A dust scattering model of M82

Perkins, H. G.

A DUST SCATTERING MODEL OF M82

by

H.G. PERKINS B.Sc., M.Sc.

A THESIS SUBMITTED TO THE

UNIVERSITY OF DURHAM FOR THE

DEGREE OF DOCTOR OF PHILOSOPHY

November, 1978.

PREFACE

The work presented in this thesis was carried out by the author when a research student at the Department of Physics, Durham University for the period 1975 to 1977 while under the supervision of Dr. S. M. Scarrott.

During this period the author made several visits to the Royal Greenwich Observatory at Herstmonceux, and also visited the George and Florence Wise observatory, University of Tel-Aviv, Israel in May 1976.

ABSTRACT

This thesis contains an investigation into polarisation produced by light scattered within nebulae and galaxies.

In the first chapter a general outline of mechanisms producing polarisation is given. This is followed in chapter two by a detailed analysis of the theory of scattering. Here we show the formulation of the theory for scattering from small particles (Rayleigh scattering) and scattering from larger particles, (Mie theory). Chapter three gives an overview of interstellar grains, their composition, growth, destruction, size distributions and the possible sources of their origins.

This is followed in the next chapter by a study of the galaxy M82. Here is given the scientific development of the galaxy showing previous models developed and the controversy which has built up over the years on whether the galaxy actually exploded or not. Chapter five contains a dust scattering model of the galaxy. This is based upon the hypothesis that the galaxy has drifted into an enormous intergalactic dust cloud. The results and consequences of the model are presented in chapter six. The dust scattering model used for M82 assumed Rayleigh scatterers. Chapter seven shows the results from model nebulae consisting of Mie particles. Here discussion is given to the effect on the predicted results when varying the properties of the grains. We also mention the potentials of other forms of polarisation techniques.

CONTENTS

CHAPTER I.

POLARISED LIGHT

It was shown by Maxwell that light travels in a sinusoidal wave form. Moreover, being an electromagnetic phenomenon, it has an electric vector $\underline{E}$, perpendicular to a magnetic vector $\underline{H}$, which are both perpendicular to the direction of propogation of the wave.

Any restriction on the orientation of the vibrations yields polarised light.

1.1 Description of polarised light.

In natural light the electric vector $\underline{E}$ is randomly orientated. When the $\underline{E}$ - vector is confined to vibrate in a particular direction, the light is said to be plane-polarised. Resolving the $\underline{E}$ - vector into two components with respect to a fixed co-ordinate system yields three quantities, the amplitude of the $\underline{E}$ - vector, the angle it makes with respect to the co-ordinate system, and the ratio of the two components.

Elliptically polarised light occurs when two component waves of plane polarised light are differentially interfered. The result is a phase difference between the two waves. This is physically represented by a rotation of the $\underline{E}$ - vector in both time and space and so the $\underline{E}$ - vector describes an ellipse. When the major and minor axes of the ellipse are equal (phase difference equal to $\frac{\pi}{2}$) the $\underline{E}$ - vector will describe a circle. This phenomenon is known as circularly polarised light.

Any beam of light may consist of a mixture of natural and polarised light. With the aid of Stokes' parameters, the beam can be split into the two respective components.

1.2 Stokes Parameters.

All polarised light can be represented by Stokes parameters. These parameters have the property that they may be added i.e. they are vectors.

The most general form of polarised light is elliptical (see figure 1).

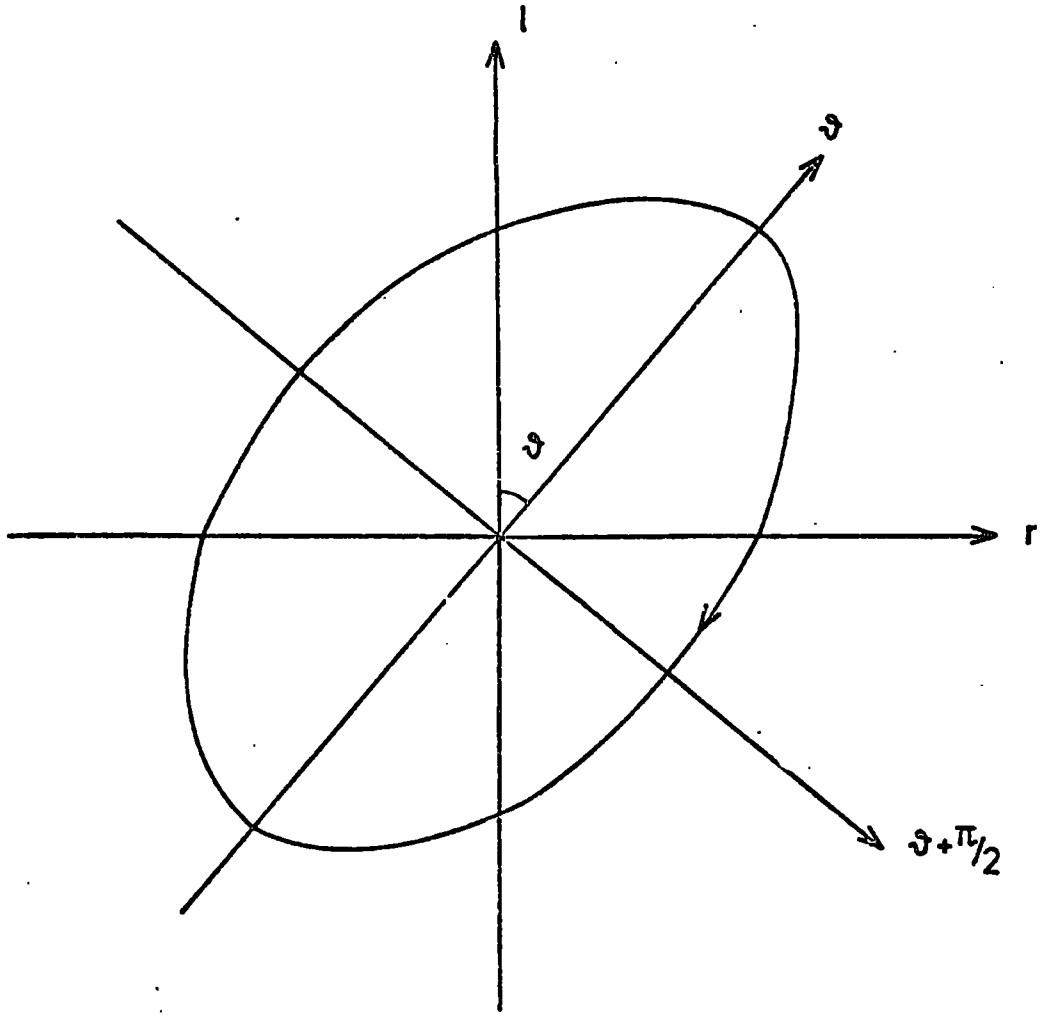

FIG.1 ELLIPTICALLY POLARISED LIGHT.

Circular and plane-polarised light are just special cases of this.

Resolving the $\underline{E}$ - vector along the l and r axes (l and r denoting parallel and perpendicular) we have.

$$\begin{aligned} \xi_l &= \xi_l^{(0)} \sin(\omega t - \epsilon_l) \\ \xi_r &= \xi_r^{(0)} \sin(\omega t - \epsilon_r) \end{aligned} \tag{1.1}$$

where ϵ_l and ϵ_r are constants and ω is the circular frequency. However, we may describe the ellipse as

$$\begin{aligned} \xi_\theta &= \xi^{(0)} \cos\beta \sin\omega t \\ \xi_{\theta+\pi/2} &= \xi^{(0)} \sin\beta \cos\omega t \end{aligned} \tag{1.2}$$

Here, $\tan\beta$ is the ratio of the axes of the ellipse (b/a) Note also that

$$\begin{aligned} (\xi^{(0)})^2 &= (\xi_l^{(0)})^2 + (\xi_r^{(0)})^2 \\ &= I_l + I_r \\ &= I \end{aligned} \tag{1.3}$$

where I denotes the intensity.

Comparing (1.1) and (1.2), it is readily shown that:

$$\begin{aligned} \xi_l &= \xi^{(0)} (\cos\beta \cos\theta \sin\omega t - \sin\beta \sin\theta \cos\omega t) \\ \xi_r &= \xi^{(0)} (\cos\beta \sin\theta \sin\omega t + \sin\beta \cos\theta \cos\omega t) \end{aligned} \tag{1.4}$$

by putting

$$\begin{aligned} \xi_l^{(0)} &= \xi^{(0)} (\cos^2\beta \cos^2\theta + \sin^2\beta \sin^2\theta)^{1/2} \\ \xi_r^{(0)} &= \xi^{(0)} (\cos^2\beta \sin^2\theta + \sin^2\beta \cos^2\theta)^{1/2} \end{aligned} \tag{1.5}$$

along with

$$\begin{aligned} \tan\epsilon_l &= \tan\beta \tan\theta \\ \tan\epsilon_r &= -\tan\beta \cot\theta \end{aligned} \tag{1.6}$$

We then have

$$\begin{aligned} I_l &= [\xi_l^{(0)}]^2 = I(\cos^2\beta \cos^2\theta + \sin^2\beta \sin^2\theta) \\ I_r &= [\xi_r^{(0)}]^2 = I(\cos^2\beta \sin^2\theta + \sin^2\beta \cos^2\theta) \end{aligned} \tag{1.7}$$

and we immediately see that

$$I = I_l + I_r$$

We define

$$Q = I_l - I_r = (\xi_l^{(0)})^2 - (\xi_r^{(0)})^2$$

Using equations (1.5) this may be written as.

$$\begin{aligned} Q &= I\{\cos^2\beta(\cos^2\theta - \sin^2\theta) + \sin^2\beta(\sin^2\theta - \cos^2\theta)\} \\ &= I\{\cos 2\theta(\cos^2\beta - \sin^2\beta)\} \\ &= I \cos 2\theta \cos 2\beta \end{aligned}$$

Similarly, we define U and V such that

$$U = 2\xi_l^{(0)} \xi_r^{(0)} \cos(\epsilon_r - \epsilon_l) = I \cos^2\beta \sin 2\theta$$

and $$V = 2\mathcal{E}_e^{(0)}\mathcal{E}_r^{(0)}\sin(\epsilon_r - \epsilon_e) = I\sin 2\beta$$

The quantities (I, Q, U, V) are Stokes parameters, and written fully are

$$\begin{aligned} I &= I_e + I_r \\ Q &= I\cos^2\beta\cos 2\theta = I_e - I_r \\ U &= I\cos^2\beta\sin 2\theta = (I_e - I_r)\tan 2\theta \\ V &= I\sin 2\beta \quad = (I_e - I_r)\tan 2\beta\sec 2\theta \end{aligned} \tag{1.8}$$

Immediately we find

$$I^2 = Q^2 + U^2 + V^2$$

with

$$\tan 2\theta = U/Q \;,\; \sin 2\beta = V/(Q^2+U^2+V^2)^{1/2}$$

For plane-polarised light, $\beta = 0$ (since tan = b/a this implies b = 0), and the equations (1.8) reduce to

$$\begin{aligned} I &= I_e + I_r \\ Q &= I\cos 2\theta \\ U &= I\sin 2\theta \\ V &= 0 \\ I^2 &= Q^2 + U^2 \end{aligned} \tag{1.9}$$

In practice, the beam is usually a mixture of natural and polarised light, so this quantity, $Q^2 + U^2$ is called the polarised intensity and is denoted by I_p. So

$$\begin{aligned} I &= I_e + I_r \\ Q &= I_p\cos 2\theta \\ U &= I_p\sin 2\theta \end{aligned} \tag{1.10}$$

Since light is a mixture, it can be shown that the intensity is written as

$$I^2 \geqslant Q^2 + U^2 + V^2$$

and that it is possible to set up two independent groups thus

$$(I - (Q^2+U^2+V^2)^{1/2}, 0, 0, 0) \tag{1.11}$$

and

$$((Q^2+U^2+V^2)^{1/2}, Q, U, V)$$

The former represents natural light while the latter describes elliptically polarised light.

In fact this is an important result that states that a beam, consisting of a mixture of light, can be separated into natural and polarised light and thus analysed separately. A full analysis of this is given by Chandrasekhar (1960).

1.3 Astrophysical processes producing polarisation.

There are three main processes that produce polarisation. They are synchrotron emission, transmission of light through aligned dust grains, and scattering by electrons and dust grains.

a). Synchrotron emission is a phenomenon that occurs when energetic charged particles are introduced into a magnetic field. The particles describe circular motions around the magnetic field lines and also have a linear motion parallel to the magnetic field lines. During this process they lose energy which is given off in the form of synchrotron radiation. This radiation is usually very highly plane-polarised and the $\underline{E}$ - vector lies perpendicular to the magnetic field. Only relativistic particles however, are capable of emitting radiation in the visible part of the spectrum. An example of such an object is the Crab nebula which shows up to 60% polarisation (White 1977). Only a few objects will have such an input of relativistic particle (such as Supernovae remnants) but other objects possessing magnetic fields will emit synchrotron radiation. These however, are usually detected by radio measurements since the component in the visible is far too small.

b). It was shown by Greenstein and Davis (1951) that anisotropic grains can be aligned in a magnetic field. Usually the long axis of the particle is perpendicular to the magnetic field and the grain spins around an axis parallel to the magnetic field. The grain precesses by an amount depending on the strength of the magnetic field and if the field is situated in a turbulent medium (eg. H II region) the colliding electrons and protons will tend to increase the precession.

The effect of aligning those grains is that light passing through, from stars say, will be polarised in such a way that the $\underline{E}$ - vector is parallel to the magnetic field. Our own galaxy possesses a magnetic field and interstellar polarisation of starlight was discovered by Hall (1949).

However, we do not necessarily need a magnetic field to align grains. In H II regions where conditions are hot, electrons and protons, flowing from a source,

will collide with the dust grains. The result is that the grains will align themselves such that they offer least resistance i.e. the long axis of the grain will be parallel to the particle flow.

Radiation pressure may also align grains in the same manner if it is strong enough. Some believe that this is what is happening within the Kleinman - Low infra-red nebula in M 42. (Pallister 1977).

c). Scattering occurs in most astronomical objects such as nebulae and 'ordinary' galaxies and is probably the cause for most polarisation observed. Electrons behave like radiating dipoles so their scattered intensities are given by Rayleigh scattering theory.

$$I = \frac{(1+\cos^2\theta)\, k^4 |\alpha|^2 I_0}{i r^2} \qquad (1.12)$$

where r is the distance from the light source to the electron, θ is the scattering angle, $K(=\frac{2\pi}{\lambda})$ the wave number and α is the polarizability of the particle.

For an electron, the polarizability is given by

$$\alpha = \frac{-e^2}{m\omega^2} \qquad (1.13)$$

where ω is the circular frequency. Substituting into equation (1.12), we find the wave length dependence no longer exists.

The amount of polarised light to the total light (defined by $p = \frac{(Q^2+U^2)^{1/2}}{I}$) for Rayleigh scattering is given by

$$p = \frac{1-\cos^2\theta}{1+\cos^2\theta} \qquad (1.14)$$

Here, also there is no wavelength dependance.

Very small grains in a radiation field will also radiate like an oscillating dipole if the size of the grain is small compared to the incident radiations' wavelength, so equation (1.12) may be applied in this case.

For these grains the polarizability is usually wavelength independant, meaning that the scattered intensity will have wavelength dependance. However the polarisation is still wavelength independant.

As the grains increase in size we arrive at the stage where the size of the

grain is comparable to that of the incident lights' wavelength. In this region, and beyond, Mie scattering theory has to be applied. The formulation for this will be given in a later chapter but we can say now that there is no analytical form for the variation of polarisation and intensity with wavelength, except to say that they are functions of wavelength.

In all these types of scattering the $\underline{E}$ - vector will lie perpendicular to the scattering plane, defined by the incident radiation and the scattered light. It is possible however to get scattering from aligned grains. In Mie theory we assume the grains to be spherical since they are randomly orientated, but for aligned grains, as mentioned earlier, the long axis is perpendicular to the magnetic field (assuming the Greenstein - Davis mechanism). It follows that the $\underline{E}$ - vector is this case will be parallel to the long axis.

To sum up then, the scattering properties are summarised below.

Type of Scatterer	Intensity $I(\lambda)$	Polarisation $p(\lambda)$
Electron	$I(\lambda)$ = constant	$p(\lambda)$ = constant
Rayleigh Dust Particle	$I(\lambda) \propto \lambda^{-4}$	$p(\lambda)$ = constant
Mie Particle	No Analytical Expression	No Analytical Expression

1.4 Measurement of linear polarisation with the Durham polarimeter.

The Durham polarimeter used in conjuction with a four centimetre electronographic camera is capable of simultaneously measuring the quantities I,Q,U, at 4,000 points within an extended astronomical object. The reduction procedure automatically removes the effect of sky brightness and polarisation by determining the Stokes parameters for the sky observed along with the object, and then correcting the parameters determined for the object.

The polarimeter and reduction technique has been described in detail elsewhere (Pallister1976). The data used in this thesis was taken and reduced mainly by Pallister and Scarrott and the author was presented with the data for the analysis

in this thesis.

One pertinent factor to be considered when interpreting the data is the errors of the measured quantities. Figure 2 shows the errors as a function of signal level for both the degree of polarisation and position angle for measurements on the galaxy M 82. These errors have been used in the analysis described later in this thesis.

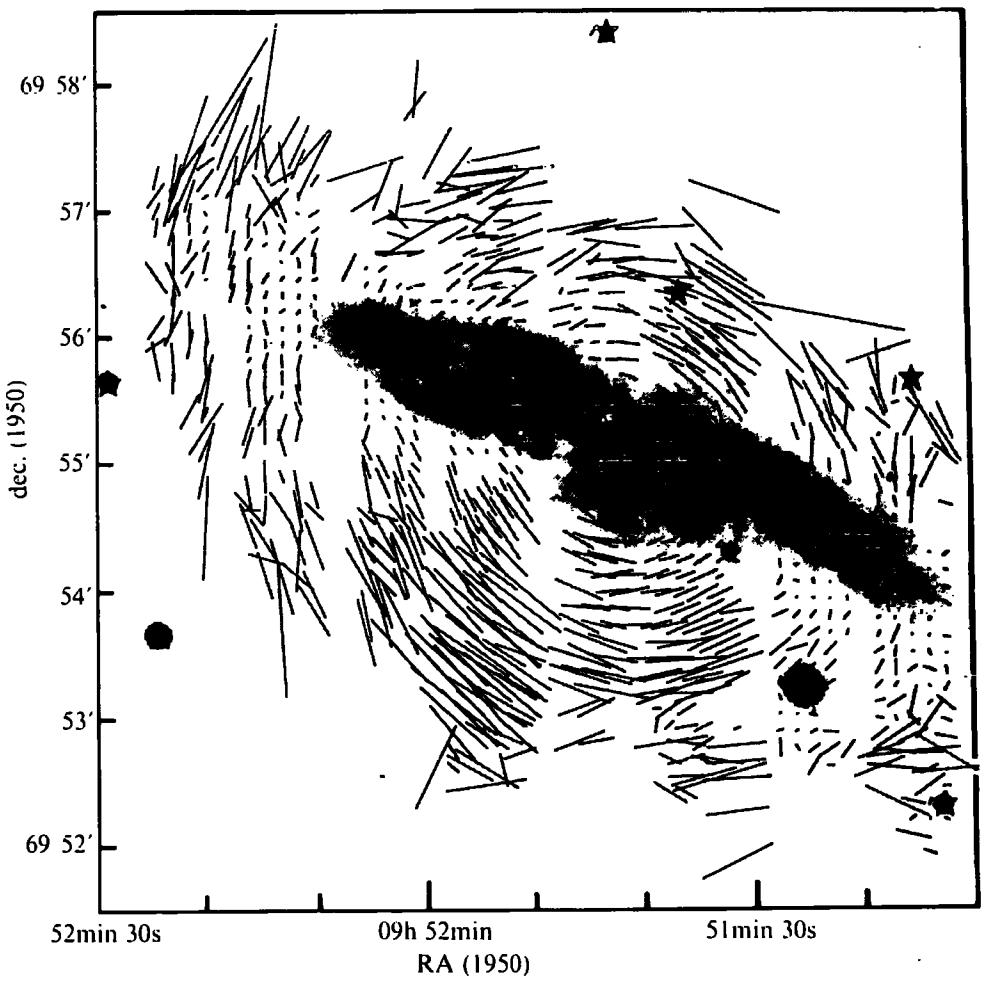

Fig. 1 The linear optical polarisation of M82 in the B waveband. ★ represent fiducial stars, ◆ the centre of symmetry, —, 10% polarisation.

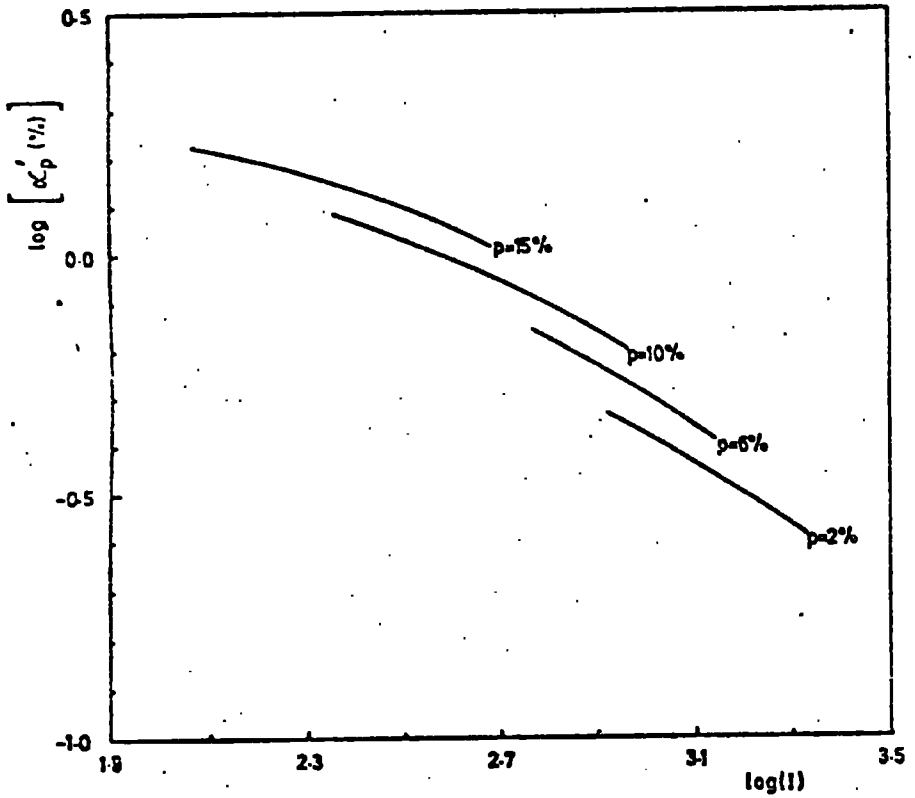

ERRORS IN POLARISATION DEGREE

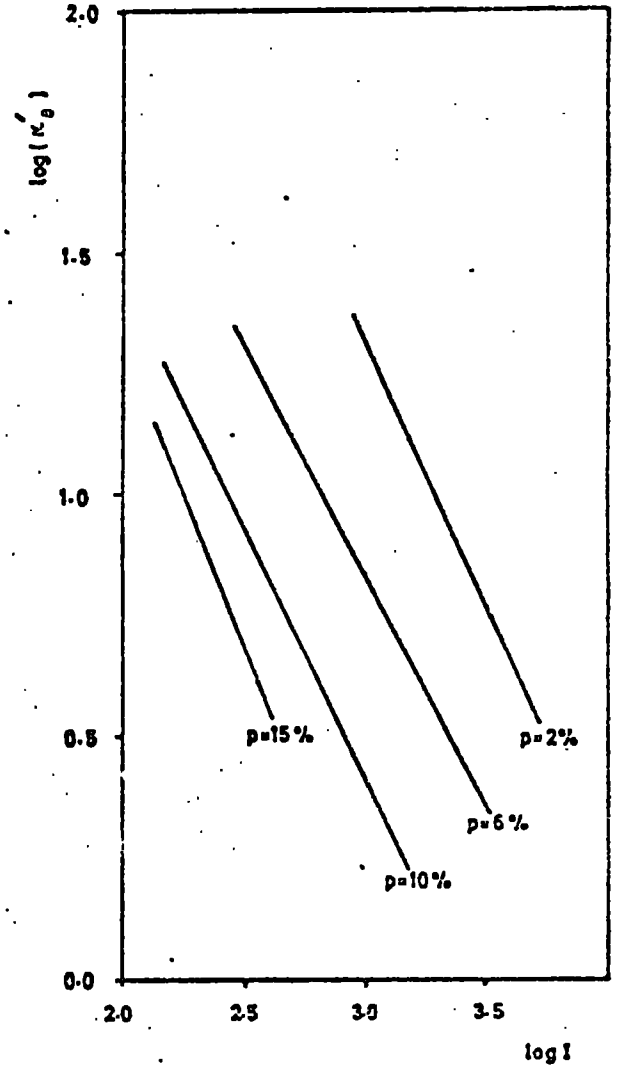

ERRORS IN POLARISATION ORIENTATION

FIG. 2. (PALLISTER 1976)

CHAPTER 2

MIE AND RAYLEIGH SCATTERING THEORY

As mentioned earlier in this thesis, the scattering of light by dust grains etc., is one of the more important processes that produces linear polarisation in astrophysical situations. This chapter is devoted to a detailed description of the scattering formulation on which models of nebulae are built to describe the polarisation measurements. Two types of scattering of light by spherical particles will be considered here. Rayleigh scattering occurs when the particle size is smaller than the wavelength (λ) of the incident radiation and the scatterer acts as a simple dipole. In the other case, as described by Mie scattering, the particle size is of the same order as the wavelength of light and the refractive index of the material of the particle has to be included.

The nomenclature used in the following derivations is of Van de Hulst (1957).

2.1 Fundamentals of Scattering theory

Consider a beam of radiation of intensity Io being scattered by a particle. The scattered radiation then has intensity I defined by

$$I = \frac{I_o F(\theta, \phi)}{k^2 r^2} \qquad (2.1)$$

where $k = \frac{2\pi}{\lambda}$, r is the distance from the particle to the observer, and $F(\theta,\phi)$ is a dimensionless function that describes the amount of radiation scattered in a particular direction, defined by θ and ϕ, the scattering and azimuthal angles respectively.

Each scattering particle can be represented by two cross-sections; Csca (the scattering cross-section), measuring the amount of radiation scattered from the incident beam and Cabs (the absorption cross-section). The total amount of radiation lost from the incidents beam is represented by Cext (the extinction cross-section) and is just the sum of Csca and Cabs.

For our purposes Csca is the most important factor and is defined by

$$C_{sca} = \frac{1}{k^2}\int_{\Omega} F(\theta,\varphi)\, d\omega \tag{2.2}$$

Where $d\omega = \sin\theta\, d\theta\, d\varphi$

Radiation carries momentum, and the amount of momentum removed from the incident beam depends on Cext. The portion removed by scattering naturally depends on Csca and is proportional to I $\cos\theta$, the forward component of the scattered light. The total forward momentum is then proportional to

$$\langle\cos\theta\rangle C_{sca} = \frac{1}{k^2}\int_{\Omega} F(\theta,\varphi)\cos\theta\, d\omega \tag{2.3}$$

where $\langle\cos\theta\rangle$ denotes the weighted mean of $\cos\theta$. This is just the phenomenon of radiation pressure and its cross-section is given by

$$C_{pr} = C_{ext} - \langle\cos\theta\rangle C_{sca} \tag{2.4}$$

The force applied to the particle is just Io Cpr/c.

If the particle is a sphere of radius a we can define the 'efficiency factors' as the cross-sections divided by the 'physical' projected area of the particle. These efficiency factors are denoted by Q's.

So that

$$\begin{aligned} Q_{ext} &= C_{ext}/\pi a^2 \\ Q_{sca} &= C_{sca}/\pi a^2 \\ \text{and}\quad Q_{abs} &= C_{abs}/\pi a^2 \end{aligned} \tag{2.5}$$

A relationship can be obtained giving the intensity and state of polarisation after scattering, as follows,

If I, Q, U and V represent Stokes' parameters for the scattered light, then

$$\{I, Q, U, V\} = \frac{1}{k^2 r^2}\,\underset{\sim}{F}\cdot\{I_o, Q_o, U_o, V_o\} \tag{2.6}$$

where Io, Qo, Uo and Vo are Stokes' parameters for the incident light. The matrix $\underset{\sim}{F}$ contains sixteen components, so that for example,

$$I = \frac{1}{k^2 r^2} \{ F_{11} I_0 + F_{12} Q_0 + F_{13} U_0 + F_{14} V_0 \} \tag{2.7}$$

But from equation (2.1) we have

$$I = \frac{F(\theta,\varphi) I_0}{k^2 r^2}$$

so that $$F = F_{11} + F_{12} Q_0/I_0 + F_{13} U_0/I_0 + F_{14} V_0/I_0 \tag{2.8}$$

For unpolarised incident light $F = F_{11}$

If instead of a single particle we have a medium containing N different particles, then for the ith particle

$$I_i = \frac{1}{k^2 r^2} F_i(\theta,\varphi) I_0 \tag{2.9}$$

From this, a definition for $F(\theta,\varphi)$ may be obtained for a whole medium, so that

$$F(\theta,\varphi) = \sum_i F_i(\theta,\varphi) \tag{2.10}$$

(This is based on the assumption that phase effects may be neglected)
In the medium however, the light is attenuated by a factor $e^{-\gamma S}$ where S is the path length traversed by the light. As well as this, the particle sizes are given by a distribution function N(a) such that between radii a and a + da there are N(a) da particles. We now have

$$\gamma = \int_0^\infty N(a) Q_{ext}(a) \pi a^2 da \tag{2.11}$$

where $N = \int_0^\infty N(a)\, da$ is the total number of grains.

Note that Qext is a function of a as well as θ (here $\theta = 0$).

2.2 Formulation of extinction and scattering cross-sections

Consider an arbitrary particle in a radiation field. We may write the incident field in the form.

$$U_0 = e^{-i(kz - \omega t)} \tag{2.12}$$

This is sometimes called the disturbance. We may write the disturbance of the scattered wave as

$$u = \frac{S(\theta,\varphi)}{ikr} e^{-i(kr-\omega t)} \tag{2.13}$$

since the scattered wave in the distant field is a spherical outgoing wave with amplitude inversely proportional to the distance r between the scatterer and the observer. Here $S(\theta,\varphi)$ is called the amplitude function, and it is the solution of this function which is one of the prerequisites for modelling nebulae. Equation (2.13) can be written

$$u = \frac{S(\theta,\varphi)}{ikr} e^{-ik(r-z)} \tag{2.14}$$

and since intensity is proportional to the square of the modulus of the disturbance

$$I_{sca} = \frac{|S(\theta,\varphi)|^2 I_0}{k^2 r^2} \tag{2.15}$$

If we now try to calculate the amount of extinction by a particle, we must consider the combination of the incident and scattered wave, since the particle is placed in a radiation field.

Consider an observer at a large distance from the scattering particle, he will observe the intensity over a finite area (see figure 3). Let P(x, y) be a point within the 'collecting' area. (This may, for example, be a mirror of a telescope). Since $r \gg (x, y)$ we write

$$r = z + \frac{(x^2+y^2)}{2z} \tag{2.16}$$

Then

$$u+u_0 = u_0 \left(1 + \frac{S(0)}{ikr} e^{-ik(r-z)}\right) \tag{2.17}$$

or using (2.16)

$$u+u_0 = u_0 \left(1 + \frac{S(0)}{ikz} e^{-ik\left(\frac{x^2+y^2}{2z}\right)}\right) \tag{2.18}$$

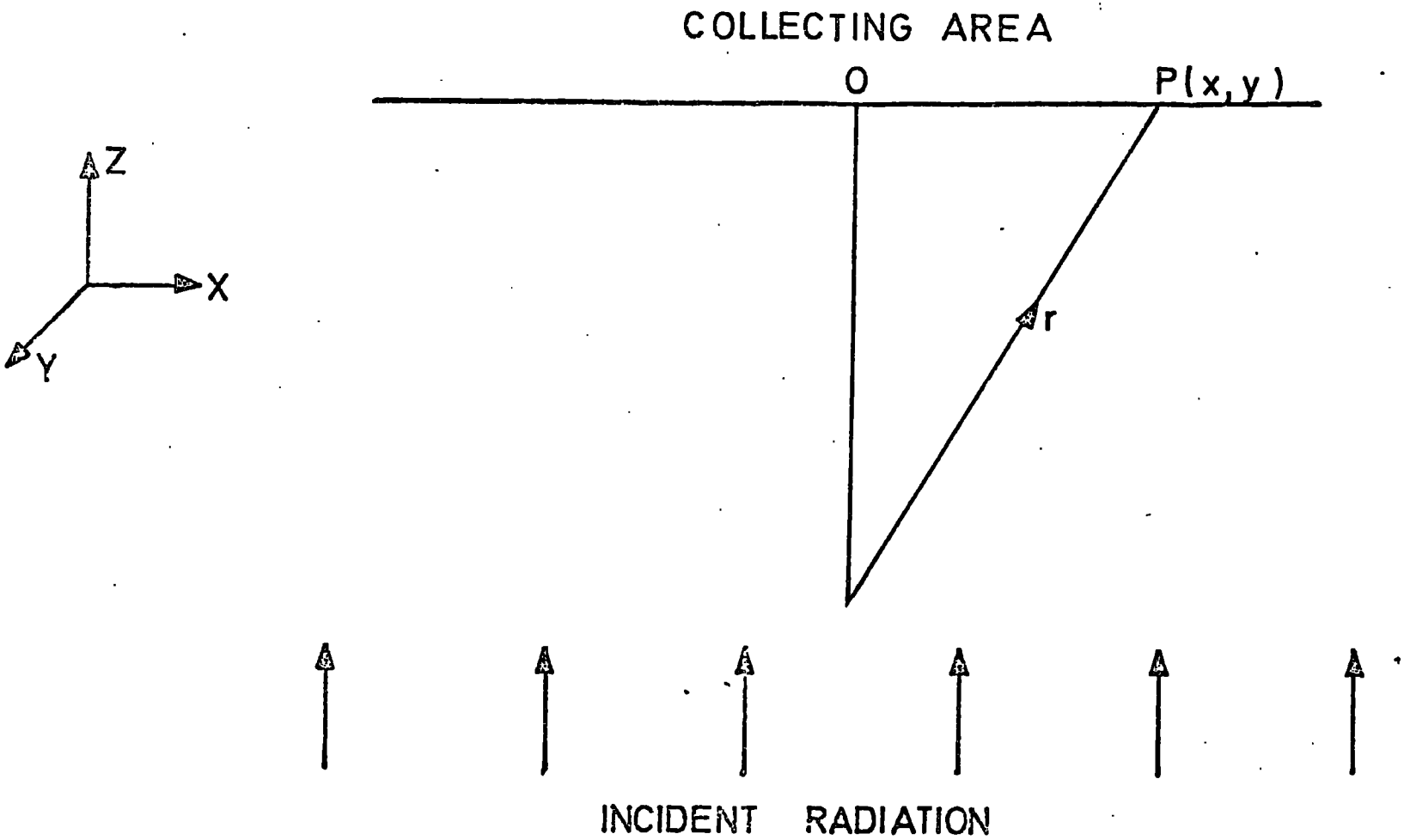

FIG. 3.

(N.B., $\theta = 0$)

and

$$|u+u_0|^2 = 1 + \frac{2}{kz}\Re\left\{\frac{S(0)}{i}e^{-ik\left(\frac{x^2+y^2}{2z}\right)}\right\} \tag{2.19}$$

Integrating this expression over the area, dxdy, and using the property of the Fresnel integral viz.

$$\int_0^\infty e^{-as^2}ds = \tfrac{1}{2}\sqrt{\pi/a}$$

we find

$$C_{ext} = \frac{4\pi}{k^2}\Re\{S(0)\} \tag{2.20}$$

The physical significance of this is that the particle does not block the wave, but causes an interference phenomenon.

For many scattering particles we may, as before, write each particle as having an individual scattering function $S_i(\theta,\varphi)$. To find the amplitude function for the whole medium would mean reforming all the individual amplitudes to a common origin and then summing. This would involve large phase shifts and so the individual intensities, and not the amplitudes, have to be added thus.

$$I(\theta,\varphi) = \sum_i I_i(\theta,\varphi) \tag{2.21}$$

Integrating over all areas gives

$$C_{sca} = \sum_i C_{i,sca} \tag{2.22}$$

We can express the amplitude function as

$$S(\theta,\varphi) = s\,e^{i\sigma} \tag{2.23}$$

where $S=S(\theta,\varphi)>0$ and $\sigma=\sigma(\theta,\varphi)$ is real.

Note that σ depends on the choice of origin, except for $\theta = 0$ when

$$S(0) = s(0)\,e^{i\sigma(0)} \tag{2.24}$$

and the phase, $\sigma(0)$ is independent of the choice origin. So

$$S(0) = \sum_i S_i(0) \tag{2.25}$$

in which case it follows that

$$C_{ext} = \sum_i C_{i,ext} \tag{2.26}$$

Consider now a 'slab' containing scatterers all identical and all orientated the same way such that they have the same scattering amplitudes $S_i(\theta,\phi)$ (see figure 4). Let the particle density be N. The radiation received at P is a combination of both extinction and dispersion, so that the total amplitude received at P is

$$u = u_0 \left\{ 1 + S(0) \sum \frac{1}{ikr} e^{-ikr\left(\frac{x^2+y^2}{2r}\right)} \right\} \tag{2.27}$$

If there are many particles, we may replace the summation by integration giving

$$u = u_0 \left\{ 1 + S(0) \iiint \frac{N}{ikr} e^{-ikr\left(\frac{x^2+y^2}{2r}\right)} dx\,dy\,dz \right\} \tag{2.28}$$

This then gives

$$u = u_0 \left\{ 1 - \frac{2\pi}{k^2} N \ell S(0) \right\} \tag{2.29}$$

Now if this slab is replaced by a slab containing homogeneous material with complex refractive index $\tilde{m}$ such that $|\tilde{m}| \simeq 1$, the amplitude of the wave is changed by an amount proportional to

$$e^{-ik\ell(\tilde{m}-1)} \simeq 1 - ik\ell(\tilde{m}-1) \tag{2.30}$$

This is saying that uo is changed to u by an amount shown in equation (2.30) so on comparison we find

$$1 - ik\ell(\tilde{m}-1) = 1 - \frac{2\pi}{k^2} N \ell S(0) \tag{2.31}$$

or

$$\tilde{m} = 1 - \frac{2\pi N i S(0)}{k^3} \tag{2.32}$$

Representing the refractive index by $\tilde{m} = n - in'$ the real part becomes

$$n = 1 + \frac{2\pi N}{k^3} \mathcal{J}\{S(0)\} \tag{2.33}$$

This determines the lagging or advancement of phase of the wave travelling through the medium.

This is dispersion and the phase velocityof the wave travelling the medium is c/n

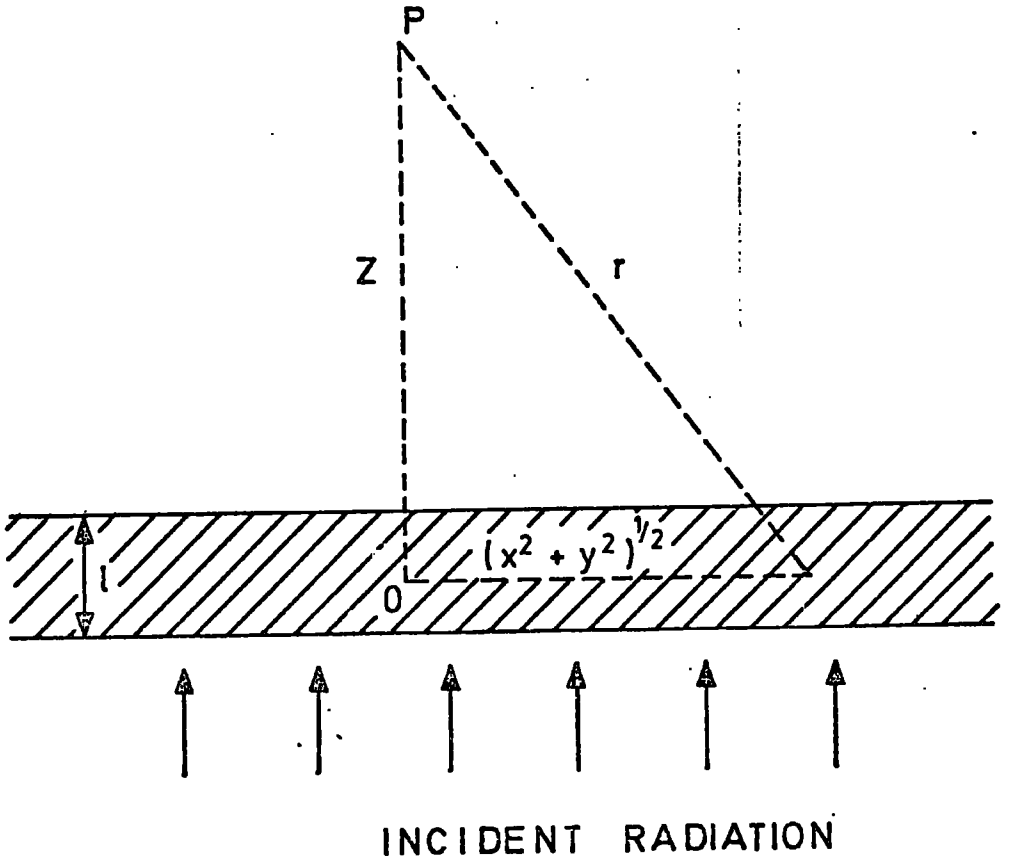

FIG. 4.

The imaginary part of $\tilde{m}$ is

$$n' = \frac{2\pi N}{k^3} \Re\{S(0)\} \tag{2.34}$$

This determines the decrease in intensity of the wave. It may also be shown that

$$\gamma = \frac{4\pi N}{k^2} \Re\{S(0)\} \tag{2.35}$$

2.3 Mie formulation

The solution of scattering of radiation from finite spheres (i.e. spheres with $2\pi a \sim 1$) is obtained by solving Maxwells equations with appropriate boundary conditions. Some of the derivations will however be omitted.

With the usual notation, Maxwells equations are

$$\nabla \times \underset{\sim}{H} = \frac{4\pi}{c} \underset{\sim}{J} + \frac{1}{c} \frac{\partial \underset{\sim}{D}}{\partial t} \tag{2.36}$$

$$\nabla \times \underset{\sim}{E} = -\frac{1}{c} \frac{\partial \underset{\sim}{H}}{\partial t} \tag{2.37}$$

where $\underset{\sim}{D} = \epsilon \underset{\sim}{E}$ and $\underset{\sim}{J} = \sigma \underset{\sim}{E}$

These, along with the conservation of charge equation viz.

$$\nabla \cdot \underset{\sim}{J} + \frac{\partial \rho}{\partial t} = 0 \tag{2.38}$$

give us sufficient equations (along with boundary conditions) to solve the problem.

First, with equation (2.36) we write

$$\nabla \cdot (\nabla \times \underset{\sim}{H}) = \frac{4\pi}{c} \nabla \cdot \underset{\sim}{J} + \frac{1}{c} \frac{\partial}{\partial t} (\nabla \cdot \underset{\sim}{D}) \tag{2.39}$$

i.e.

$$\frac{4\pi}{c} (\nabla \cdot \underset{\sim}{J}) + \frac{1}{c} \frac{\partial}{\partial t} (\nabla \cdot \underset{\sim}{D}) = 0 \tag{2.40}$$

Using equation (2.38), the above equation can be written as

$$\frac{4\pi}{c}\frac{\partial \rho}{\partial t} = \frac{1}{c}\frac{\partial}{\partial t}(\nabla \cdot \underset{\sim}{D}) \tag{2.41}$$

i.e.

$$\nabla \cdot \underset{\sim}{H} = 0 \tag{2.42}$$

We assume circular frequency ω viz.

$$A = (\alpha + i\beta)e^{i\omega t}$$

but interest will only be given to the real part of this.

Since $\underset{\sim}{H} \propto e^{i\omega t}$

then $$\frac{\partial \underset{\sim}{H}}{\partial t} = i\omega \underset{\sim}{H} \tag{2.43}$$

So that $$\nabla \times \underset{\sim}{E} = -ik\underset{\sim}{H} \tag{2.44}$$

where $k = \frac{\omega}{c} = \frac{2\pi}{\lambda}$

Equation (2.36) gives

$$\nabla \times \underset{\sim}{H} = \frac{4\pi}{c}\sigma \underset{\sim}{E} + \frac{\varepsilon}{c}\frac{\partial \underset{\sim}{E}}{\partial t} \tag{2.45}$$

and since $\underset{\sim}{E} \propto e^{i\omega t}$

then $$\frac{\partial \underset{\sim}{E}}{\partial t} = i\omega \underset{\sim}{E}$$

Equation (2.45) yields

$$\nabla \times \underset{\sim}{H} = \frac{4\pi}{c}\sigma \underset{\sim}{E} + \frac{i\varepsilon}{c}\omega \underset{\sim}{E} = ikm^2 \underset{\sim}{E} \tag{2.46}$$

where $m^2 = \varepsilon - \frac{4\pi\sigma}{\omega} i$ is the complex refractive

index of the medium at frequency ω.

Taking

$$\nabla \cdot (\nabla \times \underset{\sim}{H}) = \nabla \cdot (ikm^2 \underset{\sim}{E}) = 0 \tag{2.47}$$

gives

$$\nabla \cdot (m^2 \underset{\sim}{E}) = 0 \tag{2.48}$$

For a homogeneous medium, m = constant and so

$$\nabla \cdot \underset{\sim}{E} = 0 \tag{2.49}$$

giving $\rho = 0 \quad (\underset{\sim}{D} = \varepsilon \underset{\sim}{E})$

The components of $\underline{E}$ and $\underline{H}$ satisfy the scalar wave equation viz.

$$\nabla^2 \psi = -k^2 m \psi \tag{2.50}$$

The simplest type of solution of this equation corresponds to a plane wave travelling in the Z-direction i.e.

$$\psi = e^{ikmz + i\omega t} \tag{2.51}$$

Now let us consider the boundary conditions. Let the two media be denoted by 1 and 2, so that medium 1 has quantities $(\varepsilon_1, \sigma_1, m_1)$ and medium 2 $(\varepsilon_2, \sigma_2, m_2)$.

If $\hat{n}$ denotes the normal to the boundary then we may write

$$\begin{aligned} \hat{n} \times (\underline{H}_2 - \underline{H}_1) &= 0 \\ \hat{n} \times (\underline{E}_2 - \underline{E}_1) &= 0 \end{aligned} \tag{2.52}$$

As well as

$$\begin{aligned} \hat{n} \cdot (m_2^2 \underline{E}_2 - m_1^2 \underline{E}_1) &= 0 \\ \hat{n} \cdot (\underline{H}_2 - \underline{H}_1) &= 0 \end{aligned} \tag{2.53}$$

The scalar wave equation has elementary solution of the following type

$$\psi_{\ell n} = \left.\begin{matrix} \cos \ell\phi \\ \sin \ell\phi \end{matrix}\right\} P_n^{\ell}(\cos\theta) Z_n(mkr) \tag{2.54}$$

where n and l are integers ($n \geq \ell \geq 0$). Here, $P_n^{\ell}(\cos\theta)$ is the associated Legendre polynomial and Z_n (mkr) the spherical Bessel function.

Now from (2.44) and (2.45), one obtains the vector wave equation

$$\nabla^2 \underline{A} + k^2 m^2 \underline{A} = 0 \tag{2.55}$$

To solve this, we make use of the following theorem. If ψ satisfies the scalar wave equation, then the vectors $\underline{M}\psi$ and $\underline{N}\psi$ satisfy the vector equation (2.55) where

$$\begin{aligned} \underline{M}\psi &= \nabla \times (\underline{r}\psi) \\ mk\underline{N}\psi &= \nabla \times \underline{M}\psi \end{aligned} \tag{2.56}$$

and

$$mk\,\underline{M}\psi = \nabla \times \underline{N}\psi$$

If the scalar wave equation has solutions u and v, and the vector fields components are $\underset{\sim}{M}u$, $\underset{\sim}{N}u$, $\underset{\sim}{M}v$ and $\underset{\sim}{N}v$. Then Maxwells equations are satisfied by

$$\underset{\sim}{E} = \underset{\sim}{M}_1 - i\underset{\sim}{N}u \tag{2.57}$$

and $$\underset{\sim}{H} = m(-\underset{\sim}{M}u + i\underset{\sim}{N}v)$$

The full components of $\underset{\sim}{M}\psi$ and $\underset{\sim}{N}\psi$ are

$$M_r = 0$$

$$M_\theta = \frac{1}{r\sin\theta}\frac{\partial}{\partial\phi}(r\psi) \tag{2.58}$$

$$M_\phi = -\frac{1}{r}\frac{\partial}{\partial\theta}(r\psi)$$

and

$$mkN_r = \frac{\partial^2}{\partial r^2}(r\psi) + m^2k^2r\psi$$

$$mkN_\theta = \frac{1}{r}\frac{\partial^2}{\partial r\partial\theta}(r\psi) \tag{2.59}$$

$$mkN_\phi = \frac{1}{r\sin\theta}\frac{\partial^2}{\partial r\partial\phi}(r\psi)$$

So $\underset{\sim}{E}$ and $\underset{\sim}{H}$ may be written in terms of the derivatives of the scalar solutions. We can now solve the problem of scattering of a plane wave by a homogeneous sphere.

We assume the second media to be a vacuum i.e. $m_2 = 1$.

If the incident beam lies along the positive Z-axis and the X-axis is in the plane of the electric vibration of the incident wave

Then $$\underset{\sim}{E} = \hat{a}_x e^{-ikz+i\omega t}$$

and $$\underset{\sim}{H} = \hat{a}_y e^{-ikz+i\omega t} \tag{2.60}$$

where $\hat{a}_x$ and $\hat{a}_y$ are unit vectors in the appropriate directions.

It has been shown that the solution of the scalar wave equation can be written in the form.

$$\psi_{en} = \begin{matrix}\cos l\phi \\ \sin l\phi\end{matrix}\Big\} P_n^l(\cos\theta)\, z_n(mkr) \tag{2.61}$$

It can be proved that the fields given by equation (2.60) along with equations (2.56) and (2.57) can be written as

$$u = e^{i\omega t}\cos\phi \sum_{n=1}^{\infty} (-i)^n \frac{2n+1}{n(n+1)} P_n'(\cos\theta)\, j_n(kr)$$
$$v = e^{i\omega t}\sin\phi \sum_{n=1}^{\infty} (-i)^n \frac{2n+1}{n(n+1)} P_n'(\cos\theta)\, j_n(kr) \qquad (2.62)$$

for the incident wave $j_n(kr)$ is a spherical Bessel function.

The field outside the sphere consists of the incident wave and the scattered wave. If we let the boundary conditions be satisfied at infinity then the following equations are sufficient

$$u_s = e^{i\omega t}\cos\phi \sum_{n=1}^{\infty} -a_n (-i)^n \frac{2n+1}{n(n+1)} P_n'(\cos\theta)\, h_n^{(2)}(kr)$$
$$v_s = e^{i\omega t}\sin\phi \sum_{n=1}^{\infty} -b_n (-i)^n \frac{2n+1}{n(n+1)} P_n'(\cos\theta)\, h_n^{(2)}(kr) \qquad (2.63)$$

where the subscript s denotes 'scattered'. Here, $h_n^{(2)}(kr)$ is a spherical Bessel function of the second kind so chosen because of its asymptotic behaviour i.e.

$$h_n^{(2)}(kr) \sim \frac{i^{n+1}}{kr} e^{-ikr} \qquad (2.64)$$

which makes it an ideal candidate for the solution. (This is because when it is combined with $e^{-i\omega t}$ it becomes an outgoing spherical wave)

For the field inside the sphere

$$u_i = e^{i\omega t}\cos\phi \sum_{n=1}^{\infty} m c_n (-i)^n \frac{2n+1}{n(n+1)} P_n'(\cos\theta)\, j_n(mkr)$$
$$v_i = e^{i\omega t}\sin\phi \sum_{n=1}^{\infty} m d_n (-i)^n \frac{2n+1}{n(n+1)} P_n'(\cos\theta)\, j_n(mkr) \qquad (2.65)$$

The coefficients a_n, b_n, c_n and d_n when determined give us the completion solution to the scattering problem. To solve for these we use the boundary conditions (2.52) and (2.53).

The compnents we consider are E_θ, E_φ, H_θ and H_φ. Now derivatives with respect to θ and φ are the same for waves both inside and outside the sphere, so they need not be considered.

E_θ and E_φ both contain expressions involving v and $\frac{\partial}{\partial r}(ru)$ and components

H_θ and H_φ contain mu and $\frac{\partial}{\partial r}(rv)$.

When r = a, where a is the radius of the scattering sphere, the expressions must be the same. We define the following set of functions,

$$\begin{aligned} \psi_n(z) &= z j_n(z) = (\pi z/2)^{1/2} J_{n+\frac{1}{2}}(z) \\ \chi_n(z) &= -z n_n(z) = -(\pi z/2)^{1/2} N_{n+\frac{1}{2}}(z) \\ \zeta_n(z) &= z h_n^{(2)}(z) = (\pi z/2)^{1/2} H^{(2)}_{n+1/2}(z) \end{aligned} \tag{2.66}$$

These are the Ricatti-Bessel functions

Since

$$H_n^{(2)}(z) = J_n(z) - i N_n(z)$$

we imply

$$\zeta_n(z) = \psi_n(z) + i \chi_n(z) \tag{2.67}$$

We now define two important quantities, the dimensionless quantity $x = 2\pi a/\lambda$ and $y = mx$.

For the sake of continuity we state:

Incoming wave - Scattered wave = Inside wave. This, combined with boundary conditions, give us the following continuity conditions.

1. Continuity for mu implies

$$\psi_n(x) - a_n \zeta_n(x) = m c_n \psi_n(y) \tag{2.68a}$$

2. Continuity for $\frac{1}{m}\frac{\partial}{\partial r}(ru)$ implies

$$\psi_n'(x) - a_n \zeta_n'(x) = c_n \psi_n'(y) \tag{2.68b}$$

3. Continuity for v implies

$$\psi_n(x) - b_n \zeta_n(x) = d_n \psi_n(y) \tag{2.68c}$$

and

4. Continuity for $\frac{\partial}{\partial r}(rv)$ implies that

$$\psi_n'(x) - b_n \zeta_n'(x) = m d_n \psi_n'(y) \tag{2.68d}$$

Eliminating c_n and d_n from the above equations we have

$$a_n = \frac{\psi_n'(y)\psi_n(x) - m\psi_n(y)\psi_n'(x)}{\psi_n'(y)\zeta_n(x) - m\psi_n(y)\zeta_n'(x)} \tag{2.69}$$

$$b_n = \frac{m\psi_n'(y)\psi_n(x) - \psi_n(y)\psi_n'(x)}{m\psi_n'(y)\zeta_n(x) - \psi_n(y)\zeta_n'(x)} \tag{2.70}$$

We ignore c_n and d_n since we are only interested in the scattered wave. Armed with a_n and b_n we now proceed to solve for the scattered wave.

Since the asymptotic behaviour of $h_n^{(2)}(kr) \sim \frac{i^{n+1}}{kr} e^{-ikr}$ (equation 2.64). Equations (2.63) become

$$U_s = -\frac{i}{kr} e^{-ikr+i\omega t} \cos\phi \sum_{n=1}^{\infty} a_n \frac{2n+1}{n(n+1)} P_n'(\cos\theta) \tag{2.71}$$

and

$$V_s = -\frac{i}{kr} e^{-ikr+i\omega t} \sin\phi \sum_{n=1}^{\infty} b_n \frac{2n+1}{n(n+1)} P_n'(\cos\theta)$$

On deriving the tangential field components by means of equations (2.56) and (2.57), the following functions of the scattering angle appear.

$$\pi_n(\cos\theta) = \frac{1}{\sin\theta} P_n'(\cos\theta) = -\frac{1}{\sin\theta} \frac{d}{d\theta} P_n(\cos\theta) \tag{2.72a}$$

and

$$\tau_n(\cos\theta) = \frac{d}{d\theta} P_n'(\cos\theta)$$

which may be written

$$\tau_n(\cos\theta) = \cos\theta\, \pi_n(\cos\theta) - \sin\theta \frac{d\,\pi_n(\cos\theta)}{d\cos\theta} \tag{2.72b}$$

The field components of the scattered wave can be written as

$$E_\phi = H_\theta = -\frac{i}{kr} e^{-ikr+i\omega t} \sin\phi . S_1(\theta) \tag{2.73}$$

$$E_\theta = H_\phi = -\frac{i}{kr} e^{-ikr+i\omega t} \cos\phi . S_2(\theta)$$

where

$$S_1(\theta) = \sum_{n=1}^{\infty} \frac{2n+1}{n(n+1)} \{a_n \pi_n(\cos\theta) + b_n \tau_n(\cos\theta)\} \tag{2.74}$$

$$S_2(\theta) = \sum_{n=1}^{\infty} \frac{2n+1}{n(n+1)} \{b_n \pi_n(\cos\theta) + a_n \tau_n(\cos\theta)\}$$

By defining

$$i_1(\theta) = |S_1(\theta)|^2 \tag{2.75}$$

and

$$i_2(\theta) = |S_2(\theta)|^2$$

we can express the state of light scattered from the spherical scatterer.

For natural incident light of intensity Io, the scattered intensity will be given by

$$I = \{ \frac{i_1(\theta) + i_2(\theta)}{2k^2r^2} \} I_o \tag{2.76}$$

and the state of linear polarisation of the light will be

$$\frac{i_1(\theta) - i_2(\theta)}{i_1(\theta) + i_2(\theta)} \tag{2.77}$$

2.4 Procedure to calculate coefficients

To calculate a_n and b_n we use the recurrence relationships of the spherical Bessel functions. These are written as

$$\begin{aligned} \frac{(2\ell+1)}{x} j_\ell(x) &= j_{\ell+1}(x) + j_{\ell-1}(x) \\ \frac{d}{dx}(x^{\ell+1} j_\ell(x)) &= x^{\ell+1} j_{\ell-1}(x) \\ \frac{d}{dx}(x^{-\ell} j_\ell(x)) &= -x^{-\ell} j_{\ell+1}(x) \end{aligned} \tag{2.78}$$

These differ from our quantities by an additional factor of the argument. Thus

$$\psi_n(x) = x j_n(x)$$

Equations (2.78) can then be written as

$$\frac{(2\ell+1)}{x} \psi_\ell(x) = \psi_{\ell+1}(x) + \psi_{\ell-1}(x) \tag{2.79}$$

$$\frac{d}{dx}(x^\ell \psi_\ell(x)) = x^\ell \psi_{\ell-1}(x) \tag{2.80}$$

$$\frac{d}{dx}\left(x^{-(l+1)}\psi_l(x)\right) = -x^{-(l+1)}\psi_{l+1}(x) \tag{2.81}$$

Equations (2.80) and (2.81) are given by

$$\frac{l}{x}\psi_l(x) + \psi_l'(x) = \psi_{l-1}(x) \tag{2.82}$$

$$\psi_l'(x) - \left(\frac{l+1}{x}\right)\psi_l(x) = \psi_{l+1}(x) \tag{2.83}$$

respectively.

Expressions for a_n and b_n can be re-written, using equation (2.82) and (2.83).

we have

$$a_n = \frac{\left(A_n(y)/m + n/x\right)\mathcal{R}\{S_n(x)\} - \mathcal{R}\{S_{n-1}(x)\}}{\left(A_n(y)/m + n/x\right)S_n(x) - S_{n-1}(x)} \tag{2.84}$$

and

$$b_n = \frac{\left(m A_n(y) + n/x\right)\mathcal{R}\{S_n(x)\} - \mathcal{R}\{S_{n-1}(x)\}}{\left(m A_n(y) + n/x\right)S_n(x) - S_{n-1}(x)} \tag{2.85}$$

where

$$A_n(y) = \psi_n'(y)/\psi_n(y) \tag{2.86}$$

Equation (2.79) gives us the recurrence relation for $S_n(x)$ viz.

$$S_n(x) = \frac{2n-1}{x}S_{n-1}(x) - S_{n-2}(x) \tag{2.87}$$

with

$$S_0(x) = \sin x + i\cos x$$
$$S_{-1}(x) = \cos x - i\sin x \tag{2.88}$$

Using equations (2.82) and (2.83), a recurrence relation for $A_n(y)$ is obtained

i.e. $$A_n(y) = -n/y + \{n/y - A_{n-1}(y)\}^{-1} \tag{2.89}$$

with $$A_0(y) = \cot y$$

Equations (2.72a) and (2.72b) have appropriate recurrence relationships

$$\pi_n(\theta) = \cos\theta \frac{(2n-1)}{(n-1)} \pi_{n-1}(\theta) \frac{-n}{(n-1)} \pi_{n-2}(\theta) \tag{2.90}$$

$$\tau_n(\theta) = \cos\theta\{\pi_n(\theta) - \pi_{n-2}(\theta)\} - (2n-1)\sin^2\theta\, \pi_{n-1}(\theta) + \tau_{n-2}(\theta) \tag{2.91}$$

with

$$\pi_0(\theta) = 0 \qquad \tau_0(\theta) = 0$$

$$\pi_1(\theta) = 1 \qquad \tau_1(\theta) = \cos\theta$$

$$\pi_2(\theta) = 3\cos\theta \qquad \tau_2(\theta) = 3\cos 2\theta$$

All these equations enable us to claculate a_n and b_n, thus giving us $S_1(\theta)$ and $S_2(\theta)$ which in turn enable us to find the intensity and polarisation of a scattered beam. The above analysis was formulated by Wickramasinghe, (1972).

2.5 Rayleigh scattering

We consider particles of arbitrary forms. The only condition here is that the particle is small compared to the wavelength of the incident radiation. Because of the partiicles' size, it may be considered as being placed in a homogeneous, electric field $\underline{E}o$, which will be called the 'applied' field. The effect of the particle, caused by the electric polarisation of the particle, is to modify the field (denoted by $\underline{E}$) both inside and near the particle.

If $\underline{p}$ is the induced dipole moment, then the electrostatic formula gives $\underline{p} = \alpha \underline{E}o$, where α gives the polarizability of the particle.

Usually α is a tensor, which means that the directions of $\underline{p}$ and $\underline{E}o$ coincide only if the field is applied in one of three mutually perpendicular directions, denoted by the unit vectors $\hat{n}_i$ (i = 1, 2, 3). We have then an expression for $\underline{E}o$ i.e.

$$\underline{E}o = \sum_{i=1}^{3} E_i \hat{n}_i \tag{2.92}$$

Immediately giving

$$\underline{P} = \sum_{i=1}^{3} \alpha_i E_i \hat{n}_i \tag{2.93}$$

(Note that if the extended field is periodic i.e. $E_o e^{i\omega t}$ then the induced dipole is $p e^{i\omega t}$).

The particle in the applied field radiates like an oscillating dipole, which radiates in all directions.

Consider a point P at distance $r(\gg\lambda)$ from the particle under consideration (see figure 5). The scattered wave observed at P is

$$E = k^2 \frac{p}{r} \sin\gamma \, e^{-ikr} \tag{2.94}$$

The intensities are

$$I_o = \frac{c}{8\pi} |\underline{E}_o|^2 \tag{2.95a}$$

for the incoming wave and

$$I = \frac{c}{8\pi} |\underline{E}|^2 \tag{2.95b}$$

for the outgoing wave

To find the energy scattered per unit time in all directions (W), we integrate over a sphere of radius r. So that

$$W = \frac{cr^2}{8\pi} \int_{\Omega} |\underline{E}|^2 d\omega = \frac{cr^2}{8\pi} \int_0^{2\pi} \int_0^{\pi} k^4 \frac{|\underline{p}|^2}{r^2} \sin^3\gamma \, d\gamma \, d\varphi$$

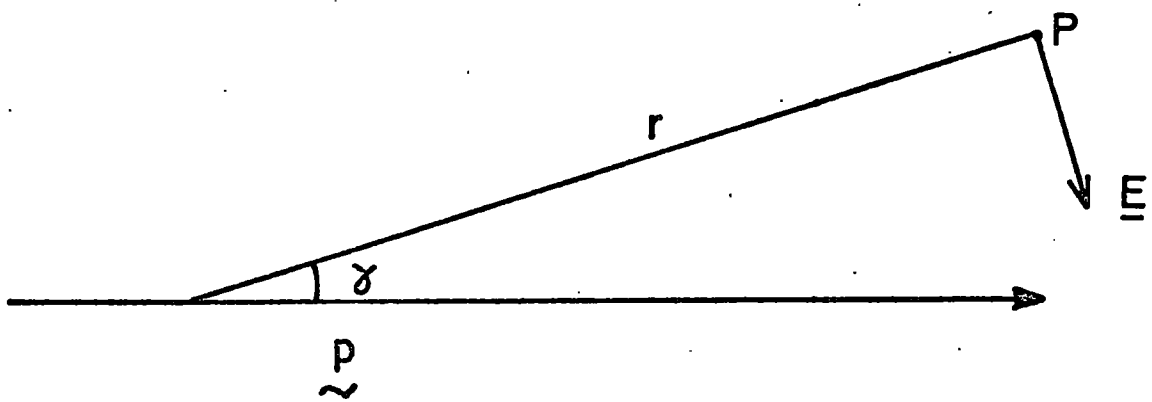

FIG. 5.

$$= \frac{k^2 c}{4} |\underset{\sim}{p}|^2 \int_0^{\pi} \sin^3\gamma \, d\gamma \tag{2.96}$$

which simply reduces to

$$W = \frac{k^4 c}{3} |\underset{\sim}{p}|^2 \tag{2.97}$$

Dividing by Io gives the scattering cross-section. With $|p|^2 = |\alpha E_0|^2$ along with equation (2.95a), we find

$$C_{sca} = \frac{W}{I_0} = \frac{8\pi}{3} k^4 |\alpha|^2 \tag{2.98}$$

where

$$|\alpha|^2 = l^2|\alpha_1|^2 + m^2|\alpha_2|^2 + n^2|\alpha_3|^2$$

and l, m and n are the direction cosines of $\underline{E}o$.

Consider now a particular type of Rayleigh particle. The case when

$$\alpha_1 = \alpha_2 = \alpha_3 \equiv \alpha$$

In this situation the directions of $\underset{\sim}{p}$ and $\underline{E}o$ always coincide, in which case the polarizability, α is a scalar. If θ is the scattering angle then the perpendicular component (r-component) has $\gamma = \pi/2$, while the parallel component (l-component) has $\gamma = \pi/2 - \theta$. It follows therefore, that the scattered intensity is given by

$$I = \frac{(1 + \cos^2\theta)}{2r^2} k^4 |\alpha|^2 I_0 \tag{2.99}$$

where Io is the intensity of the incident light. Consider an assembly containing non-spherical scatterers which are randomly orientated. If we concentrate on one particle we can give it a co-ordinate system (see figure 6). The scattered light lies in the ZOY plane. Denote unit vectors $\hat{n}_x$, $\hat{n}_y$, $\hat{n}_3$ along the x, y and z axes respectively, and if $\hat{l}_o$ and $\hat{r}_o$ denote the unit vectors in directions of Eo_ℓ and Eo_r then

$$(\hat{\ell}_o, \hat{r}_o) = (\hat{n}_y, \hat{n}_x)$$

For the scattered wave we have

$$(\hat{\ell}, \hat{r}) = (\hat{n}_y \cos\theta - \hat{n}_3 \sin\theta, \hat{n}_x)$$

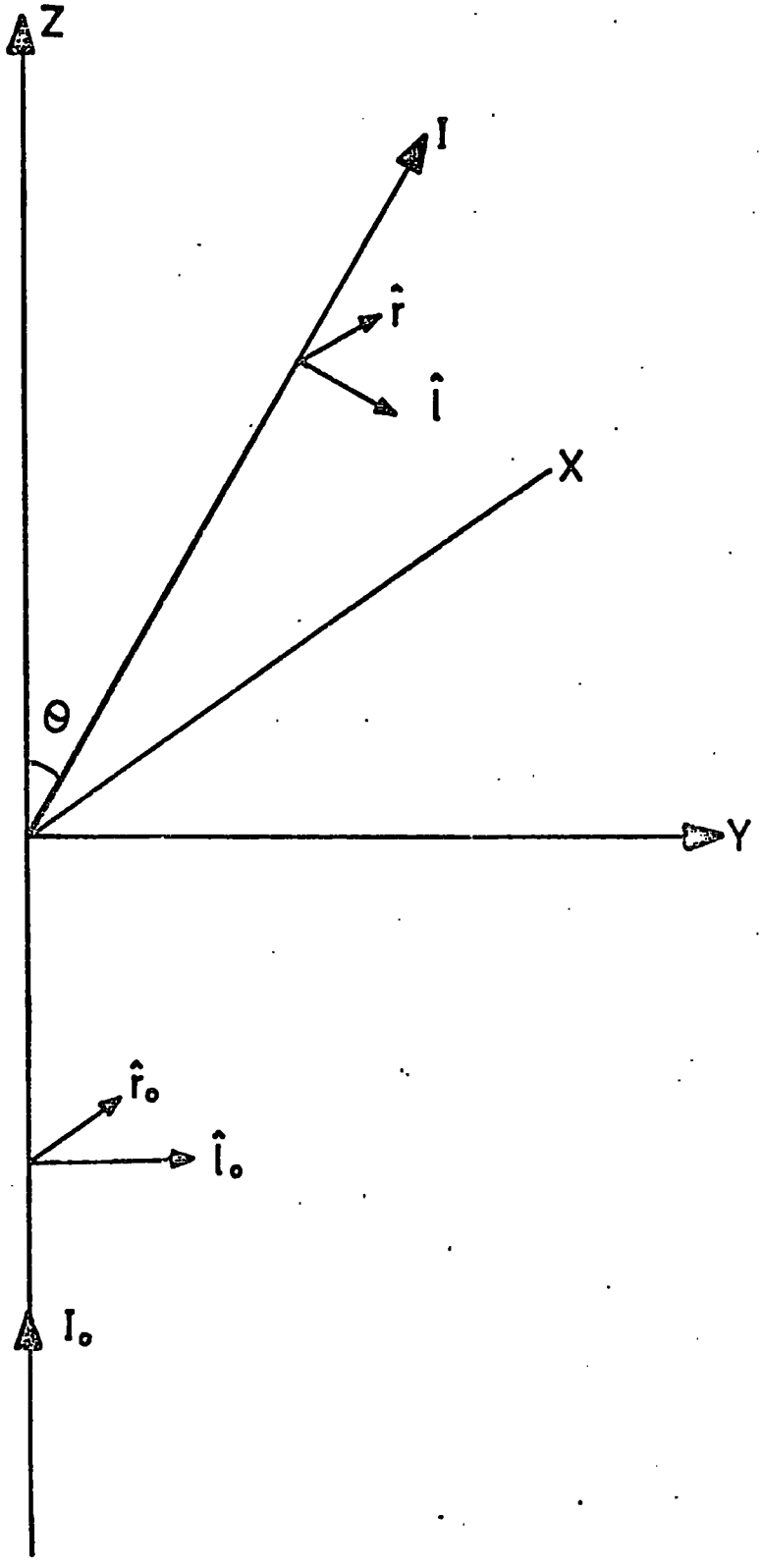

COMPONENTS OF SCATTERED LIGHT

FIG. 6.

The electric vector may be written as

$$\underline{E}_0 = E_{0\ell}\,\hat{n}_y + E_{0r}\,\hat{n}_x$$

Now the particle orientated in space is characterized by three unit vectors $\hat{n}_1$, $\hat{n}_2$ and $\hat{n}_3$. So that

$$\begin{aligned}\hat{n}_x &= C_{11}\hat{n}_1 + C_{12}\hat{n}_2 + C_{13}\hat{n}_3\\ \hat{n}_y &= C_{21}\hat{n}_1 + C_{22}\hat{n}_2 + C_{23}\hat{n}_3\\ \hat{n}_3 &= C_{31}\hat{n}_1 + C_{32}\hat{n}_2 + C_{33}\hat{n}_3\end{aligned} \qquad (2.100)$$

The components of the induced dipole moment $\underset{\sim}{P}$ are found to be

$$\begin{aligned}P_x &= E_{0r}P_{11} + E_{0r}P_{12}\\ P_y &= E_{0r}P_{21} + E_{0r}P_{22}\\ P_3 &= E_{0r}P_{31} + E_{0r}P_{32}\end{aligned} \qquad (2.101)$$

i.e.

$$P_{ik} = P_{ki} = \sum_{j=1}^{3} C_{ij}C_{kj}\alpha_j$$

Multiplying the component of $\underline{p}$ perpendicular to the radius vector, by $\frac{k^2 e^{-ikr}}{r}$ gives the electric field of the scattered wave. Then

$$\underline{E} = E_\ell(\hat{n}_y\cos\theta - \hat{n}_3\sin\theta) + E_r\,\hat{n}_x$$

giving

$$E_\ell = (P_y\cos\theta - P_3\sin\theta)\,k^2 e^{-ikr}/r \qquad (2.102)$$

which gives the scattering matrix for one particle as:

$$\begin{pmatrix} S_2 & S_3\\ S_4 & S_1\end{pmatrix} = ik^3\begin{pmatrix} P_{22}\cos\theta - P_{23}\sin\theta & P_{12}\cos\theta - P_{13}\sin\theta\\ P_{12} & P_{11}\end{pmatrix} \qquad (2.103)$$

We can now compute the combined effects for all particles. Taking averages of the products over all possible orientations, we have the relationship given on the opposing page.

The effect therefore of an assembly of randomly orientated non-spherical particles is to depolarise the light. A full treatment of this phenomenon can be found in Chandrasekhar (1960). The derivations in this chapter give the intensity and polarisation as a function of particle size and refractive index for both Rayleigh and Mie scattering.

$$\begin{bmatrix} I \\ Q \\ U \\ V \end{bmatrix} = \frac{k^4}{r^2} \begin{bmatrix} 4A + B - \frac{1}{2}(2A + 3B)\sin^2\theta & \frac{1}{2}(2A + 3B)\sin^2\theta & 0 & 0 \\ -\frac{1}{2}(2A + 3B)\sin^2\theta & (2A + 3B)(1-\frac{1}{2}\sin^2\theta) & 0 & 0 \\ 0 & 0 & (2A + 3B)\cos\theta & 0 \\ 0 & 0 & & 5B\cos\theta \end{bmatrix} \begin{bmatrix} I_o \\ Q_o \\ U_o \\ V_o \end{bmatrix}$$

where $$15A = \sum_{i=1}^{3} \left(\alpha_i \ \alpha_i^* \right)$$

$$15B = \sum_{i=1}^{3} \alpha_i \left[\sum_{i \neq j}^{3} \alpha_j^* \right]$$

By invoking a geometry and dust distribution for the nebula and using this formalism we will be in a position to create models to describe the observed data.

CHAPTER 3

THE NATURE OF INTERSTELLAR GRAINS

Many years ago the observation of dark obscurring clouds in the Galaxy suggested the existence of matter in the form of dust grains in the interstellar medium. The possible constituents of the dust has varied over the past few decades. Initially Schalen (1939) proposed iron, later Van de Hulst (1949) proposed ice and more recently Hoyle and Wickramasinghe (1962) suggested graphite. At the present time a variety of materials, e.g. silicate, SiC, graphite, seem to be able to explain observations.

There are a number of ways of explaining this dust. For interstellar grains we have the reddening laws and interstellar polarisation. In other objects, such as H II regions and planetary nebulae, we employ the study of absorption features, colour diagrams and polarisation measurements. We shall see however, that although we can observe these quantities, many of the deduced properties remain questionable.

3.1. Extinction by interstellar grains

Let us first examine how we obtain information from the extinction of starlight through interstellar grains. Using the quantities of the previous chapter, we can say that the observed intensity of starlight, seen at wavelength λ, can be written as

$$I(\lambda) = I_0(\lambda) \exp(-N\pi a^2 Q_{ext}(a,\lambda)) \tag{3.1}$$

where $I_0(\lambda)$ denotes the intrinsic intensity of the star and N is the grain density. Defining the optical depth as

$$\tau = N\pi a^2 Q_{ext}(a,\lambda). \tag{3.2}$$

we have the familiar equation of transfer.

$$I(\lambda) = I_0(\lambda) e^{-\tau} \tag{3.3}$$

or in terms of magnitudes

$$\Delta m(\lambda) = 1.086 \int_0^\infty \pi a^2 Q_{ext}(a,\lambda)\, n(a)\, da \tag{3.4}$$

where $\Delta m(\lambda)$ denotes the attenuated light at a wavelength λ. Note that we have integrated over a grain size distribution, n(a). The quantity $A(\lambda i)$ denotes interstellar extinction at wavelength λ_i, defined by

$$m(\lambda i) = M(\lambda i) - 5 + 5 \log_{10} D + A(\lambda i) \tag{3.5}$$

where $M(\lambda i)$ is the absolute magnitude at wavelength λi and D is the distance of the star from the earth. Further, if i and j denote magnitudes at wavelength λi and λj then

$$\text{observed } (i-j) = \text{Intrinsic } (i-j) + A(\lambda i) - A(\lambda j) \tag{3.6}$$

Defining the Colour excess as

$$Ei-j = \text{observed } (i-j) - \text{Intrinsic } (i-j)$$

it follows that

$$Ei-j = A(\lambda i) - A(\lambda j) \tag{3.7}$$

to that at any wavelength

$$\frac{E\alpha-v}{E_{B-V}} = \frac{A(\lambda\alpha) - A(\lambda v)}{A(\lambda B) - A(\lambda v)} \tag{3.8}$$

where subscripts i and j have been substituted with the B and V wavebands from the U-B-V system. By equation (3.3) we can compute various models for extinction.

The effect of the dust on the light is to preferentially scatter the blue thus leaving the redder light to be transmitted so that the observed light is redder than the intrinsic light.

In this way, the plot of $E\alpha-v$ against wavelength is called interstellar reddening curve. The method of obtaining this curve is to observe a suspected 'reddened' star and to compare the intensities, at different wavelengths, to that of an unreddened star of the same spectral type. If an unreddened star is unavailable, a model spectra is used (since the spectral type of the reddened star can be obtained from spectral analysis). Using this method, Stebbins (1934, 39) found, by using obviously reddened stars, that over the U-B-V range, the extinction curve posessed a law such that

$$\Delta m(\lambda) \propto 1/\lambda \qquad (3.9)$$

But recent extensive observations in the Ultra-Violet shows curves that depart from this law. Indeed, recently Schild (1977) showed that this law does not exist at all. Even so, different parts of the galaxy show differing reddening laws. The Orion region, for example, is markedly different from other parts of our galaxy. This is mainly because the Orion is a hot, nebulous region. Stecher (1969), Bless and Savage (1970) found that when measurements were extended into the Ultra-Violet, a suspicious hump occurs at $\lambda^{-1} = 4{\cdot}4\mu m^{-1}$. Other measurements were taken away from ζ and ϵ Persei (where their original data was obtained) to stars of the same spectral type separated greatly over the galaxy. All showed this characteristic hump.

Johnson (1968) extended observations into the infra-red using B stars, because they have structureless features in the infra-red. He found deviations from the $1/\lambda$ law. However, it must be pointed out that some of these stars may have circumstellar dust clouds associated with them. Deep infra-red observations were undertaken using M type stars. Here again care must be taken since these stars have great structure in their infra-red spectra. A search was undertaken to try and detect the 3.1μm absorption band of ice but this was not observed however. This does not mean that ice does not exist, it may be due to the intrinsic properties of the stars used since they possess peculiar spectra.

Hackwell (1970), observing towards the galactic centre, discovered the 10μm feature of silicate and Knacke et.al. (1969) observing 119 Tauri found a similar feature.

3.2. Interstellar polarisation

As mentioned in Chapter 1, interstellar polarisation was discovered by Hiltner and Hall (1949). The mechanism producing this is beyond doubt the Davis - Greenstein effect aligning grains in a magnetic field. Denoting the difference in magnitude between the maximum intensity by Δm_p, Schmidt (1958) found an

upper limit of $\frac{\Delta m_\rho}{\Delta m} \leq 0.065$

3.3. Diffuse galactic light

From diffuse galactic light it is possible to obtain some information of the properties of the interstellar scattering particles. Henyey and Greenstein (1941) using a slab model and Eddingtons' approximation, solved the radiative transfer equation, and showed that the particles had an albedo $(\gamma) > 0.05$ and a forward throwing phase function(g).

Observations by Witt (1968) led him to believe that $\gamma \sim 1$ and $g = \langle \cos\theta \rangle \simeq 0$ Van de Hulst and de Jong (1969) using previous measurements solved for γ and g using the slab model but this time included multiple scattering. They found that plotting γ against g gave two discrete loci for the wavelengths λ_B and λ_V i.e. there are many solutions. Measurements in the Ultra-Violet led Hayakawa et. al. (1969) to the result $\gamma \simeq 1$ and $g = 0.56$.

3.4. Reflection and Emission nebulae.

From Hubbles observations of reflection nebulae, an emperical law was established viz.

$$M_* + 4.9 \log_{10} a = 19.74 \qquad (3.9)$$

where M_* is the apparent magnitude of the star and a is the angular separation from the star to the farthest observable point. Wickramasinghe (1967), making a naive model of isotropic scattering, showed $\gamma \geq 0.5$ but, as he points out, not much weight should be given to this result.

O'Dell (1965), Elvius and Hall (1967) have made polarisation measurements, particularly of the Morope nebula in the Pleiades. Both colour and polarisation indicate the presence of dust.

Observations of H II regions by O'Dell and Hubbard (1965) and O'Dell et. al. (1965) established beyond doubt that dust was present within these objects. Using the $H\beta$ emission line, an estimate of the effective gas to dust ratio is possible

viz. $N_H / N_d C_{sca}$

where N_H is the ion density, N_d is the dust density and Csca is the effective scattering cross-section. However, the temperature determines the type of grain that can survive. In M42, it was shown that great variations exist in the gas to dust ratio. A more detailed discussion of dust within nebulae will be given later.

3.5. Circumstellar Dust.

Any anomalies occurring in the infra-red spectra of stars which cannot be accounted for in stellar spectra, is attributed to a dust shell surrounding the star. Stellar radiation, less than 1 μm, will be absorbed by dust and is re-radiated further into the infra-red. A determination of the radius and mass of a shell is possible from the following analysis.

We assume a spherical shell of thickness $\delta R \ll$ Rshell, where Rshell is the radius of the shell.

Then

$$Q_{abs} \cdot \frac{L_{TOTAL}}{4\pi R^2_{SHELL}} = 4\pi^2 \epsilon \sigma T^4_{SHELL} \qquad (3.10)$$

where Ltotal is the total luminosity, Tshell is the temperature of the shell, a is the radius of the grains and Qabs and ϵ are the mean absorption efficiencies of the grains in the red and infra-red respectively. Wickramasinghe (1972) finds $\epsilon / Q_{abs} \simeq 0.1$. Further, we can write

$$e^{-\tau} = L_{SHELL} / L_{TOTAL}$$

implying that

$$\tau = -\log_e (L_{SHELL} / L_{TOTAL}) \qquad (3.11)$$

Within the shell

$$M_{grains} = 4/3 \pi a^3 \rho N \cdot 4\pi R^2_{SHELL} \delta R \qquad (3.12)$$

where N is the number density of grains and ρ their mean density

From definition

$$\tau = N \pi a^2 Q_{abs} \cdot \delta R$$

Combining (3.11) and (3.12) we find

$$M_{grains} = \frac{16\pi a \rho R^2_{SHELL}}{Q_{abs}} \log_e \left(\frac{L_{TOTAL}}{L_{SHELL}} \right) \qquad (3.13)$$

Typical values calculated for various stars (e.g. VYCMa) gives Tshell $\sim$ 600 K , Rshell $\sim 2 \times 10^{15}$ cm and Mgrains $\sim 10^{29}$ gms.

There are however, difficulties arising. Since we do not know what type of grains are present, Qabs and ρ have to be roughly estimated. Also a grain size distribution is not employed.

Woolf and Ney (1969), Knacke et.al. (1969), Ney and Allen (1969) and Stein et.al. (1969) showed several cool oxygen rich stars of Mira type exhibiting infra-red excess in the 8-14μm spectral range. Stars exhibiting this include o Ceti, χ Cyg, and α Ori. These excesses have been attributed to the presence of silicates within a circumstellar dust cloud. Time dependent polarisation observations of cool giants also indicate circumstellar dust.

Circumstellar dust shells are not necessarily restricted to old stars. Infra-red excesses have been reported T - Tauri stars, F and G supergiants and Be stars. Reddish (1967) concludes that very young stars have circumstellar dust clouds with diameters of the order $\lesssim$ 1 pc and masses $\sim 30 M_\odot$ but this phenomenon, he reports, is short lived.

3.6. Grain formation

Linblad (1935) suggested that interstellar dust grains may condense within clouds of interstellar gas, forming ice. This idea was extended by Van de Hulst (1949) showing the following sequence of events. First diatomic molecules are formed, such as CH, CH^+, CN and CN^+, These grow into a condensation nuclei (about 10 - 20 atoms). From these nuclei, grains are mormed with radii $\sim 10^{-5}$ cm. Bates and Spitzer (1951) showed, for a gas temperature $\sim$100 K and with typical values of the abundance of C, H and C^+, showed that the molecules formed (CH and CH^+) had densities of the order of $10^{-10} - 10^{-11}$ cm^{-3}. These values are of the order a hundred too low from the observed densities of these molecules. It was then suggested that grains up to radii $\sim 10^{-7}$ cm are formed in circumstellar envelopes and are then ejected into interstellar clouds. Calculations show that after a time of about 10^9 years, the radii will grow up to 3×10^{-5} cm. However,

there may exist partial destruction by cloud - cloud collisions and encounters with hot stars.

Platt (1956) and Platt and Donn (1956) suggest that interstellar condensation processes result in the formation of large unsaturated molecules of the order 10Å across consisting mainly of water. However, the theory behind these particles is not quite understood.

Hoyle and Wickramasinghe (1962) recommended graphite as a possible candidate for interstellar material. They suggest that it can be formed on the surface of Carbon stars (N type) which have temperatures $\sim$ 1500 - 3000 K.

These stars also have temperature fluctuations with a period of approximately one year. The density at the surface is high and below a critical temperature ($\sim$2400 K), thermodynamic equilibrium is quickly established and, mainly due to three-body collisions, graphite nuclei can be formed. They condense to radii of about 10^{-6} - 10^{-5} cm, and since the radiation pressure on the surface of these stars exceeds gravity by a factor 10^{3} - 10^{4}, the grains are ejected from the surface of the star. Using a value of 10^{5} N type stars, over a period of 10^{9} years, a substantial amount of graphite can be ejected into the interstellar medium (10^{9} years is the 'turn-over' time of star formation). Bahng (1966) has found that these N type stars have Black-Body spectra in the region 1-10μm, showing that grains absorb and re-emit in optically thick layers.

In cool oxygen rich stars (carbon/oxygen<1), with temperatures of the order 2000 - 3000 K, certain species may condense, as shown by Hoyle and Wickramasinghe (1968). In particular Fe, MgO and SiO_2. These then go on to form grains of radii of the order of 10^{-5} - 10^{-6} cm, which are ejected by radiation pressure. These species may exist in other forms e.g. $MgSiO_3$ and $MgFeSiO_4$. However, there is strong evidence for SiO_2 and/or silicate in the atmospheres of these cool oxygen rich stars as stated by Low and Krishna-Swamy (1970).

Supernovae can also be a possible area of grain formation as argued by Hoyle and Wickramasinghe (1970a). It is thought that 10% of the material expelled by

supernovae can be formed into grains. This material consists mainly of carbon, iron and silicon. Calculations show a grain growth, after one year, giving radii of the order of 10^{-5} cm, and high speed ejection into the interstellar medium. Using a value of one supernova every thirty years, a value of 7×10^{-27} gms/cm is obtained for density in the interstellar medium after 10^{9} years. This is close to what is required from infra-red models.

Other possibilities include the formation of an ice mantle on a graphite core after the graphite has been ejected into a cool cloud. Hartman (1970) suggests iron condensation in T - Tauri stars followed by silicate accretion. This gives radii of the order of 3×10^{-5} cm.

3.7. Theoretical extinction curves

A theoretical fit to the extinction curve was first attempted by Van de Hulst (1949) using two grain size distributions viz. $n(a) \propto \exp(-a/a_0)$ with $a_0 = 0.075 \mu m$ and the other, a single particle size of $a_0 = 0.3 \mu m$. The latter fitted better of the two. It must be remembered that this fit was achieved over the visible range. When the ultra-violet measurements were obtained the Van de Hulst model deviated strongly in this region. The absence also of the $3.1 \mu m$ ice band in highly reddened stars soon placed the ice model out of favour.

A graphite model by Wickramasinghe and Guillaume (1965), using a size distribution of

$$n(a) \propto \exp(-(a-\bar{r})^2/2\sigma^2) \qquad (3.14)$$

fitted the reddening curve, but deviated sharply for $\lambda < 2000$Å. It was also found that the model depended weakly on the size distribution. Using graphite cores with dielectric mantles, Wickramasinghe (1963) attempted a model using a distribution given by

$$n(a) = A \exp(-5(10a)^3) + B \exp(-5(2a)^3)$$

The result was better than previous models but not extremely satisfactory. This led astronomers to think on the lines of a mixture of different materials. Wickramasinghe and Nandy (1970), following this approach, used a mixture of

graphite, silicate, and iron particles, and a size distribution of

$$n(a) = A a^{3/2} \exp(-\tfrac{1}{2}(a/am)^3) \qquad (3.15)$$

choosing a different am for each particle type used. They defined the quantities

$$Xgr = \frac{\text{Extinction of graphite component of mixture at } 4500\text{Å}}{\text{Extinction of silicate component of mixture at } 4500\text{Å}}$$

and

$$Xiron = \frac{\text{Extinction of iron component of mixture at } 4500\text{Å}}{\text{Extinction of silicate component of mixture at } 4500\text{Å}}$$

They used radii of the following range.

graphite: 0.04 - 0.065 μm

iron: 0.015 - 0.03 μm

silicate: 0.12 - 0.16 μm

It was found that good fits produced a relationship between Xiron and Xgr such that

$$A.Xiron = B + Xgr$$

Using Stechers' (1969) observations of ζ-ϵ Persei, the extinction curve was fitted using Xgr: Xiron: 1 = 1:5/6: 1

and for the Orion extinction curve, with

am (graphite) = 0.05 μm

am (iron) = 0.02 μm

am (silicate) = 0.17 μm

and Xiron = 1/6 Xgr + 2/9 (Xgr = 0.3 and 0.6), good fits were obtained.

Other mixtures have produced fits also, Gilra (1971) using a mixture of silicate, silicon carbide (SiC) and graphite, fitted the extinction curve for ζ Oph, and σ Sco. Other materials attempted include quartz and diamond grains, and quartz grains irradiated by cosmic rays and X-rays.

3.8. Theoretical models of interstellar polarisation

Cylinders are used in most interstellar polarisation models. If the incident radiation has $\underline{E}$ - vector parallel to the cylinder axis, the amount of extinction in magnitudes is given by

$$\Delta m_1 = 1.086\, C_{11}(m, a, \lambda) \qquad (3.16)$$

Similarly, with the $\underline{E}$ - vector perpendicular to the long axis

$$\Delta m_{\perp} = 1.086\, C_{\perp}(m, a, \lambda) \tag{3.17}$$

where the C's denote the extinction cross-sections, calculated in a similar fashion to the Mie theory. Using silicate needles and a size distribution

$$n(a) \propto \exp\left(-(a - \bar{r}_{sil})^2 / 2\sigma^2\right)$$

with $\bar{r}_{sil}$, mean cylinder radius set to the range 0.08 - 0.1μm and σ = 0.02μm, agreement is achieved between theoretical and observed values of polarisation with wavelength. Employing $\bar{r}_{sil} = 0.1\mu m$, the ratio of polarisation to extinction at $\lambda = 5000\text{Å}$ is

$$\frac{\Delta m_p}{\Delta m} = \frac{2(C_{\parallel} - C_{\perp})}{(C_{\parallel} + C_{\perp})} \simeq 0.8 \tag{3.18}$$

Since the maximum value for Δm_p is 0.065, this implies a 10% effective line up of particles in the magnetic field.

Small graphite flakes used by Greenberg (1966) with radii approximately 0.05μm explain extinction curves but not polarisation with wavelength. Later, Greenberg (1968) showed that dielectric cylinders such as ice produce a better fit for the polarisation than metallic grains. However, all the calculations depend strongly on the shape of the particle, which is unknown.

3.9. Rotation of grains

Grains situated in a gaseous medium will be effected by atoms and ions colliding with the grains. These impinging particles will impart momentum to the grain. We can therefore write

$$\tfrac{1}{2} I \omega^2 = \tfrac{3}{2} kT \tag{3.19}$$

where I is the moment of inertia and T is the kinetic temperature of the ambient gas.

Assuming spherical grains

$$I = \tfrac{2}{5} M_g a^2$$

where

$$M_g = \tfrac{4}{3} \pi a^3 \rho_g$$

writing $\omega = 2\pi\nu$ equation (3.19) reduces to

$$\nu = 3\times10^{8}\left(\frac{10^{-6}}{a}\right)^{2.5}\left(\frac{T}{100}\right)^{1/2}\ \text{Hz}. \tag{3.20}$$

for T ~100 K and a $\sim 10^{-6}$ cm we get $\nu \sim 300$ MHZ

while for a $\sim 10^{-5}$ cm, $\nu \sim 1$ MHz

The timescale required for the equipartition of angular velocity, ω is

$$\tau_{eq} \simeq \frac{(I\omega)^2}{\langle Mva\rangle^2 \langle v\rangle (4\pi a^2)} \tag{3.21}$$

where n is the density of the ambient medium.

For a typical interstellar cloud $\tau_{eq} \leq 10^{5}$ years, a very short time. The consequence is that most grains are spinning.. It was proposed by Hoyle and Wickramasinghe (1970b) that these spinning grains will emit radio waves, and what was previously thought to be radio waves emitted by synchrotron radiation in many objects, are in fact due to spinning grains.

3.10. Accretion and destruction of dust in ionized nebulae

Osterbrock (1974) has set out the following conditions for grains in a hot medium.

Within ionized nebula, typical temperatures are of the order of 10,000 K so that ions and photons are of high energy. Collisions with high energy ions and photons tend to detach atoms and molecules from the surface i.e. theytend to destroy the particle. The photons will cause electrons to be ejected from the surface so causing an increase in positive charge on the surface. The rate of increase of positive charge due to photoejection is given by

$$(dz/dt)_{pe} = \pi a^2 \int_0^{\infty} \frac{4\pi J_\nu}{h\nu}\,\phi_\nu\, d\nu \tag{3.22}$$

where J_ν is the mean intensity of the radiation and ϕ_ν is the photodetachment probability ($0 \leq \phi_\nu \leq 1$).

If the particle is neutral or negative, $\nu_K = \nu_c$ = threshold frequency of the material. If the material is positive however, lowest energy electrons cannot escape, so we write

$$\nu_R = \begin{cases} \nu_c + 2e^2/a\hbar & z > 0 \\ \nu_c & z \le 0 \end{cases} \qquad (3.23)$$

($-\frac{ze^2}{a}$ is the potential energy of an electron at a surface of charge z).

Rate of increase of charge due to capture of electrons is

$$(dz/dt)_{ce} = -\pi a^2 N_e \sqrt{\frac{8kT}{\pi m_e}}\, \zeta_e \gamma_e \qquad (3.24)$$

where ζ_e is the electron sticking probability ($0 \le \zeta_e \le 1$) and Ye is the attraction or repulsion of the charge on the particle, given by

$$\gamma_e = \begin{cases} 1 + ze^2/akT & z > 0 \\ e^{ze^2/akT} & z \le 0 \end{cases} \qquad (3.25)$$

Rate of increase of charge due to protons is

$$(dz/dt)_{cp} = \pi a^2 N_p \sqrt{\frac{8kT}{\pi m_H}}\, \zeta_p \gamma_p \qquad (3.26)$$

with

$$\gamma_p = \begin{cases} e^{-ze^2/akT} & z > 0 \\ 1 - ze^2/akT & z \le 0 \end{cases}$$

For equilibrium

$$dz/dt = (dz/dt)_{pe} + (dz/dt)_{ce} + (dz/dt)_{cp} = 0 \qquad (3.27)$$

Showing this equation, the following results are obtained for the inner part of the nebula, photoejection dominates causing the particles' charge to be positive. The outer regions however, receive a small ultra-violet flux and photoejection is negligible, causing the particles to be negatively charged. As an example, consider a 'dirty' ice grain of radius 3×10^{-5} cm. $\zeta_e \sim \zeta_p \sim 1$, $\phi_\nu \simeq 0.2$ (for $h\nu > h\nu_c \sim 12eV$), and an O5 star with $L_* = 5 \times 10^6$ $L_\odot$, T ~ 50,000 K, in a nebula with $N_e \sim N_p \sim 16/cm^3$ It is found that z ~380 at r = 3.5 pc (r is the distance from the star), and z = 0 at r = 8.5 pc, while $z \to -360$ as $J_\nu \to 0$.

We can now estimate the rate of sputtering i.e. the knocking out of atoms by energetic positive ions. In the inner part of the nebula, where z~400, the positive charge raises the threshold which decreases the sputtering. In the outer

part however, the particles are negative and so the sputtering rate is increased. The lifetime of a particle against sputtering is about 10^{15} a/Np years where z = 0, and 3×10^{12} a/Np years in the outer regions (z~-400). Taking $a \sim 3 \times 10^{-5}$ cm and Np = 16 cm^{-3}, it is found that the lifetime of the particles against sputtering is long compared with the lifetime of the H II region.

Photons can destroy grains by heating the grains until they reach vaporisation temperatures. The temperature of the grain T_D, is given by the equilibrium reached between the energy absorbed (mainly in the U - V) and the energy emitted (mainly in the 1-R) i.e.

$$\int_0^\infty 4\pi J_\nu (1-A_\lambda) C_{ext_\lambda} d\nu = \int_0^\infty 4\pi B_\nu (T_D)(1-A_\lambda) C_{ext_\lambda} d\nu \qquad (3.28)$$

where A_λ is the albedo and $B_\nu (T_D)$ is the Planck function. We can now make the following approximations: L.H.S.of equation (3.28), $\lambda \ll a$ giving $(1-A_\lambda)\ C_{ext_\lambda} = \pi a^2$ R.H.S. of equation (3.27), $\lambda \gg a$ giving $(1-A_\lambda)\ C_{ext_\lambda} = \pi a^2 \epsilon \cdot \frac{2\pi a}{\lambda}$. Putting $\epsilon = 0.1$ for dielectrics. The expression

$$T_D \propto \left(L/4\pi r^2 a \right)^{1/5} \qquad (3.29)$$

is obtained, so that for $a \sim 3 \times 10^{-5}$ cm, $T_D \sim 100$ K at r = 3pc. This shows us that H_2O will evaporate within the inner regions.

Overall, sputtering is not important, possibly only in the outer regions. In the inner regions, vaporisation dominates. This implies that in these types of emission nebulae, graphite, silicate and iron are more likely to survive than ice.

3.11. Dynamics of grains in nebulae

The radiation force exerted on a grain is

$$F_{rad} = \pi a^2 \int_0^\infty \frac{\pi F_\nu}{c} Q_{pr}\, d\nu \qquad (3.30)$$

Usually, for most hot stars, the dominant radiation is such that $\lambda \ll a$, giving $Q_{pr} \sim 1$. (This is only true for ice). The grain, being pushed through the nebula, receives a drag force from gas interactions. This force can be written as

$$F_{coll} = 4/3\ N_p \pi a^2 (8kT m_H/\pi)^{1/2} w \qquad (3.31)$$

for a neutral grain. Here w is the velocity relative to the gas. When forces

balance, the terminal velocity is given by

$$W_t = \frac{3L}{16\pi r^2 C N_P} \left(\frac{\pi}{8kTM_H} \right)^{1/2} \qquad (3.32)$$

Note that there is no dependence on a.

For typical values, as before, when r = 3.3pc, w_t = 10 km/s.

If the grain posesses a charge the drag is increased and we include the additional term

$$F_{coul} \simeq \frac{2N_P Z^2/M_H}{T^{3/2}} \qquad (3.33)$$

This Coulomb force will dominate if $|z| \gtrsim 50$. Usually z is much higher than this and W becomes smaller, meaning that the grain becomes 'frozen' into the gas. If this occurs, the grain can experience large accelerations. It is believed for instance, that the central 'hole' in NGC 2244 is caused by this effect.

3.12. Grain size distributions

Deriving theoretical expressions for grain size distributions is very difficult. Particularly if we try to include all probable destruction and accretion effects. We can estimate the distribution in a size equilibrium situation. We follow the analysis of Wickramasinghe(1972).

Let P(r), the destruction probability per unit time for a grain of radius r, be expressed as

$$P(r) = Ar^{\eta}$$

Let n(r, t) dr be the number of grains with radii between r and r + dr per unit volume at time t.

We define

$$N(r,t) = \int_0^r n(x,t)\,dx \qquad (3.34)$$

to be the number of grains with grains with radii less than r at time t. So that

$$n(r,t) = \frac{\partial N}{\partial r}$$

We now have

$$N(r+dr, t+dt) = N(r,t) - dt \int_0^r Ar^{\eta} n(r,t)\,dr \qquad (3.35)$$

Expanding

$$\frac{\partial N}{\partial r}\,dr + \frac{\partial N}{\partial t}\,dt = -dt\int_0^r Ar^{\eta}\,n(r)\,dr \tag{3.36}$$

When a steady - state situation is reached

$$\frac{\partial N}{\partial r} = 0$$

and so

$$\frac{\partial N}{\partial r}\cdot\frac{dr}{dt} = -\int_0^r Ar^{\eta}\,n(r)\,dr \tag{3.37}$$

Writing $dr/dt = \mu =$ constant and using (3.34)

$$\mu\,n(r,t) = -\int_0^r Ar^{\eta}\,n(r)\,dr \tag{3.38}$$

or

$$\mu\frac{\partial n}{\partial r} = -Ar^{\eta}\,n(r) \tag{3.39}$$

which becomes

$$\frac{\partial}{\partial r}\log_e n = -\frac{A}{\mu}r^{\eta} \tag{3.40}$$

Integrating

$$\log_e n = -\frac{A\,r^{\eta+1}}{\mu(\eta+1)} + \text{constant} \tag{3.41}$$

or

$$n(r) = \text{const.}\,\exp\left(-\frac{A}{\mu(\eta+1)}r^{\eta+1}\right) \tag{3.42}$$

Putting $\eta = 3$ i.e. $P(r) \propto r^3$ (i.e. destruction is proportional to the volume), then

$$n(r) = n(0)\,e^{-(r/r_0)^4} \tag{3.43}$$

and putting $P(r)$ = constant gives

$$n(0) = n(0)\,e^{-(r/r_0)} \tag{3.44}$$

Other distributions used include Gaussians. These are probably more realistic since the distributions given by

$$n(r) = n(0)\,e^{-(r/r_0)^{\alpha}} \tag{3.45}$$

gives many particles in the Rayleigh domain. Wickramasinghe (1971) also uses the distribution of Deirmendjian (1969) which is based on observations of terrestrial

clouds. It is given by

$$n(a) = A a^{\alpha} \exp(-B a^{\beta})$$

To find the maximum grain radius a_m, we find the solution of

$$\frac{d n(a)}{da} = 0 \tag{3.46}$$

This gives

$$a_m = (\alpha / B\beta)^{1/2} \tag{3.47}$$

The distribution is weakly dependent on the choice of α and β. Wickramasinghe chooses $\alpha = \frac{3}{2}$ and $\beta = 3$ giving

$$n(a) = A a^{3/2} \exp(-1/2 (a/a_m)^3) \tag{3.48}$$

Clearly, there is no real certainty in any of the distributions.

3.13. Conclusions

It is clear from the evidence given that there are a lot of questions left unanswered. The distribution of sizes, for example, will be greatly effected by processes within nebulae. As we have seen, it is probably a function of distance as well. Establishing a mixture for interstellar grains does not mean that the same mixture, or type of grain, is the same as in nebulae and galaxies, as we will see in the next chapter.

Polarisation then, is another important lever which can be used, along with other measurements, to determine the types and sizes of grains that can exist.

CHAPTER 4

THE GALAXY M82

The galaxy M82 is one of the most studied and most enigmatic of galaxies known. It is a member of the local group and is classified as an irregular type II. Plates in the Hα band showed filamentary structure radiating from the nucleus or core. It was suggested, in the view of this discovery, that the core of M82 was the scene of a violent explosion in the past. Theories arose to account for this explosion, one suggesting that an influx of dust could initiate the onset of supernovae explosions which in turn sets off further explosions.

While theorists were trying to find possible explanations for the explosion, observers were busy studying the galaxy. It was soon found that the findings did not altogether fit with the idea of an explosion in the core.

4.1. The Scientific development of M82

It was found that the filaments radiate strongly (relative to the neighbourhood) in Hα. Lynds and Sandage (1963) also found emission lines in Hβ and Hδ and the forbidden lines [N II], [S II], [O II], and [O III]. It was found that the filaments were not symmetric about the core. This was attributed to various mechanisms inhibiting istropic expansion. It was the looping appearance of the filaments which suggested that they followed the lines of a magnetic field. Combine this with an explosion (which can supply a large number of high energy charged particles) and we have grounds to suspect that the filaments will emit synchrotron radiation.

The synchrotron model was verified by various authors who had measured the spectral index. The measured spectral index was found to be $\alpha = -0.17$ (Lynds 1961) which is similar to the crab nebula ($\alpha = -0.23$).

The general trend in colour of the halo is that it tends to get bluer as we get further from the disk (one would expect it to get redder) and this is represented, to a certain extent, by the synchrotron theory.

If polarisation measurements are taken of the filaments, the $\underline{E}$ - vector should be perpendicular to the filaments if the model is correct.

Sandage and Miller (1964), using photographic techniques, found that $P \sim 100\%$ with the $\underline{E}$ - vector perpendicular to the filaments. This agrees with the synchrotron model. However, it was Elvius (1963) who made photoelectric polarisation measurements that found the polarisation to be less than that previously stated ($P \sim 30\%$). New measurements of the spectral index gave a U-V flux which was far too low to account for the Hα emission in the filaments. So the synchrotron model failed for the supposed Hα emission and the low polarisation measured.

Solinger (1969 a, b, c) had proposed a shock front mechanism, caused by the explosion, heating the halo and creating filaments. These then would be sufficient free electrons to create the Hα emission, and the polarisation would be caused by free electrons i.e. Thompson scattering. If the Hα line was intrinsic to the filaments, one would expect the polarisation to be less than observed in the continuum, since the extra radiation would decrease the polarisation.

Polarisation measurements taken within the filaments showed values of about 27% in the Hα. However, observations taken in the continuum showed no increase in percentage polarisations as one would expect if the Hα line is intrinsic to the filaments.

Solingers' blast wave model declined in favour. There could be only one possible explanation to account for the polarimetric observations of the filaments, and that was that the filaments scatter light emitted from the galaxy.

4.2. The possibility of dust scattering

The two possible processes of scattering are electron i.e. Thompson scattering and dust scattering. A simple analysis by Schmidt and Angel (1976) showed that electron scattering was not feasible. Consider the following naive model. We have an infinite plane of brightness B_D, representing the galactic disk. If we assume non-absorbing scatterers, the amount of light scattered is given by

$$4\pi B_S = 2\pi B_D (1 - e^{-\tau}) \qquad (4.1)$$

where τ is the optical depth of the scatterers. Equation (4.1) follows since light taken out by transmission is reduced by a factor $\exp(-\tau)$ i.e.

$$I_T = I_0 e^{-\tau} \tag{4.2}$$

and since there is no absorbtion then the light must be scattered i.e.

$$I_S = I_0 (1 - e^{-\tau}) \tag{4.3}$$

Assuming $\tau << 1$ it follows that

$$B_S = \frac{B_D \tau}{2} \tag{4.4}$$

A better approximation can be made if we say that the galactic disk may subtend only half the solid angle of an infinite plane, in which case

$$B_S = \frac{B_D \tau}{4} \tag{4.5}$$

By taking a value for the surface brightness of a particular filament of V = 22.83 arc sec^{-2} and a value of V = 19.1 arc sec^{-2} for the disk which is seen edge on, one obtains a value of the optical depth of $\tau \sim 0.1$. If the scattering process is due to electron scattering, the optical depth is defined by

$$\tau_{es} = n_e \sigma_e l \tag{4.6}$$

where σ_e is the Thompson cross-section and l is the line of sight depth, taken to be equal to the diameter of the disk, which assigning a value of 3.3 Mpc for the distance of M82 becomes 5.8 Kpc. Substituting into (4.6) we arrive at a value for the electron density of $n_e = 8$ for $\tau_{es} = 0.1$. Bearing in mind that there is no intrinsic Hα emission from the filaments, an estimate can be obtained for the maximum electron density allowed without line emission. This is found to give a value of $n_e = 0.3$ which would give $\tau_{es} = 0.004$. If the cause is due to electron scattering then we would expect intrinsic Hα emission.

It was Elvius (1972) who put forward the idea of scattering by dust in the halo of M82. The relatively high level of polarisation observed tends to suggest that the scatters are Rayleigh type particles. This idea is also boosted by the relatively flat spectra of polarisation against wavelength (Sandage and

Visvanathan 1972).

The problem of the increase of blue light with distance from the disk was still unanswered. Mathis (1973) tried to solve this problem by concocting a mixture of grains of various refractive indices, giving not only the correct polarisation but also creating a non-reddening effect. He used the Oort - Van de Hulst distribution viz.

$$n(a) = n(0)\exp(-0.693(a/\bar{a})^{2.6}) \qquad (4.7)$$

and refractive indices (n - ik) of n = 1.33 and 2.7 with k = 0.05 in both cases. The values correspond to ice and silicon carbide respectively. The mixture was arranged such that

$$n(a) = \sum_i w_i n_i(a) \qquad (4.8)$$

where w_i represents a weighting function. His method for determining the parameters of the mixture was to use a simple minded model in which the final percentage polarisation was of the order of 26%, as observed in the filaments. This was achieved by taking a point source of light and integrating along the line of sight (the 'integration' consisted of adding up two points along the halo, situated such that the scattering angles were 60° and 120°). The 'greyness' of polarisation was achieved by using the following mixture.

a	w	n - ik
0.05	1.0	1.33 - 0.05
0.05	0.46	2.7 - 0.05
0.10	0.336	2.7 - 0.05

It was pointed out however that this mixture was in no way unique in satisfying the relevant conditions of the model. A solution is reached owing to the distributions used. It supplies enough Rayleigh particles to account for the polarisation and also just enough Mie particles to produce a non-reddening mixture. The model seems highly contrived and also a difference in distribution would have caused a distribution of sizes as a function of distance from the disk.. Note also that the model excluded light from a disk.

Another feature unaccounted for was the velocity field. This shows red-shifts in the North and blue-shifts in the South. Estimates for tilt of the galaxy (defined as the angle the minor axis makes with the sky) give a value of about 8^{o}. In all models considered so far, the filaments must lie along the rotation axis of the galaxy (the minor axis). This is because we only see the radial component of the velocity vector when observing the doppler shift. If the synchrotron model, however, the doppler measurements cannot be fitted at all if we are to believe that the filaments are expanding radially. This can readily be seen if we imagine the scattering particles to behave like mirrors. Since the mirrors are moving away from the light source (to fit with the explosion hypothesis) the light received by the mirror will be red-shifted. The scattered light will then be bluened or reddened depending on whether the mirrors are approaching or receeding from us. The red-shift is easily accounted for since the two doppler effects i.e. mirror moving away from the source and from us, adds up to a total red-shift. The blue-shift is impossible however, if the motion of the 'mirrors' are radial to the nucleus. This can be explained in the following way. Define θ to be the angle between the minor axis and the plane of the sky (see figure 7). If the velocity of a mirror at a general point is V, the scattered light is reddened. In order to obtain a blue-shift, the velocity of approach V_0 will have to be such that $V_0 > V$, but for this particular case

$$V_0 = V\sin\phi \tag{4.9}$$

implying that $\sin\phi > 1$, which is impossible for a real ϕ.

In order for the inequality to hold we must replace expression (4.9) with $V_0 = V\sin\phi + v$ (4.10)

so that

$$V\sin\phi + v > V$$

or

$$v > V(1-\sin\phi) \tag{4.11}$$

i.e. we must introduce a non-radial component of velocity into the argument.

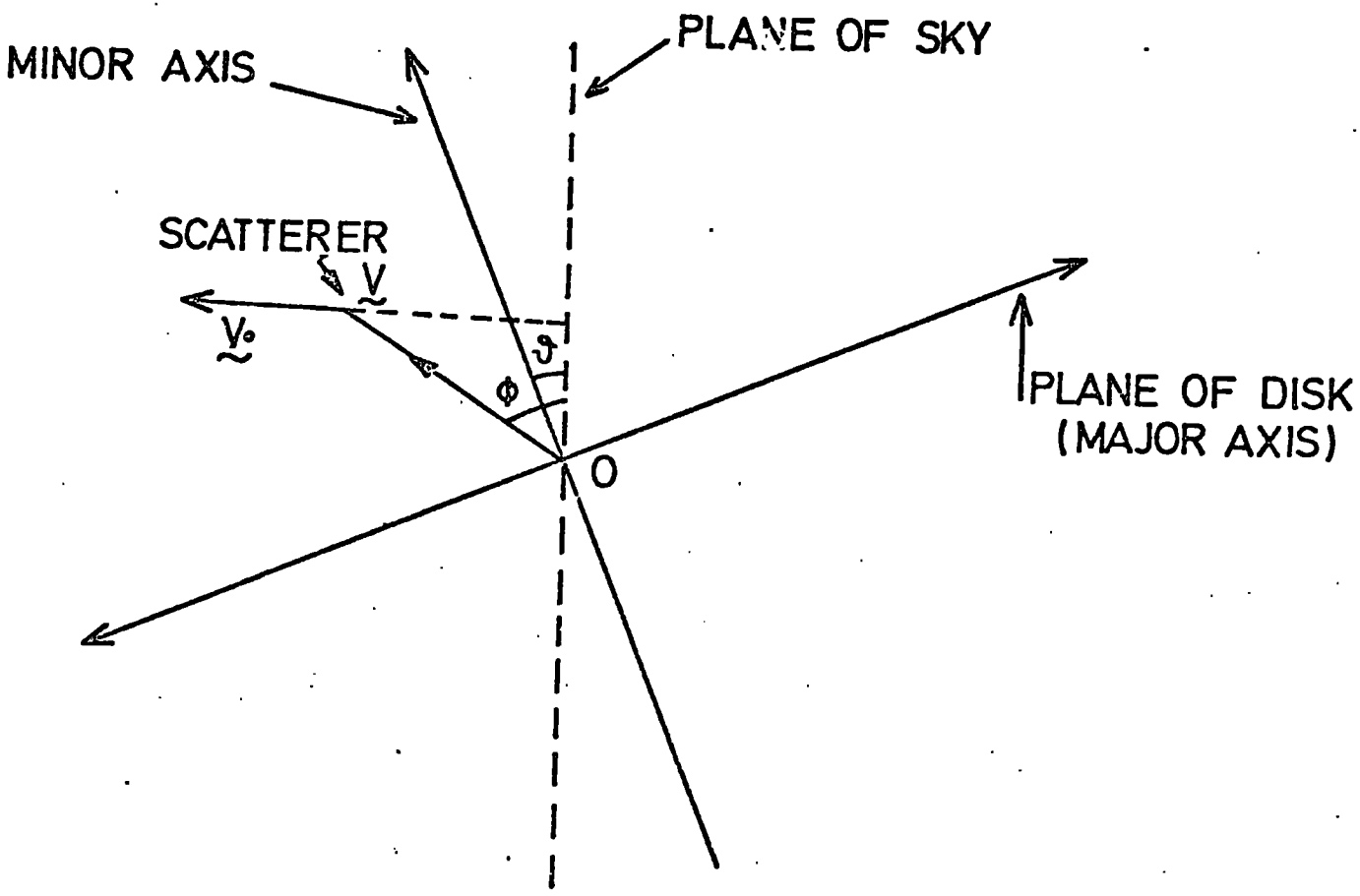
MINOR AXIS
PLANE OF SKY
SCATTERER
V
V₀
ϑ
φ
O
PLANE OF DISK
(MAJOR AXIS)

FIG. 7

This was proposed by Sanders and Balamore (1971).

Recently, Axon and Taylor (1978), using Hα spectral analysis, found two velocity components within the filaments close to the galaxy. They intepret this as arising from an expanding hollow cone of ionized gas created by an explosion in the centre of the galaxy. However, a mechanism to produce this cone has yet to be established.

It was the idea of Elvius (1972) that accounted for the difference in doppler shifts observed. The proposal was that M82 had drifted into an inter-galactic cloud of dust and gas. In this case, the doppler shift controversy can be quickly resolved since the mirrors coming towards M82 will be blue-shifted while the receeding mirrors will be red-shifted. This model was later built upon by Solinger (1977).

4.3. The model of Solinger

Solinger considered the possibility that M82 is an interloper. We take the analysis of Solinger where he discusses each point of the galaxy in turn.

a) The nucleus or core of M82 has been studied extensively in many wavebands. It is found that the maxima at each frequency range considered do not coincide (Bingham 1976) suggesting that the nucleus is complex, extended and over-luminous.

Infra-red photographs taken near 1 μm display several localised intensity maxima which was interpreted by Van den Bergh (1971) as being due to very luminous associations of very early type stars. They appear in the infra-red because the optical depth at this wavelength is less than in the optical. Solinger states that no one source dominates in the wavebands considered, whereas an explosion in the nucleus would imply a single source.

Solinger argues that the nucleus can be explained by star formation, stellar collisions, supernovae and stellar wind interactions.

b) The main body of the galaxy has a spectrum which is easily attributed to stellar spectra. The setting is of a rotating spiral disk, heavily embedded in

obscuring dust which is not lying with the spiral lanes.

c) Outside the main disk is the halo. One of the great problems of the halo are the filaments. As pointed out previously, it is a natural reaction to assume that these filaments are associated with a great catostrophic explosion that occurred within the nucleus of the galaxy. Solinger's explanation of the filaments is based on inhomogeneities within the medium i.e. clouds of dust. Predictions of the isophotes using randomly placed clouds were obtained by Solinger who found reasonable fits to the isophotes. The filaments, he says, are caused by an effect which he calls 'star-spiders'. He draws the analogy between these star-spiders and what is observed in a partially clouded sky when shafts of light pass through while the inner clouds cast shadows. Likewise in M82, the dust clouds within the galaxy allow shafts of light from the disk (emission regions and bright stars) to pick out occasional apparent linear 'filaments' of randomly reflecting matter.

The other puzzling property of the halo is the colour which tends to get bluer as we get further from the disk, whereas one would expect to see a reddening effect. Solinger points out that previously people had been considering a point-source situation of the galaxy. Consider now the effect of introducing a disk. As with a normal spiral the nuclear stars are red while those in the spiral arms are blue. A point observed just above the nucleus will receive more red light than blue light whereas if we observe far enough away from the galactic disk the light received has as much chance of coming from the disk as from the nucleus. In fact there will be even more light from the edges than from the nucleus since, as we shall see later, the nucleus is not a particularly dominant source.

4.4. Conclusion of Solingers' model

Solinger sets out the following picture for M82. The core is a combination of very luminous stars, obscuring dust, and perhaps supernovae remnants. The filamentary structure is due to inhomogeneities within the halo plus the star-spider effect. The doppler measurements, which show red-shifts in the North and

blue-shifts in the South can generally be explained by the galaxy drifting through an intergalactic cloud or vice versa. Note that in either case the relative motion is for the galaxy to be moving southwards with respect to the cloud. The apparent increase in blue of the halo light is attributed to the mixture of light from the disk (blue) and the nucleus (red), the amounts depending on the position of the point observed.

Solinger suggests that M82 entered as a small spiral galaxy into the M81 group some 10^8 years ago, and encountered a gas cloud. The internal gas of M82 was shocked around the periphery of the disk producing usual H II regions. Accretion in the core caused a brief period of extra luminous star formation. These stars produced considerable dust which was expelled into the main body of the galaxy, seen now as a vast dust domain.

4.5. Radio measurements of the extra galactic dust cloud

Measurements by Roberts (1972) had shown the possible existence of a H I bridge between M81 and M82 and also towards the other irregular II companion NGC 3077. An interesting survey was completed by Weliachew and Gottesman (1977). Using a 4.4′ resolution (as opposed to the 10′ beam by Roberts), they found a large scale lumpy envelope of gas extending from M81 and encompassing M82 itself. An interesting feature was that the velocity gradient increases for South to North (M81 lies south of M82), Weliachew and Gottesman interpreted the finding as an encounter between M81 and M82 many years ago, from which M82, following a hyperbolic orbit, proceeded to 'drag out' material from M81. As a result, the gaseous material is falling into M82. It was also found that as much as 10% of the matter seems to be associated with M82 itself.

More recently, Cotrell (1977) made measurements using 2′ x 2.1′ resolution. He arrives at the same results as Weliachew et. al. An estimate of some 1.8×10^8 years is put on the occurrence of the interaction. The velocity field above and below the disk of M82 is interpreted as rotation of the gas about the major axis. He also argues that the gas is bound to the dynamics of the

filaments which he says '...are filled with charged dust particles and plasma frozen together by magnetic fields...' Radiation pressure from the infra-red source will be transmitted to the plasma by the dust and a 'hole' in the H I distribution will develop. This follows an idea put forward by Hargrave (1974). Cotrell's analysis is as follows. Consider a grain situated a distance Z above the disk, the grain radius being represented by a. The radiation pressure it receives will be

$$P_r = \frac{L a^2 Q_{pr}}{4 c Z^2} \tag{4.12}$$

where Qpr is the radiation pressure efficiency of the grain, L is the luminosity from the galaxy. The gravitational force it receives will be

$$F = \frac{G m_g M}{Z^2} \tag{4.13}$$

where m_g is the mass of the grain and M is the mass of the galaxy. We denote the ratio Pr/F by η. Then

$$\eta = \frac{a^2}{4 \rho_g m_g c} \left(\frac{L}{M}\right)_{IR} \tag{4.14}$$

where it is assumed that $Q_{pr} \sim 1$

If $\eta > 1$, the radiation pressure dominates and the grain is forced away, whereas if $\eta < 1$ the grain is gravitationally attracted towards the centre. It must be remembered that this is the case for a point source, whereas in the case of M82 we have a disk which will totally alter the gravitational potential field. In applying this, Cotrell assumed that the dominant part was the infra-red source of the nucleus. He took $M = 10^{10} M_\odot$ and $L_{IR} = 2 \times 10^{37}$ J (Harper and Low 1973). He found that for $Z \sim 4$ Kpc (240 arc seconds) the radiation pressure dominates (the change is due to the variation of $(M/L)_{IR}$ with distance. In the nuclear regions $(M/L)_{IR} \sim 0.001$ whereas for Z = 4 Kpc, $(M/L)_{IR} \sim 0.2$). The value of m_g ($\sim 10^{-16}$ Kg), was calculated using a specific density of about one (corresponding to ice) and $a = 0.3 \mu m$. In the B band of the U - B - V system ($\lambda = 0.45 \mu m$) such a value of a will give $x \left(= \frac{2\pi a}{\lambda}\right) \sim 4.2$. This clearly means that the particle chosen here lie in the Mie scattering domain which contradicts the observed

apparent flatness of the polarisation. The upper limit required for the particles to be in the Rayleigh domain is approximately $x \sim 1$ giving $a \sim 0.07\mu m$ an obvious factor of 4.2 different. Within the nuclear regions, Cotrell finds $\eta \sim 20$ implying the radiation dominates. In setting the Rayleigh restricted value for a, it is found that $\eta \sim 1.1$ implying that radiation pressure is not so dominant. Clearly the point of inversion of the two competing forces will not lie at $Z \sim 4Kpc$.

From the data it would seem reasonable to say that Elvius' suggestion of M82 immersed in an intergalactic cloud seems the more probable. Radio astronomers found velocities that suggest it to be bound, whereas Solinger says that it is not since it is moving some one and a half times faster than the Keplerian orbital velocity associated with binding to M81. Whether the galaxy is tidally bound to M81 is not in question here, the important point is that it is possible to predict the polarisation and intensity in M82. This is discussed in the next chapter.

CHAPTER 5

A dust scattering model of M82

Solinger (1975) using the idea of Elvius that M82 has encountered a dust cloud and the polarisations arise from the scattering of galactic light by this dust cloud produced a model to explain the orientation of the polarisations, this model gives insight into the luminous structure of the galaxy. This chapter describes Solinger's model and more recent variants of it and then describes my model that predicts both the orientation and degree of polarisation.

5.1 The Solinger (1975) Model

The optical polarisation maps of M82 show a centro-symmetric pattern centred on the nuclear region of M82. If the pattern is perfectly centro-symmetric this indicates the source of illumination is point like, any deviation from centro-symmetry would indicate an extended source. Solingers' model assumes that the source is a combination of a disk seen edge on and a point nucleus. He assumed that the disk luminosity falls off as exp(-kr) where the fall off parameter k is a model parameter. The ratio (R) of total disk luminosity (L_D) to the nucleus luminosity (L_N) is another model parameter, along with the position of the nucleus (more precisely, the optical centre). The only other model parameter is the orientation of the disk on the sky, this be called θ . With this geometrical arrangement of the luminous sources Solinger was able to predict the orientation of the polarisation at various points in the halo of M82. Using a minimum chi-squared test he optimised his predictions to fit the observations (those of Elvius,(1963) and Sandage and Visvanathan,(1972)). This model assumed Rayleigh scattering and also that the scattering took place in the plane of the sky, these assumptions obviously make it unreasonable to predict the degree of polarisation.

When the Durham map of M82 became available (with 3000 points measured rather than the 60 used by Solinger) Pallister (1976) ran the Solinger model on this new data. The pertinent model parameters of Solinger and Pallister are compared below

Parameter	Solinger	Pallister
k^{-1} (Kpc)	1	0.5
R	0.05	0.05

The Solinger and Pallister parameters agreed well except for k, the disk luminosity fall off parameters.

The model I describe late in this chapter uses the luminosity geometry of the Solinger model but includes integration along the line of sight and realistic dust density distributions. Before describing my model I will review variants on the Solinger model used by other workers in the last two years.

5.2 Previous models of M82

An attempt to predict the polarisation and intensity of the halo was made by Schmidt et. al. (1976). In their model they used Solingers galactic parameters. The cylindrical disk was embedded in a cylindrical dust cloud of radius 200 arc seconds, which appears to be the visible extent of the disk.

The scatterers were Rayleigh type, and the cloud had a constant dust density. Using their own data which was obtained photographically, they obtained traces of the intensity of polarisation along the minor axis. This data was initially normalised to Elvius' data. The predicted intensity had a much slower fall-off rate than actually observed, and their resulting percentage polarisation showed itself to be a factor of two higher than observed. Overall, the theoretical predictions were not very impressive.

In their model, an optically thin halo was assumed (see page 45) and by a simple analysis, an estimate of the dust density was obtained. Denoting the observed intensity by $I(z)$, the dust density $\rho(z)$, and the predicted intensity for a uniform dust density denoted by $I_M(z)$, where z is the distance along the minor axis from the nucleus. They concluded the following relationship

$$I(z) \propto \rho(z) . I_M(z) \tag{5.1}$$

(They predicted two cases, one with a uniform disk and another using Solingers value of k. In both cases very little variation occurred in the predicted intensities.) The relationship noted for the observed intensity was

$$I(z) \propto z^{-2.7} \tag{5.2}$$

whereas it was found that

$$I_M(z) \propto z^{-0.73} \tag{5.3}$$

They concluded that

$$\rho(z) \propto z^{-2.0} \tag{5.4}$$

Note that by making the dust density a function of z only, it avoids integration along the line of sight.

The model predictions show anomolous effects however. In particular their predictions using $k^{-1} = 1$Kpc shows a minimum polarisation for $z \sim 20''$, and then the trend is for the polarisation to increase to 100% as we go towards the origin. In this case they point out that for small z the polarisation is dominated by the point source (i.e. the nucleus), but even for a point source the trend should be for the polarisation to decrease for smaller z, and it is physically impossible to achieve 100% polarisation for $z = 0$.

The model is not accurate then for small z, this is probably due to the fact that only thirteen scatterers were taken along the line of sight, and although we are not interested in regions with $z \leq 30''$ (this is because the optical depth has increased to a significant amount, and also the nucleus has a finite width which may be quite considerable) it is impossible to say where predictions do become accurate.

As stated previously, the predicted polarisation from this model was too high. Abadi et. al. (1977) realised that this was a major difficulty with the Schmidt model. They attempted to reduce the polarisation by using non-spherical Rayleigh grains. These have the effect of depolarising the light even further (see page26). The model adopted for M82 was a point source. representing the galaxy, which has drifted into an intergalactic cloud which has a depth of 16 Kpc. The effect of the depolarisation mechanism is significant. It is known for example, that the minimum polarisation produced by Rayleigh scattering through a line of sight is 33% whereas Abadis' configuration reduces the polarisation to 20% albeit a point source. However, the effect of the point source was to produce a far too high polarisation and the predictions were no better than those obtained previously by Schmidt. They concluded that the scatterers are needle like metallic grains, probably graphite. Infra-red observations could determine this point.

5.3 The present model

The model proposed here consists of a disk and a nucleus surrounded by an intergalactic dust cloud. The disk intensity goes as $I \propto \exp(-kr_p)$ where Pallisters' value of k is used. In addition to the intergalactic cloud, we have introduced dust which is assumed to be intrinsic to the galaxy. A full description of each point of the model is given below.

5.4 The formulation

Basically, the problem is to calculate the three Stokes parameters (see chapter 1) along the line of sight.

This is achieved by considering the disk as small elements of light illuminating one point along the line of sight (see figure 8), the Stokes parameters are then calculated. This continues until all points along the line of sight have been considered, and the respective Stokes parameters are then summed to give the final Stokes parameters. It is obvious that for light eminating from the disk, the associated Stokes parameters will be in the form of triple integrals whereas those from the nucleus are just single integrals. The equations connecting the Stokes parameters are given on the opposing page.

Here A is a constant depending on the properties of the grain (see Appendix A for full analysis).

The integrations were preformed employing Simpsons' rule. Since they are triple integrals, an integration routine would take up too much computing time. The step lengths were halved until the change in predictions were 1 part in 10^4. The line of sight was chosen so that any further increase in the depth would not affect the results. It was found that by varying the luminosity ratio parameter, R, very little change occurred in the results, apart from the regions where $z \leq 20''$, and as already stated, these regions do not concern us. The critical factor was k. By varying k dramatic changes in the predicted polarisation occurred (see figure 9). Care has to be taken in the step length used in the disk. If k is large, the intensity falls off dramatically, consequently if the step length, δr_b is too large then the integration will 'miss-out' the fall-off completely, and assume a fairly uniform disk. This was investigated for the chosen k and a safe step length was duly established.

5.5 The dust density

Having established the various galactic parameters and assured the accuracy within the predictions, we must now turn our attention to the form of the dust density. Since we are dealing with an intergalactic gas cloud, an infinite depth in the integration along the line of sight is used.

$$I_D = A \int_{-\ell}^{+\ell} \int_{0}^{2\pi} \int_{0}^{r_o'} \frac{n_D(Z)}{R^2} \left(1 + \frac{(X - r_D\cos\phi)^2}{R^2}\right) \exp(-kr_D)\, r_D\, dr_D d\phi dx$$

$$Q_D = A \int_{-\ell}^{+\ell} \int_{0}^{2\pi} \int_{0}^{r_o'} \frac{n_D(Z)}{R^4} (Z^2 - (Y - r_D\sin\phi)^2) \exp(-kr_D)\, r_D dr_D d\phi dx$$

$$U_D = A \int_{-\ell}^{+\ell} \int_{0}^{2\pi} \int_{0}^{r_o'} \frac{n_D(Z)}{R^4} 2Z(Y - r_D\sin\phi) \exp(-kr_D)\, r_D dr_D d\phi dx$$

are Stokes parameters produced by the disk, and

$$I_N = B \int_{-\ell}^{+\ell} n_D(Z) \left(1 + \frac{X^2}{R'^2}\right) \frac{dx}{R'^2}$$

$$Q_N = B \int_{-\ell}^{+\ell} n_D(Z) \frac{Z^2 - Y^2}{R'^4} dx$$

$$U_N = B \int_{-\ell}^{+\ell} n_D(Z) \frac{2YZ}{R'^4} dx$$

are Stokes parameters produced by the nucleus,

B being a constant

where $R^2 = (X - r_D\cos\phi)^2 + (Y - r_D\sin\phi)^2 + Z^2$

$R'^2 = X^2 + Y^2 + Z^2$

and $n_D(Z) = n_o(1 + \alpha/Z^n)$

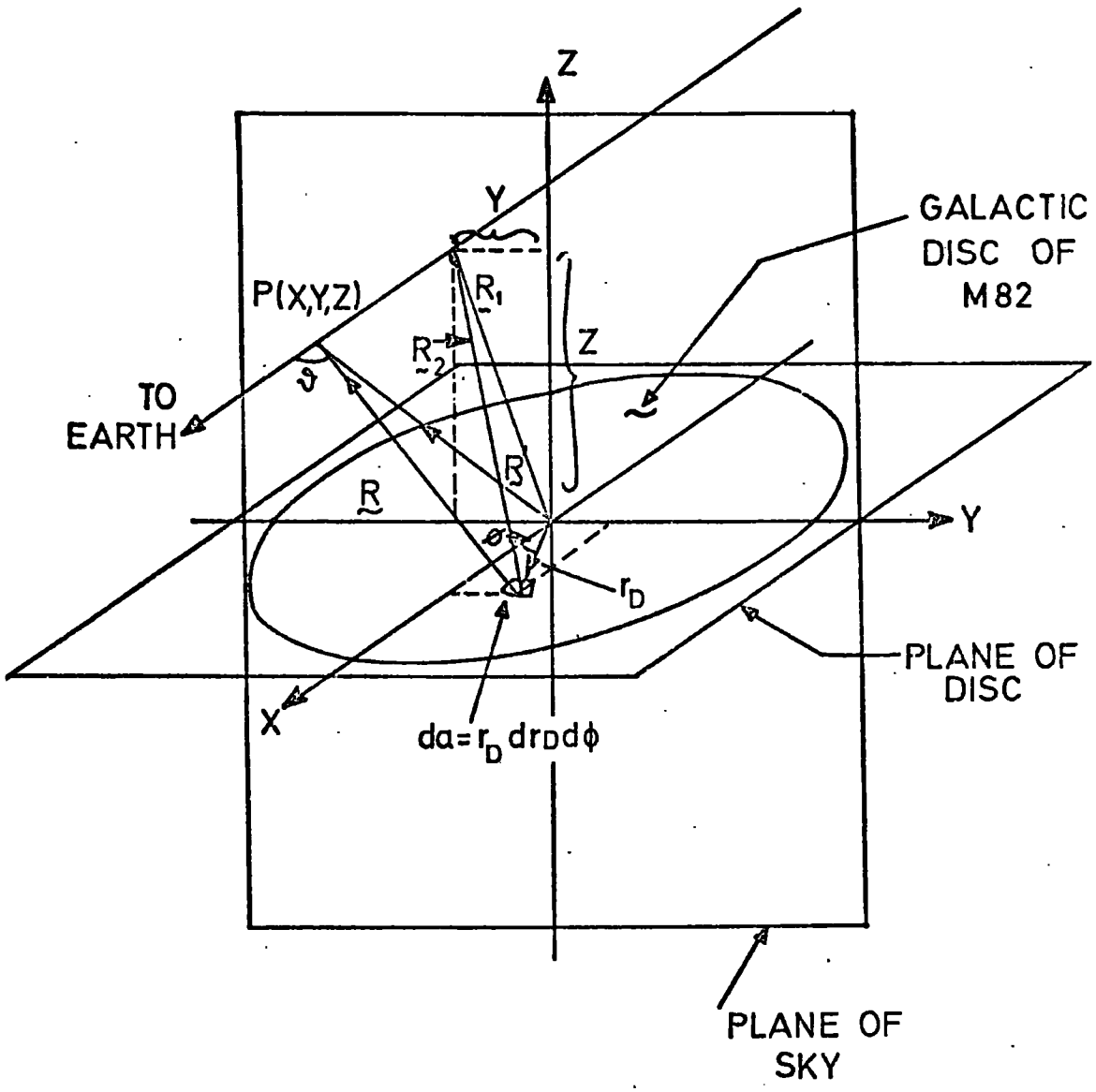
Z
Y
P(X,Y,Z)
R1
R2
Z
GALACTIC
DISC OF
M82
TO
EARTH
R
R'
Y
rD
PLANE OF
DISC
X
da=rD drD dϕ
PLANE OF
SKY

FIG. 8.

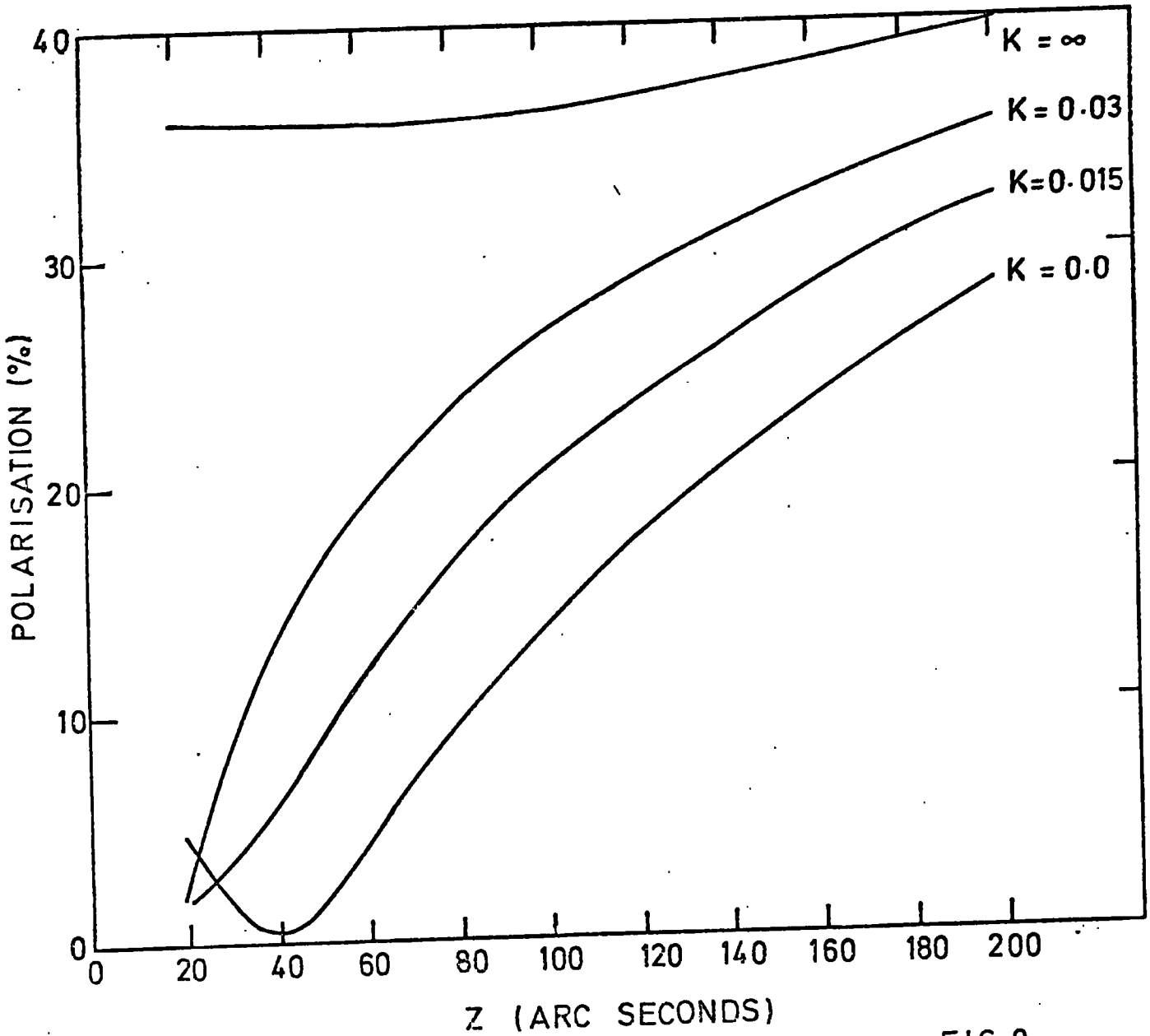
40
30
20
10
0
0
20
40
60
80
100
120
140
160
180
200
POLARISATION (%)
Z (ARC SECONDS)
K = ∞
K = 0·03
K=0·015
K = 0·0

FIG. 9

This is tantamount to using a depth of 2000 arc seconds.

The dust must be considered in two parts. Firstly, we have the intergalactic dust density (denoted by n_e) and the dust which is intrinsic to the galaxy, denoted by n_g. Both types of dust are considered as Rayleigh scatterers and by Weliachews' data, n_c is assumed constant (see figure 10). This assumed because in most observations taken in our galaxy, the dust to gas ratio is constant. Only the galactic dust n_g is given variability. We have assumed n_g to be a function of z only, and indeed in our galaxy it is the case. By making n_g a function of z it makes computations easier because none of the integrations depend on z.

Consider now the dust density. It was assumed that the intrinsic dust extended to the region of the galaxy (the radius was taken to be 200 arc seconds), therefore when scattering from the intergalactic cloud, we consider only n_c, but when scattering from regions 'above' the galaxy (i.e. $|x| \leq 200$) we consider n_c and n_g (see figure 11).

The form of the dust density was taken as

$$n_t = \begin{cases} n_g + n_c & |x| \leq 200'' \\ n_c & |x| > 200'' \end{cases} \qquad (5.5)$$

where n_t denotes total dust density.

Assume that

$$n_g(z) = n_g(0)/z^n \qquad (5.6)$$

where $n_g(o)$ is the dust density in the plane of the galaxy (obviously by putting $z = o$ we have a singularity, so we put $z = 1$, which to all intents and purposes, is in the plane).

So for $|x| \leq 200$

$$\begin{aligned} n_t &= n_c + n_g(0)/z^n \\ &= n_c \left(1 + \frac{n_g(0)/n_c}{z^n}\right) \end{aligned} \qquad (5.7)$$

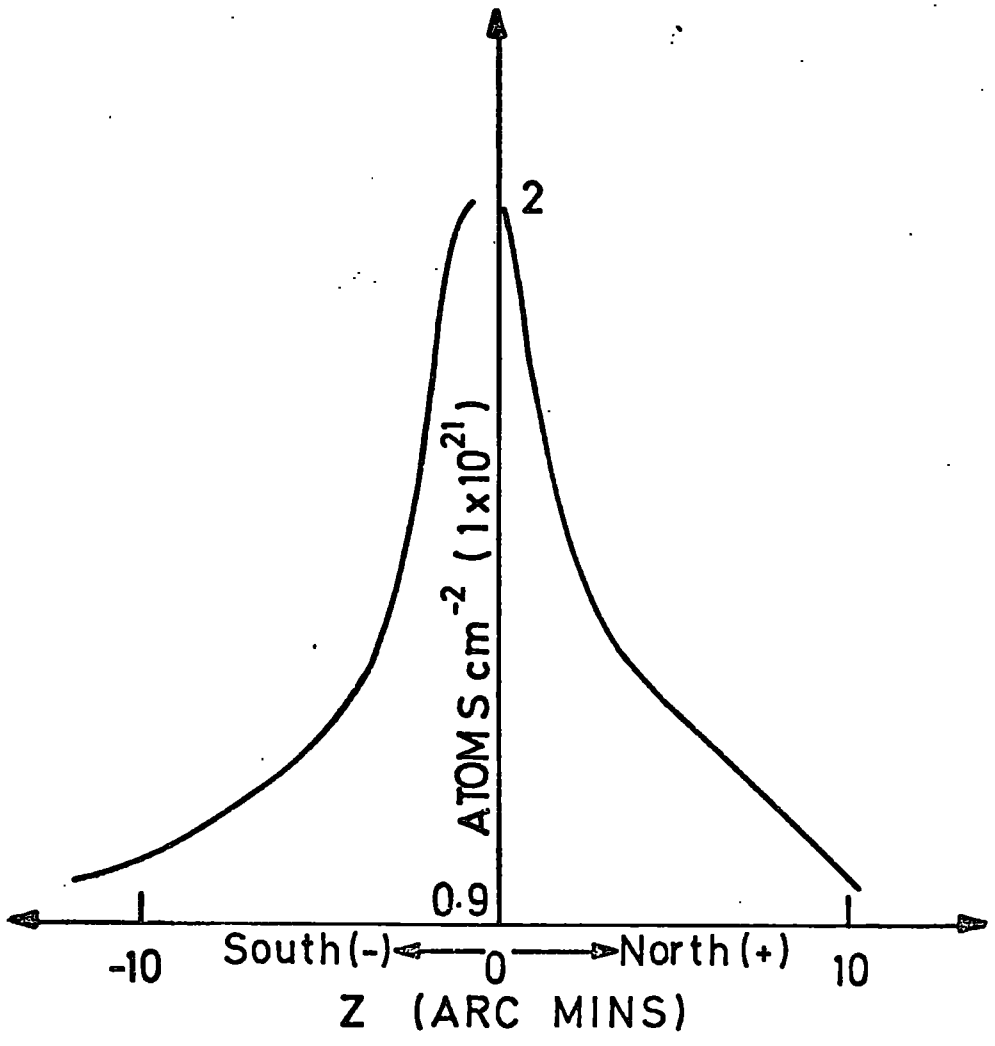

COLUMN DENSITY OF NEUTRAL HYDROGEN ALONG THE MINOR AXIS OF M82
(ORIGIN TAKEN AT OPTICAL CENTRE OF GALAXY)

FIG. 10

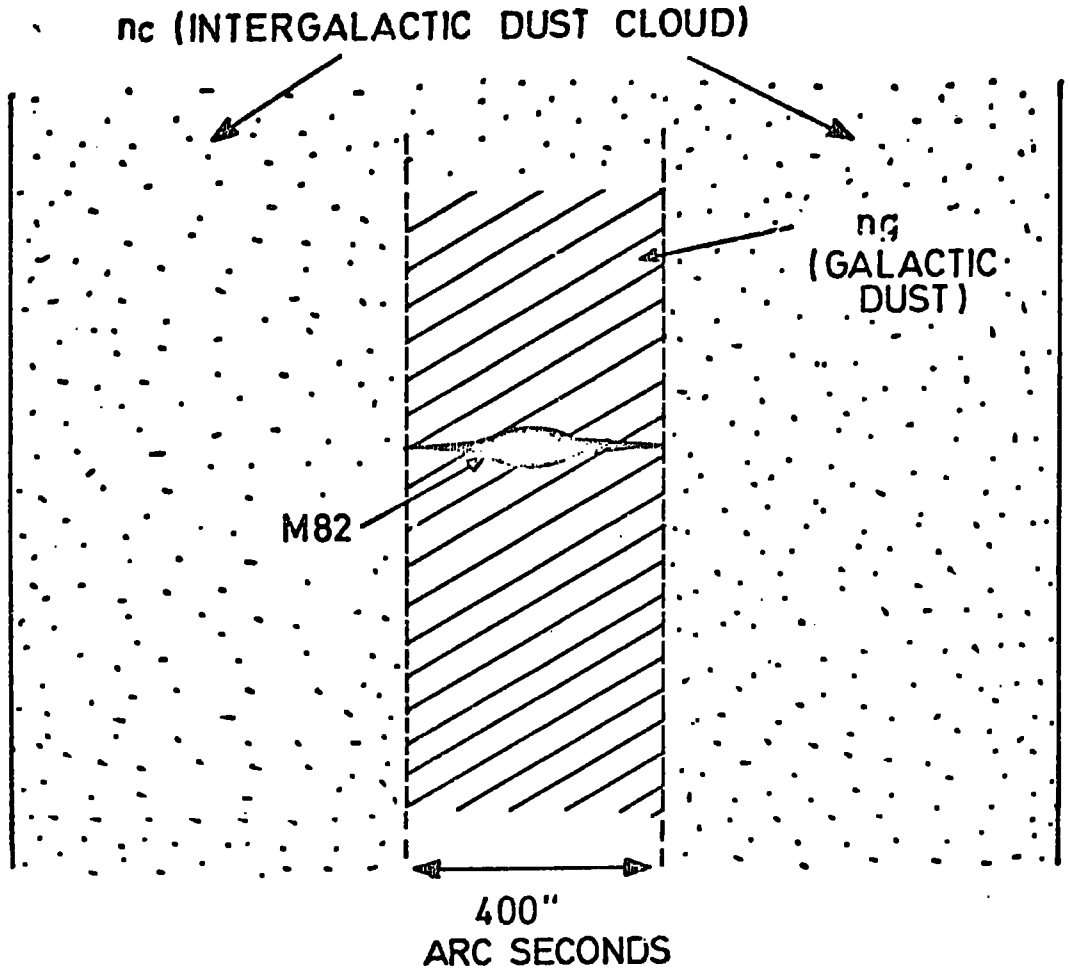
nc (INTERGALACTIC DUST CLOUD)
ng
(GALACTIC
DUST)
M82
400"
ARC SECONDS

FIG. 11

From now on we put $\alpha = n_g(o)/n_c$. We have therefore established two parameters, α and n. These two parameters alone determine the shape of the polarised intensity plots (assuming galactic parameters fixed). If we have a large value of n and α, the plot of polarised intensity against distance will have a persisting large gradient. By making the value of α less, the effect of z dependence will rapidly decrease and so on.

5.6 The selection and fitting of data

In all, twelve traces were taken, six of intensity and six of polarised intensity. Polarised intensity was used since the total intensity may be contaminated (e.g. halo stars, intrinsic light). The traces were taken through the optical centre and eighty arc seconds either side, top and bottom, perpendicular to the plane of the galactic disk. Since the polarised intensity depends only on the scatterers, theoretical predictions of polarised intensity were made. (see figures 13-24).

It is noted that the data is measured in arbitrary units. Likewise, the predicted values are also in arbitrary units. These must be normalised to the observed values since the shapes are congruent. It should be sufficient to normalise all the predictions to one value of the data. If we let the observed value to be P_o and the theoretical value be P_T, then since we plot on a logarithmic scale we can write

$$\log_{10} P_o = \log_{10} P_T + k \qquad (5.8)$$

(for $z = z'$ where z' is the point of normalisation) i.e. we merely raise the theoretical curve up until the two curves coincide. Equation (5.8) may be written as

$$\log_{10} (P_o/P_T)_{z=z'} = k. \qquad (5.9)$$

Here k is the conversion factor.

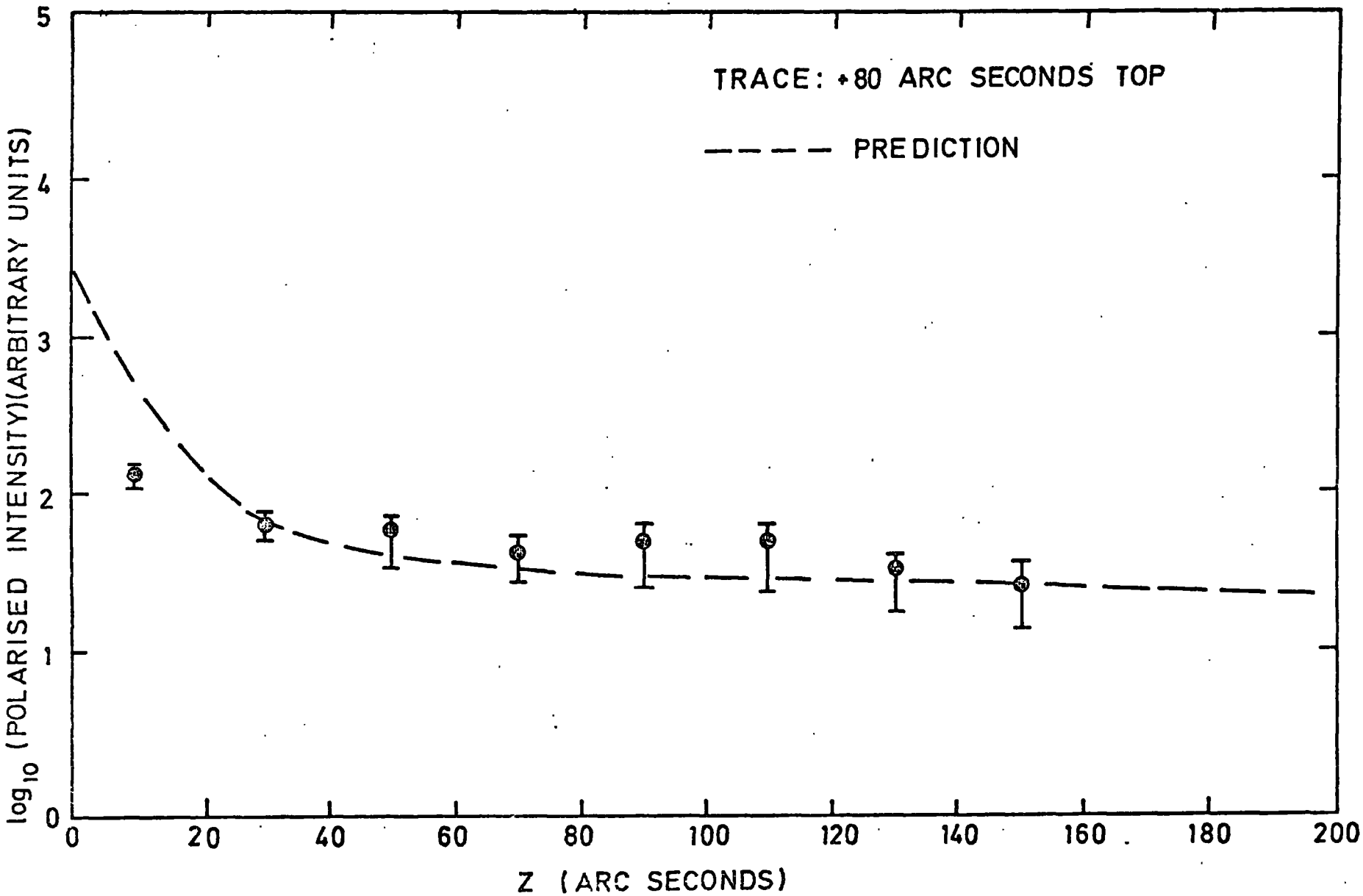
TRACE: +80 ARC SECONDS TOP
PREDICTION
log10 (POLARISED INTENSITY)(ARBITRARY UNITS)
Z (ARC SECONDS)
0
1
2
3
4
5
0
20
40
60
80
100
120
140
160
180
200

FIG. 13.

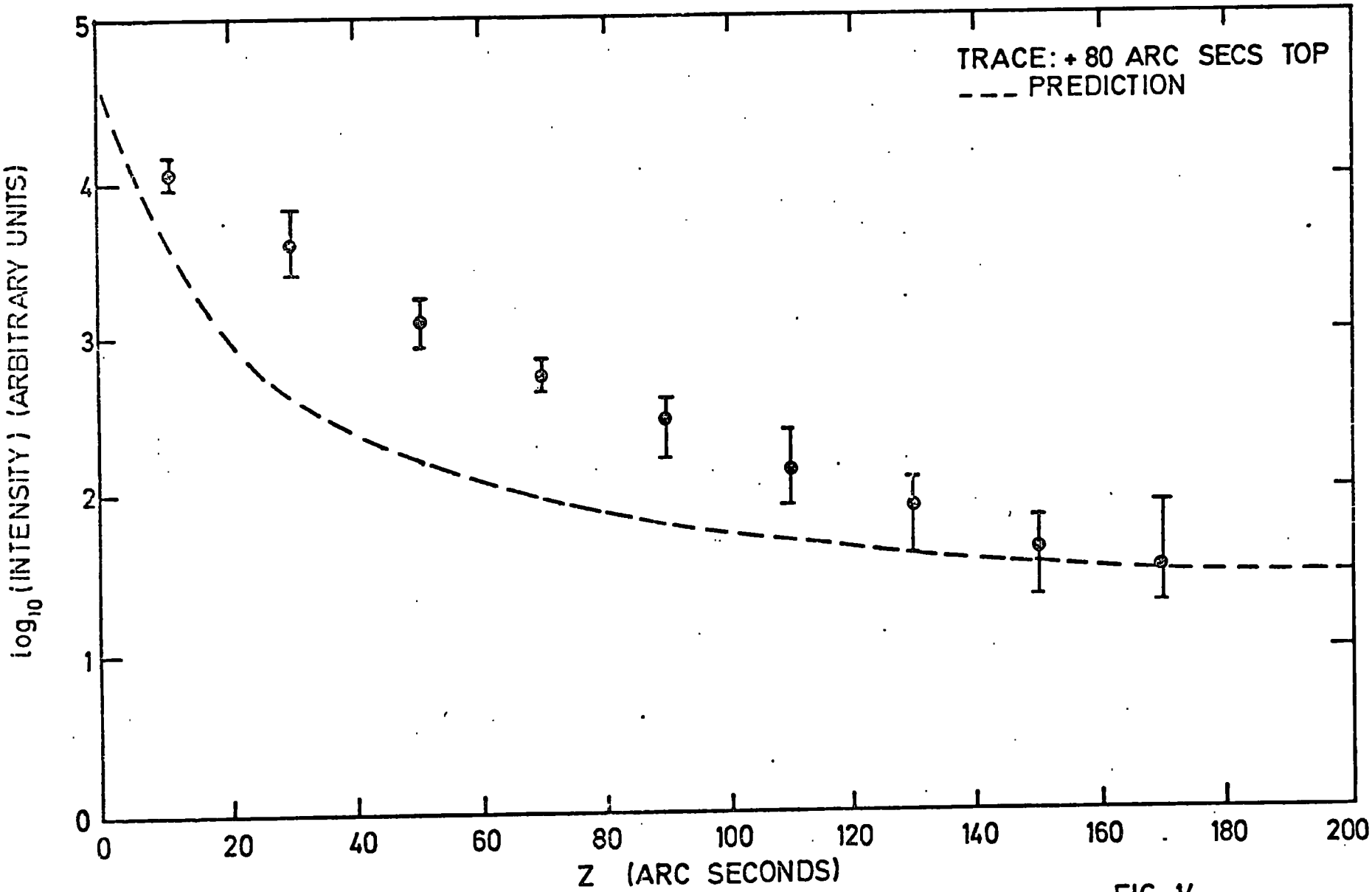
TRACE: + 80 ARC SECS TOP
--- PREDICTION
log10 (INTENSITY) (ARBITRARY UNITS)
Z (ARC SECONDS)
0
1
2
3
4
5
0
20
40
60
80
100
120
140
160
180
200

FIG. 14.

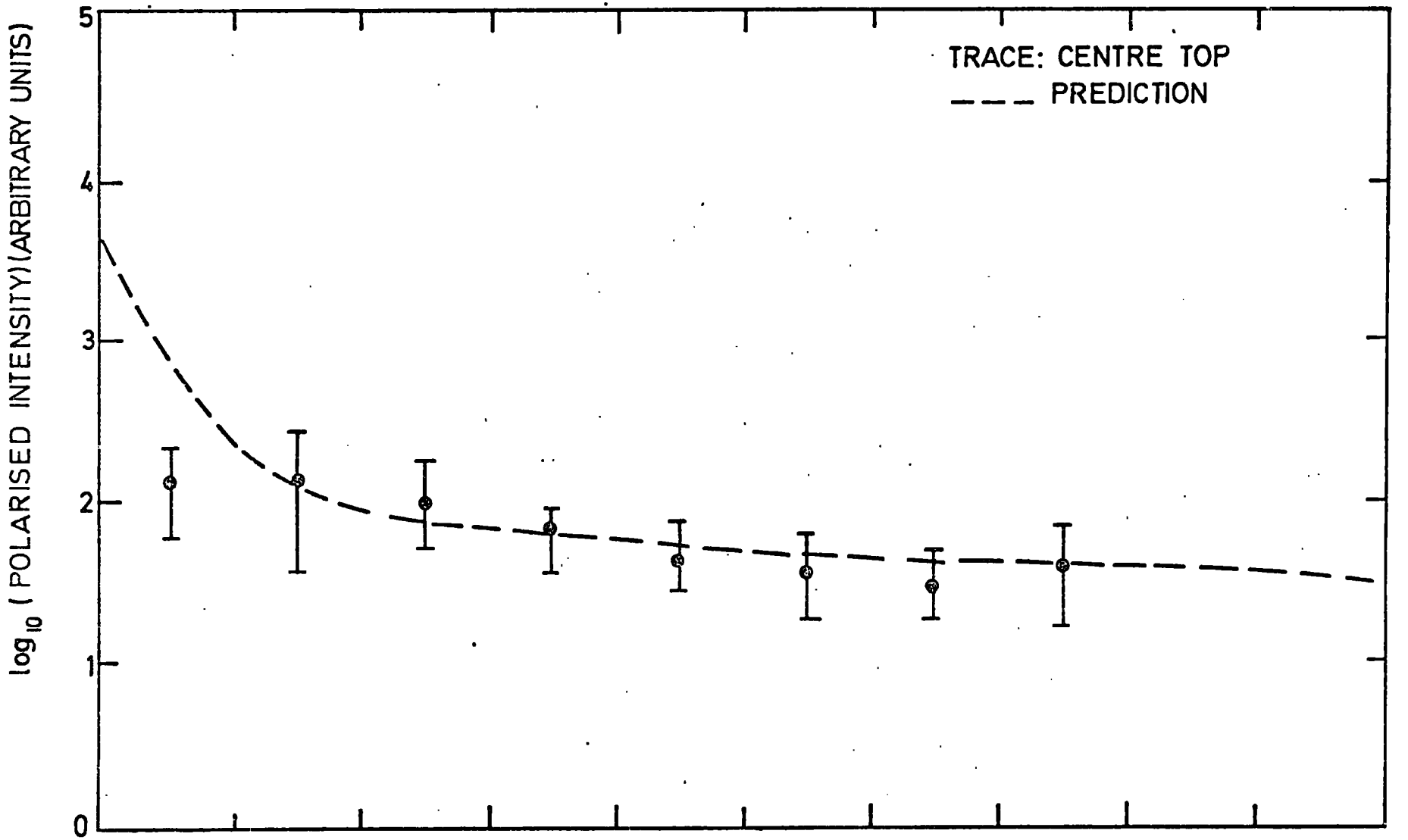
TRACE: CENTRE TOP
PREDICTION
log10 (POLARISED INTENSITY) (ARBITRARY UNITS)
Z (ARC SECONDS)
0
1
2
3
4
5
0
20
40
60
80
100
120
140
160
180
200

FIG. 15.

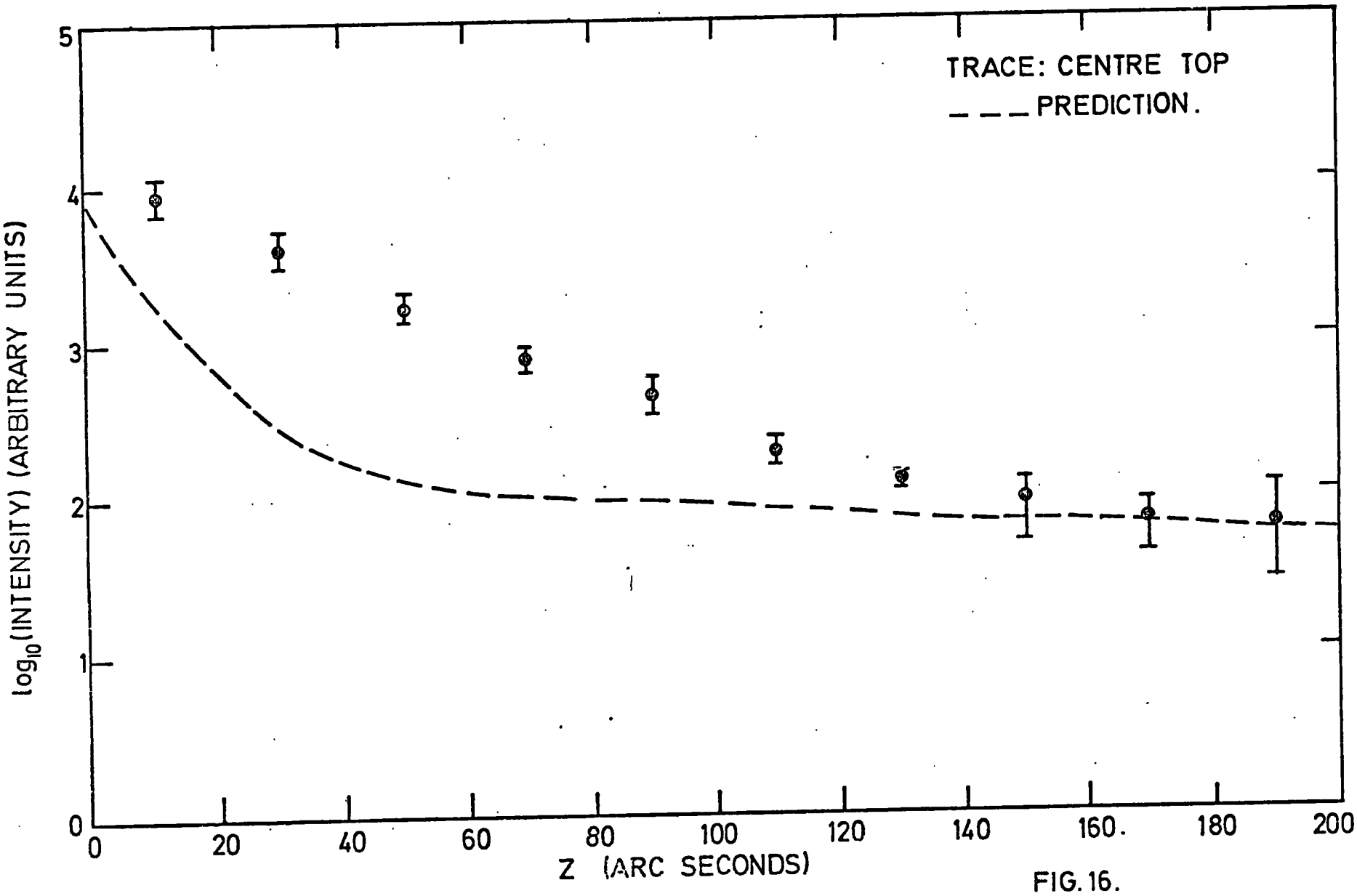
TRACE: CENTRE TOP
PREDICTION.
log10 (INTENSITY) (ARBITRARY UNITS)
Z (ARC SECONDS)
0
1
2
3
4
5
0
20
40
60
80
100
120
140
160.
180
200

FIG. 16.

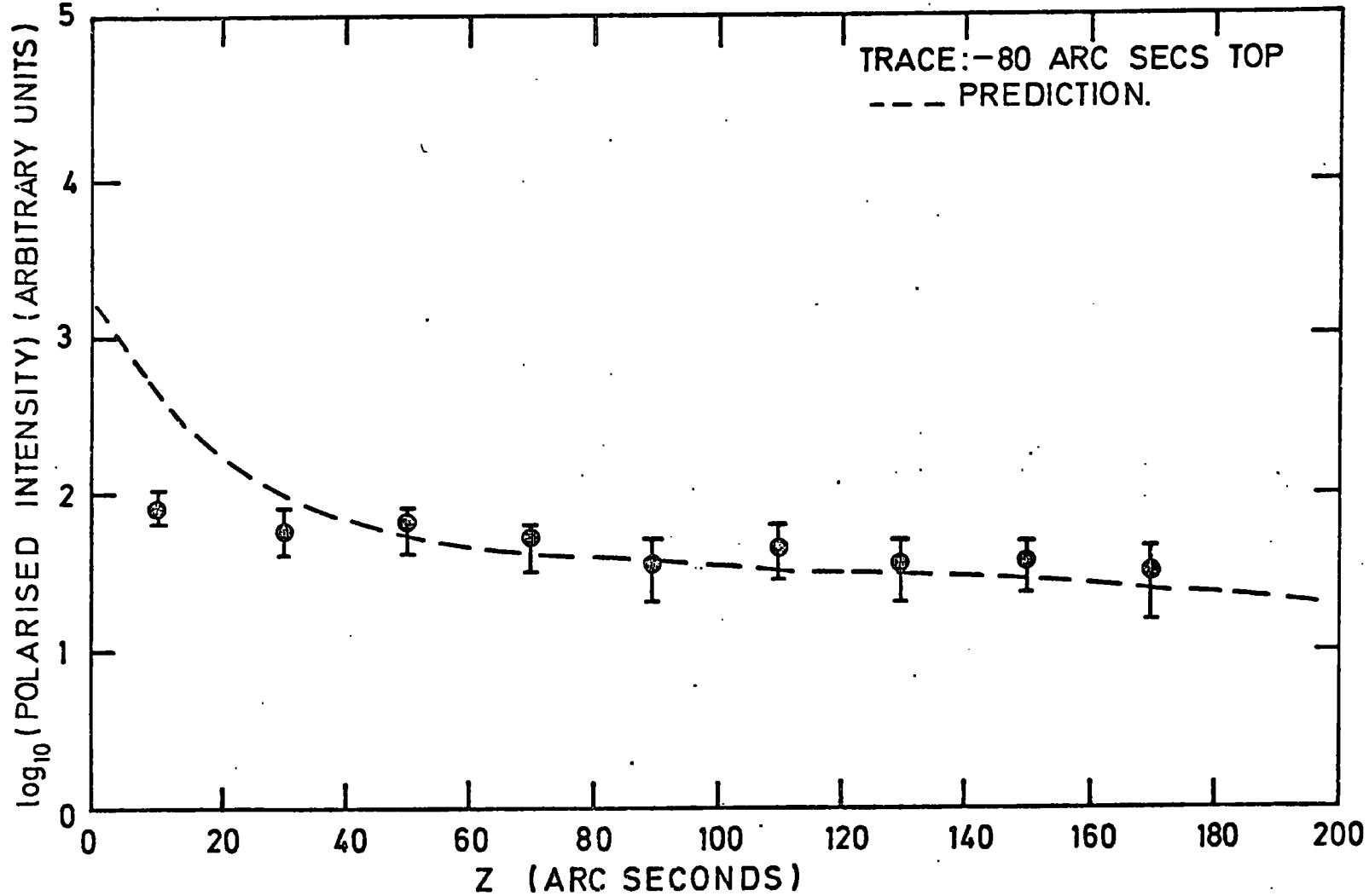
TRACE:-80 ARC SECS TOP
--- PREDICTION.
log10 (POLARISED INTENSITY) (ARBITRARY UNITS)
Z (ARC SECONDS)
0
1
2
3
4
5
0
20
40
60
80
100
120
140
160
180
200

FIG.17.

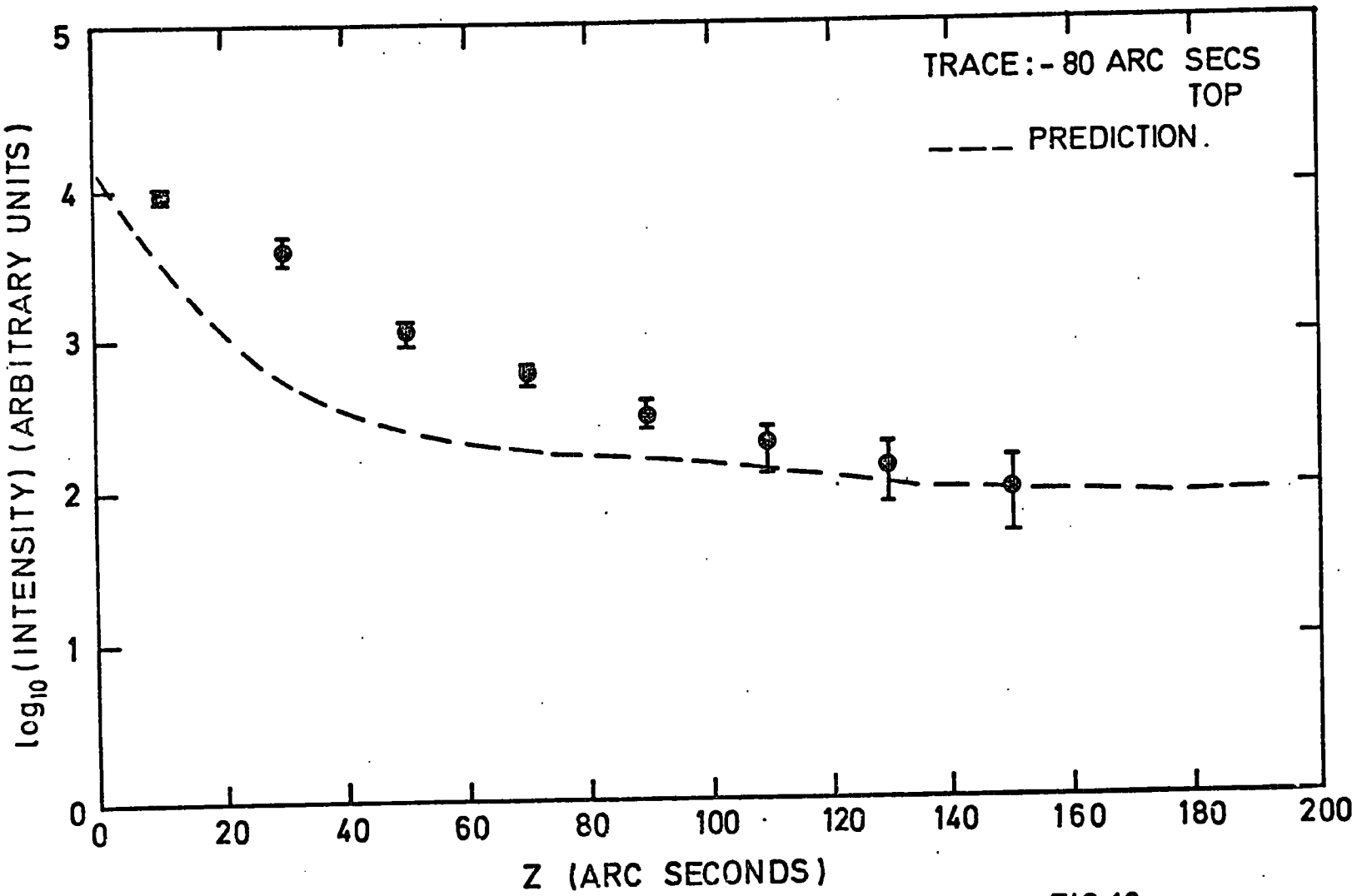
TRACE:- 80 ARC SECS
TOP
PREDICTION.
log10 (INTENSITY) (ARBITRARY UNITS)
Z (ARC SECONDS)
0
1
2
3
4
5
0
20
40
60
80
100
120
140
160
180
200

FIG.18

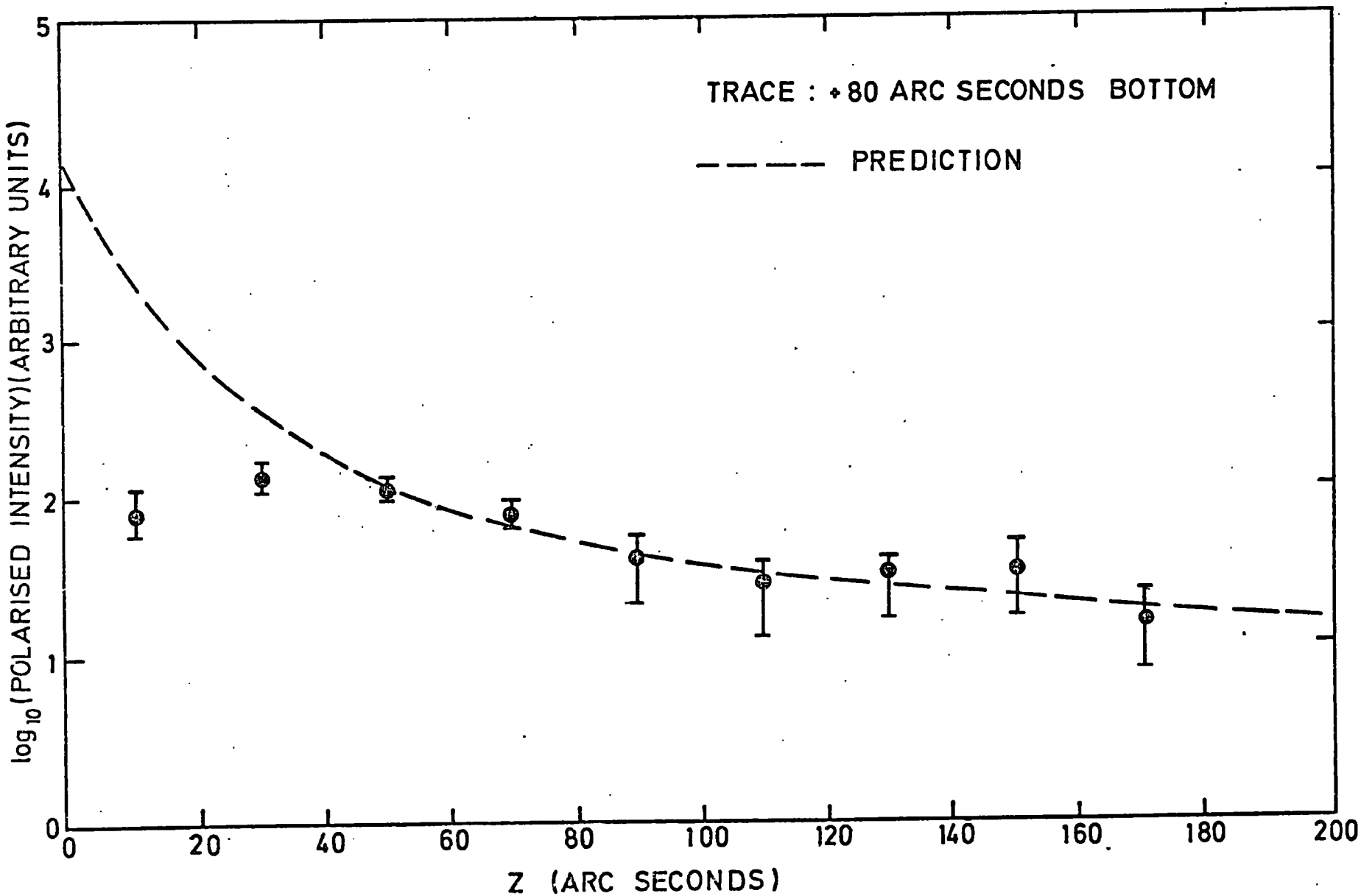
TRACE : +80 ARC SECONDS BOTTOM
PREDICTION
log10(POLARISED INTENSITY)(ARBITRARY UNITS)
Z (ARC SECONDS)
0
1
2
3
4
5
0
20
40
60
80
100
120
140
160
180
200

FIG. 19.

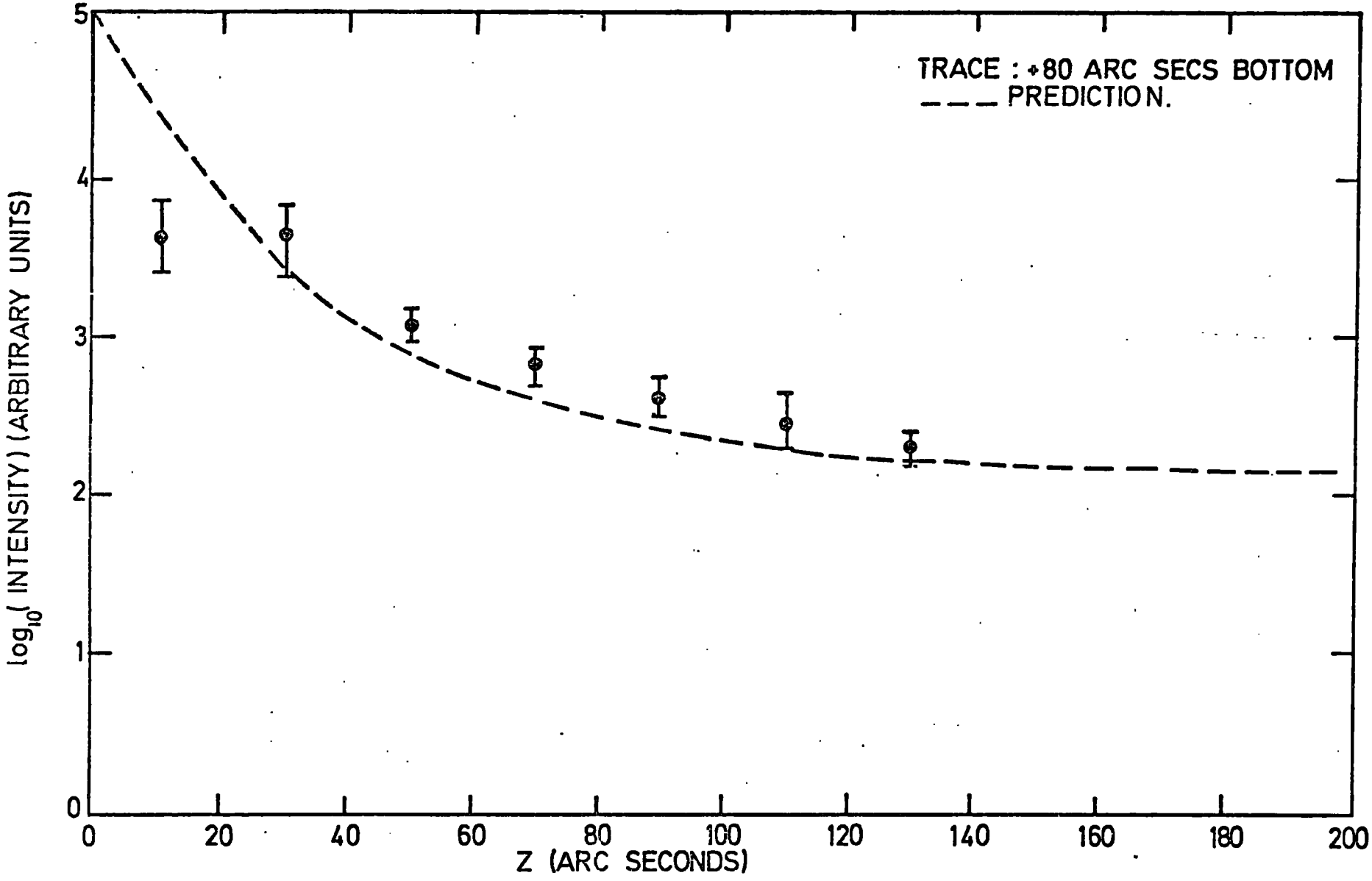
TRACE : +80 ARC SECS BOTTOM
PREDICTION.
log10 (INTENSITY) (ARBITRARY UNITS)
Z (ARC SECONDS)
0
1
2
3
4
5
0
20
40
60
80
100
120
140
160
180
200

FIG. 20

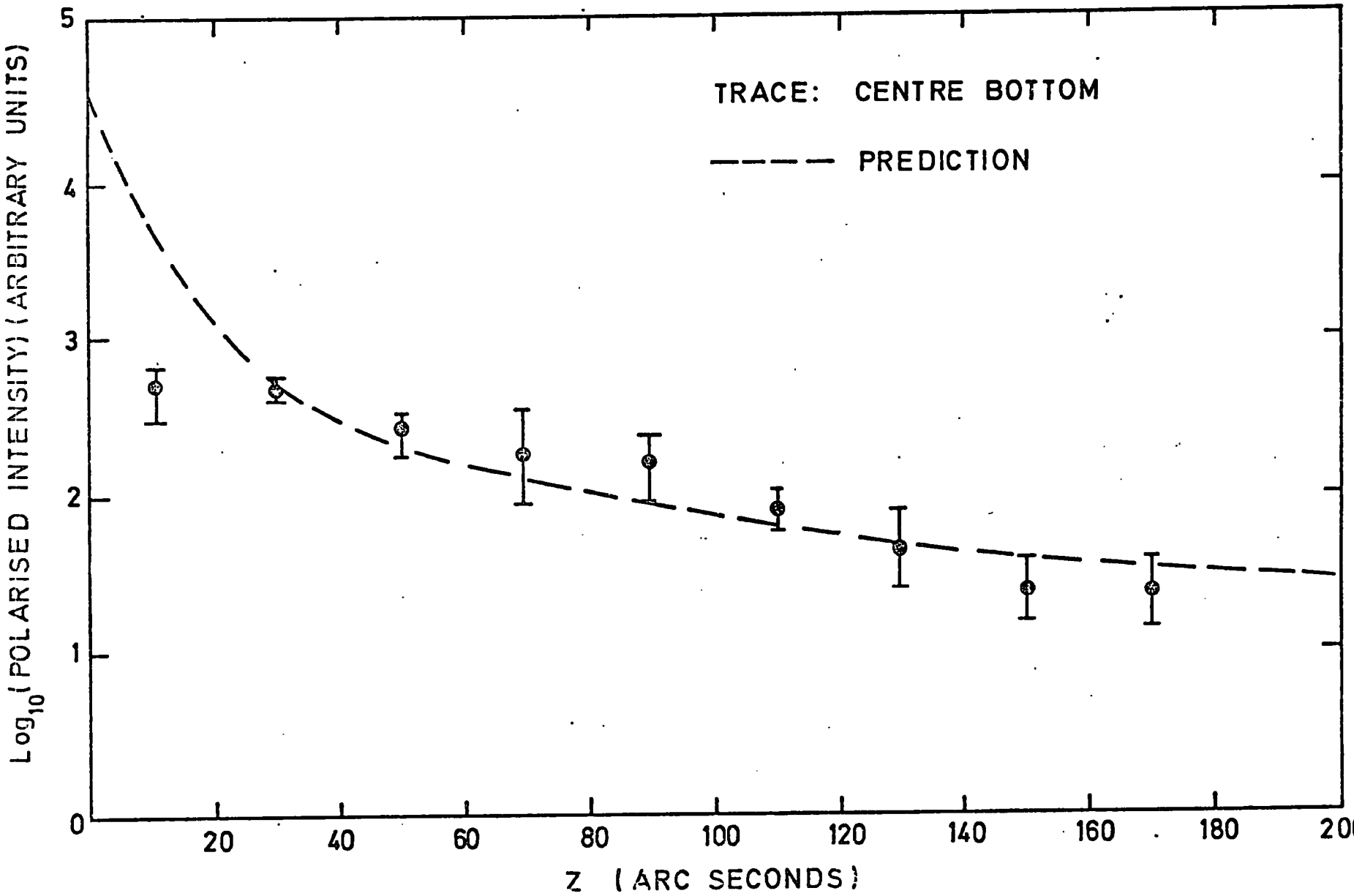
TRACE: CENTRE BOTTOM
PREDICTION
Log_{10} (POLARISED INTENSITY) (ARBITRARY UNITS)
Z (ARC SECONDS)
0
1
2
3
4
5
20
40
60
80
100
120
140
160
180
200

FIG. 21.

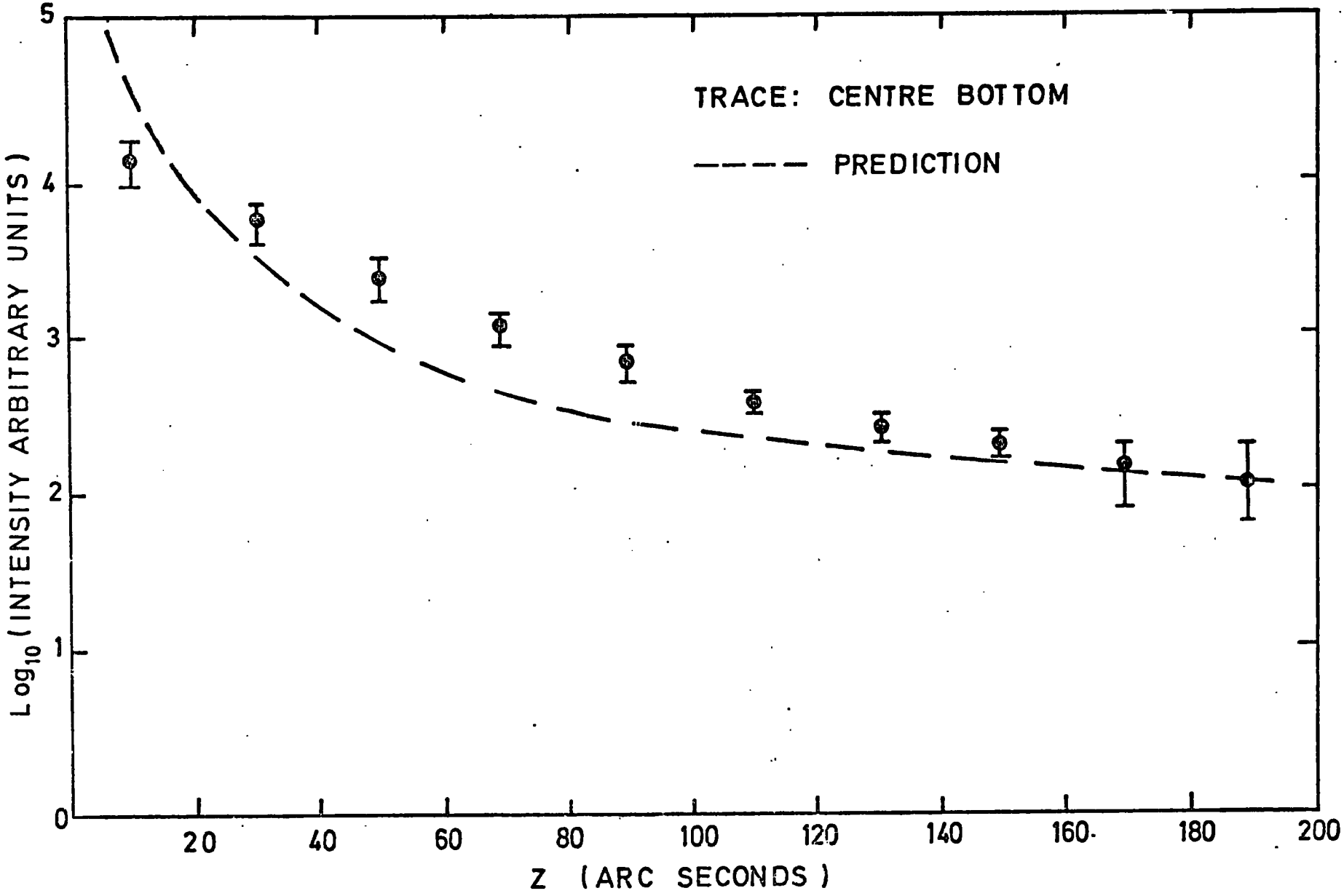
TRACE: CENTRE BOTTOM
PREDICTION
Log10 (INTENSITY ARBITRARY UNITS)
Z (ARC SECONDS)
0
1
2
3
4
5
20
40
60
80
100
120
140
160
180
200

FIG. 22.

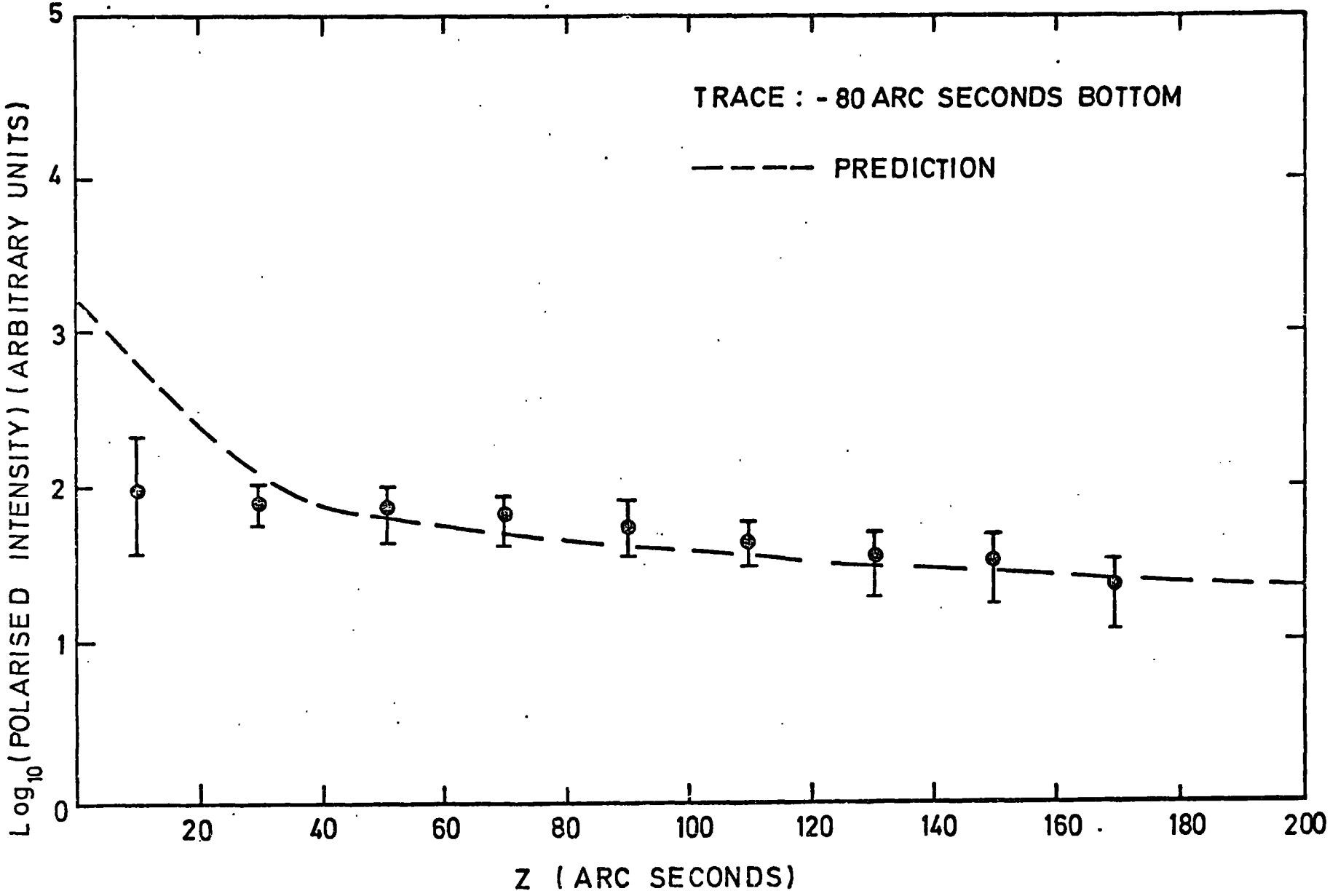
TRACE : - 80 ARC SECONDS BOTTOM
PREDICTION
Log10 (POLARISED INTENSITY) (ARBITRARY UNITS)
Z (ARC SECONDS)
0
1
2
3
4
5
20
40
60
80
100
120
140
160
180
200

FIG. 23.

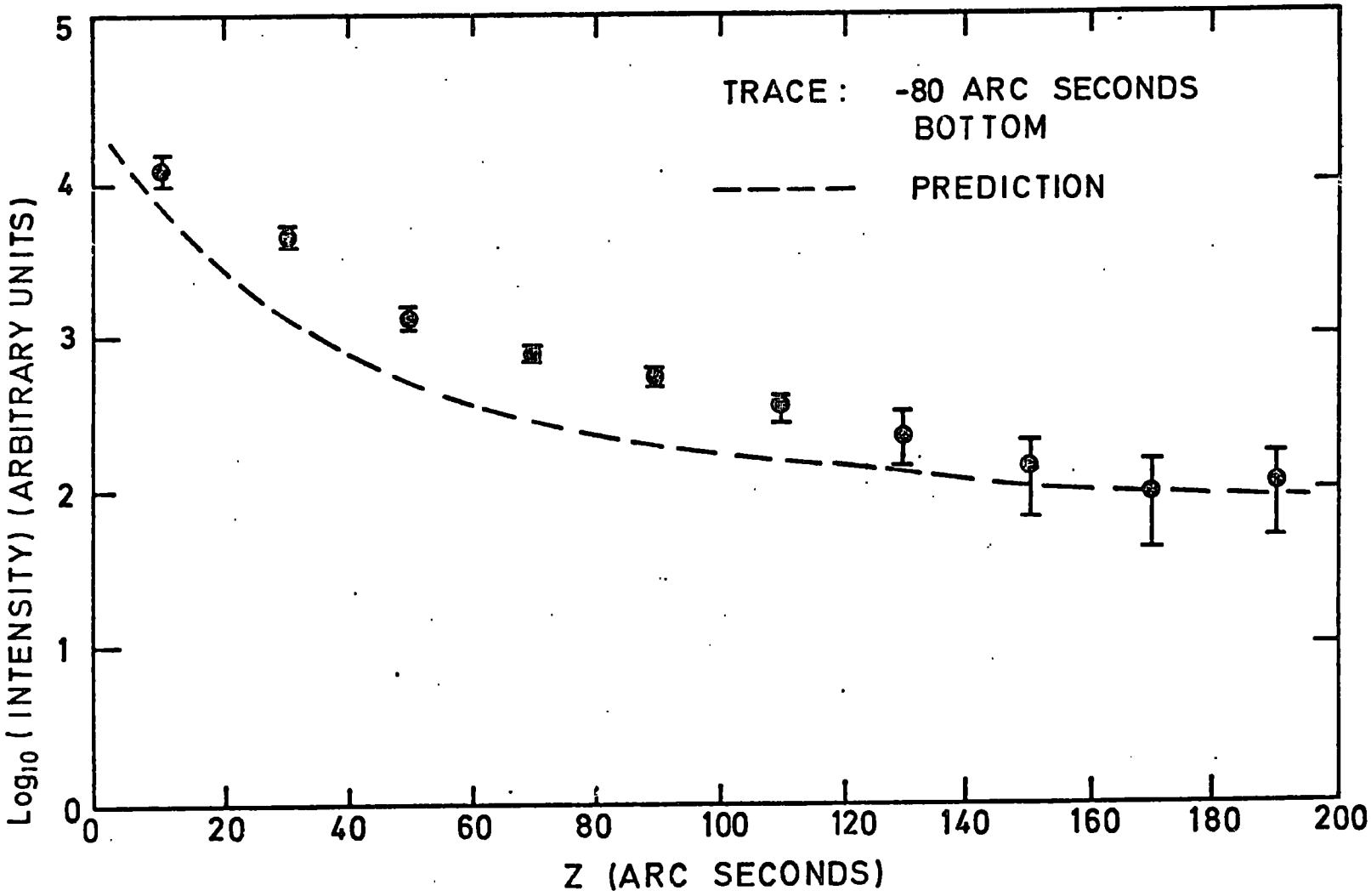
TRACE : -80 ARC SECONDS
BOTTOM
PREDICTION
Log10 (INTENSITY) (ARBITRARY UNITS)
Z (ARC SECONDS)
0
1
2
3
4
5
0
20
40
60
80
100
120
140
160
180
200

FIG.-24.

Once k has been established it should be used for all the data, including the intensity i.e.

$$\log_{10} I_o = \log_{10} I_T + k \qquad (5.10)$$

for all z. This was attempted and it was noted that the intensity did not fit the observed intensity wholly. If the model is correct, the predicted intensity, after conversion, should never be greater than the observed intensity but it is acceptable that the predicted values be less than the observed values. The latter was indeed the case.

When we use the polarised intensity, it is noted that it depends solely on the scatterers i.e. we observe the polarised scattered light. When observing the intensity however, it may be contaminated and so we predict the intensity of the scattered light alone. We see from this why it is acceptable for the predicted intensity to be less than the observed.

The most obvious explanation for this 'missing intensity' would be contamination from halo stars. If this is the case one would expect the predicted and observed intensities to coincide forlarge values of z since the halo stars in the outer region will be sparse. The following analysis shows us that the halo star density is acceptable.

5.7 Plausability for halo stars

If halo stars are the cause for the contamination then it would seem likely that away from the galactic disk, the theoretical and observed intensities should coincide. This is because the halo stars, as observed in the other galaxies, become less frequent as we go further from the disk. We first define the symbols

Line of sight = S_o

Luminosity of galactic disk = L_D

Luminosity of individual stars = L_*

Number of stars per unit volume in halo = n_*^H

Number of stars per unit volume in disk = n_*^D

Dust density = n_D

Optical depth of scattering = τ_s

Optical depth of extinction = τ_e

Effective cross-sectional area of scattering = Csca

Effective cross-sectional area of extinction = Cext

(Note: Csca = $\pi a^2 Q_{sca}$ and Cext = $\pi a^2 Q_{ext}$ where a is the radius of the scatterers). Note the assumption of constant luminosity of the disk.

Assume that light from the galaxy reaches a point P in the halo along the line of sight. The intensity of the light is approximately given by

$$I = \frac{L_D}{4\pi z^2} \tag{5.11}$$

The intensity of light scattered from point P is

$$\delta I_s = \frac{L_D n_D C_{sca}}{16\pi^2 z^2} \tag{5.12}$$

The total light scattered along the line of sight is

$$I_s = \frac{L_D n_D C_{sca} S_o}{16\pi z^2} \tag{5.13}$$

But

$$\tau_s = C_{sca} n_D S_o$$

so that (5.13) becomes

$$I_s = \frac{L_D \tau_s}{16\pi^2 z^2} \tag{5.14}$$

Now the total intensity received from halo stars along the line of sight is

$$I_* = \left(\frac{n_*^H L_*}{4\pi}\right) S_o e^{-\tau_e} \tag{5.15}$$

If τ_e is small, which is a reasonable assumption, then

$$e^{-\tau_e} \simeq (1 - \tau_e)$$

so that (5.15) becomes

$$I_* = \left(\frac{n_*^H L_*}{4\pi}\right) \zeta_0 (1-\tau_e) \tag{5.16}$$

Let Po be the observed polarisation and P_T the theoretical polarisation.

Since the polarised intensities are the same.

$$\frac{P_T}{P_0} = \frac{I_S + I_*}{I_S} = 1 + \frac{I_*}{I_S} \tag{5.17}$$

If we let the ratio have an upper limit of two (as observed from the data), then

$$\frac{I_*}{I_S} \sim 1 = \frac{n_*^H L_* \zeta_0 (1-\tau_e)\, 16\pi^2 z^2}{4\pi L_D \tau_S}$$

$$= 4\pi \left(\frac{n_*^H L_* z^2 \zeta_0}{L_D}\right) \left(\frac{1-\tau_e}{\tau_S}\right) \tag{5.18}$$

Now

$$\tau_S = n_D \pi a^2 Q_{sca}\, \zeta_0 \tag{5.19}$$

and

$$\tau_e = n_D \pi a^2 Q_{ext}\, \zeta_0$$

If we further assume that the scatterers are of Rayleigh size we can substitute values into equations (5.19) taken from Wickramasinghe (1973).

We put

$$a = 0.01\ \mu m$$

$$Q_{ext} = 10^{-2}$$

$$Q_{sca} = 10^{-4}$$

$$\zeta_0 = 7 \times 10^3 \text{ pc}$$

(Here we have used the scale one minute of arc equals 10^3 pc for M82)

Now, the condition of $\tau_e < 1$ implies

$$n_D < \frac{1}{\pi a^2 Q_{ext}\, \zeta_0} \tag{5.20}$$

and so

$$n_D < 5 \times 10^{-10} \text{ cm}^{-3}$$

Now equation (5.18) can be re-written as

$$\frac{n_*^H L_*}{L_D} \simeq \frac{\tau_s}{4\pi(1-\tau_e) z^2 S_0} \tag{5.21}$$

If we let the radius of the galactic disk be ρ then it follows that

$$L_D \simeq \pi \rho^2 n_*^D L_* \ell \tag{5.22}$$

where l is the width of the galactic disk. Substituting into equation (5.21), and assuming $\tau_e \ll 1$

$$\frac{n_*^H}{n_*^D} \simeq \frac{\tau_s \rho^2 \ell}{4 z^2 S_0} \tag{5.23}$$

Using the values of Qsca and a, we find

$$\tau_s \simeq 6 \times 10^6 n_D \tag{5.24}$$

If we substitute into equation (5.24) the value of n_D found previously i.e. $n_D \leq 10^{-10}$ then (5.24) becomes

$$\tau_s \simeq 6 \times 10^{-4}$$

and

$$n_*^H \simeq 10^{-4} \text{ stars pc}^{-3} \text{ at z = 60"}$$

Our galaxy, at an equivalent distance of 60 arc seconds, has $n_*^H \sim 5 \times 10^{-4}$ so the value of halo star density for M82 is comparable with that of our own galaxy. It must be remembered that the values found are upper limits.

To summarise, the analysis that we have shown is that the present model can be fitted to the polarised intensity but not totally to the intensity. It is noted that the predicted intensity is less than that observed and so in search of contamination, it is feasable to say that the missing light comes from halo stars and the halo star density is in order with the observed halo star density in our own galaxy. We proceed therefore on the basis of this model and in the next chapter show the results and implications of the model.

CHAPTER 6

Results from the M82 model

In the previous chapter we saw that dust density was introduced of the form

$$n(z) \propto (1 + \alpha/z^n) \tag{6.1}$$

We then have two parameters, α and n. Here α is the ratio of dust in the plane of the galaxy ($n_g(o)$) to dust in the intergalactic cloud (n_c) i.e.

$$\alpha = n_g(o)/n_c \tag{6.2}$$

The parameter n, determines the fall-off of the dust which is intrinsic to the galaxy.

6.1 The results

As mentioned previously, twelve traces were taken. Six of polarised intensity and six of intensity. These were taken through the centre and at 80 seconds of arc either side of the centre.

Various values of α and n were tried until acceptable fits were obtained. The results are shown in figures (13 - 24) and a summary is given below in Table 1

Position of trace	α	n
+ 80" TOP	10^4	2.0
CENTRE TOP	10^4	2.0
- 80" TOP	10^4	2.0
+ 80" BOTTOM	10^3	2.0
CENTRE BOTTOM	10^3	2.0
- 80" BOTTOM	3×10^3	2.0

TABLE 1

Let us now discuss the results. In all positions, the value of n was found to be two, this is in agreement with Schmidt and Angel (cf. page56). The dust ratio parameter α, is more interesting.

From table 1 it is noted that α has larger values for the north of the galaxy than for the south, the difference being of the order of ten. If the drifting dust cloud model is correct, then it may be possible for the material from the dust cloud to be 'swept-up' by the galaxy. It is also noted that the relative motion of the system is such that the galaxy is drifting in the southwards direction where the larger values of α are found.

6.2 The gas to dust ratio

Following the measurements of Weliachew (1977) we are able to make an approximation to the dust density in the intergalactic cloud and the dust belonging to M82.

Let the column density of hydrogen be n'_H and the column of dust be n'_D. For our galaxy

$$\frac{n_H'}{n_D'} = 6.7 \times 10^{12} \tag{6.3}$$

Figure (10) shows the variation of column density of hydrogen along the minor axis of M82. Weliachew finds a maximum value of 2×10^{21} atoms cm^{-2} and a minimum value of 9×10^{20} atoms cm^{-2}. We will use the minimum value since we have to be far away from the galaxy in order that no contamination is present from the intrinsic hydrogen of M82. We assume that the gas to dust ratio of the intergalactic cloud is the same as that in our galaxy. The extent of the cloud is about 30 arc minutes and we assume this to be the depth also.

The value for the average dust density becomes

$$\langle n_D \rangle = 1.3 \times 10^{-15} cm^{-3} \tag{6.4}$$

We now use the values of α found previously from the model. This means that the dust density just above the plane of the galaxy becomes

$$n_D \sim 10^{-11} - 10^{-12} cm^{-3} \tag{6.5}$$

This can be compared with the value of the dust density for our own galaxy

$$n_D \sim 0.5 \times 10^{-12} cm^{-3} \tag{6.6}$$

which is in good agreement with the predicted value for M82.

6.3 Resume and conclusions

We have seen from the last two chapters the build up to our model of M82. From the polarisation pattern of M82 we have certain parameters of the disk. We have seen which parameters are more sensative in making the comparison between the model and observations. Since there are so many parameters involved, it is important to have as much data to work from as possible since a slight error in one could affect the final results.

From the parameters and the drifting cloud hypothesis of Solinger, a model has been built up using an enormous intergalactic cloud in which M82 has drifted. Many tests have been carried out to ensure the numerical accuracy and all conceivable possibilities have been considered that might affect the model. Two dust densities have been employed, one a constant parameter for the intergalactic cloud and the other, a varying density intrinsic to the galaxy. It can be seen from the data of Weliachew that a constant dust density for the intergalactic cloud is a sufficient approximation if we assume a constant gas to dust ratio. The polarised intensity was fitted and the predicted intensity was seen to be lower than the observed. This 'missing intensity' was recovered from halo stars which, after analysis, appear to be about in order of the density of halo stars in our galaxy.

From the fits the dust density power law was found and values of the ratio of the two grain densities obtained. Working from Weliachews measurements, actual values of the two dust densities were made. In total, the values found for the halo stars and the dust density of M82 point to this galaxy being similar to that of our own. Explosions occurring in the centre of M82 will not greatly affect the scattering model. There is perhaps one approximation made to the model and that is that the model assumes Rayleigh type grains in the halo of M82.

If the grains were of Mie type, the scattering formulation would not be correct for points near the galaxy. This problem could be resolved by taking polarisation measurements at varying wavelengths, both near and far from the galaxy. If the grains of M82 are Mie type, the polarisation against wavelength measurements will show variation, whereas measurements far away from the galaxy should show no variation with wavelength. Measurements of polarisation against wavelength is a very handy lever and we will be discussing its possible potential in the next chapter.

CHAPTER 7

DUST SCATTERING MODELS OF NEBULAE

In the previous chapter we postulated that the scatterers in M82 were of Rayleigh type. We have also seen in chapter three that interstellar matter will probably partially be made up of grains in the Mie domain ($x \sim 1$).

It is evident that most nebulae will contain grains. This was shown by Schiffer and Mathis for the Orion nebula (1974). Polarisation measurements of the Orion nebula by Pallister et. al. (1977) indicated Mie type grains. It is usually easy to differentiate between the two types of grain since as the grain size approaches the Mie limit, the percentage polarisation drops dramatically for a given geometry. However, the Mie formulation is in no way easy. When dealing with Mie grains many parameters are introduced. In this chapter we look at the problems involved in modelling nebulae containing Mie particles.

7.1 The formulation

The model used here will be a simple optically thin spherical reflecting nebula, the star being placed in the centre of the nebula (see figure25). We have seen in chapter two the quantities required for the evaluation of the state of polarisation of the scattered light. The quantities required are the scattering functions $S_i(\theta, x)$. Since they are functions of x as well as θ, a grain size distribution is required. These functions must be weighted over the distribution. Thus if n(x) represents the distribution and N the total number of particles per unit volume then we can define the 'weighted' scattering functions $F_i(\theta)$ such that

$$N F_i(\theta) = \int_0^\infty n(x) |S_i(\theta, x)|^2 \, dx \qquad (i=1,2) \tag{7.1}$$

where

$$N = \int_0^\infty n(x)\, dx .$$

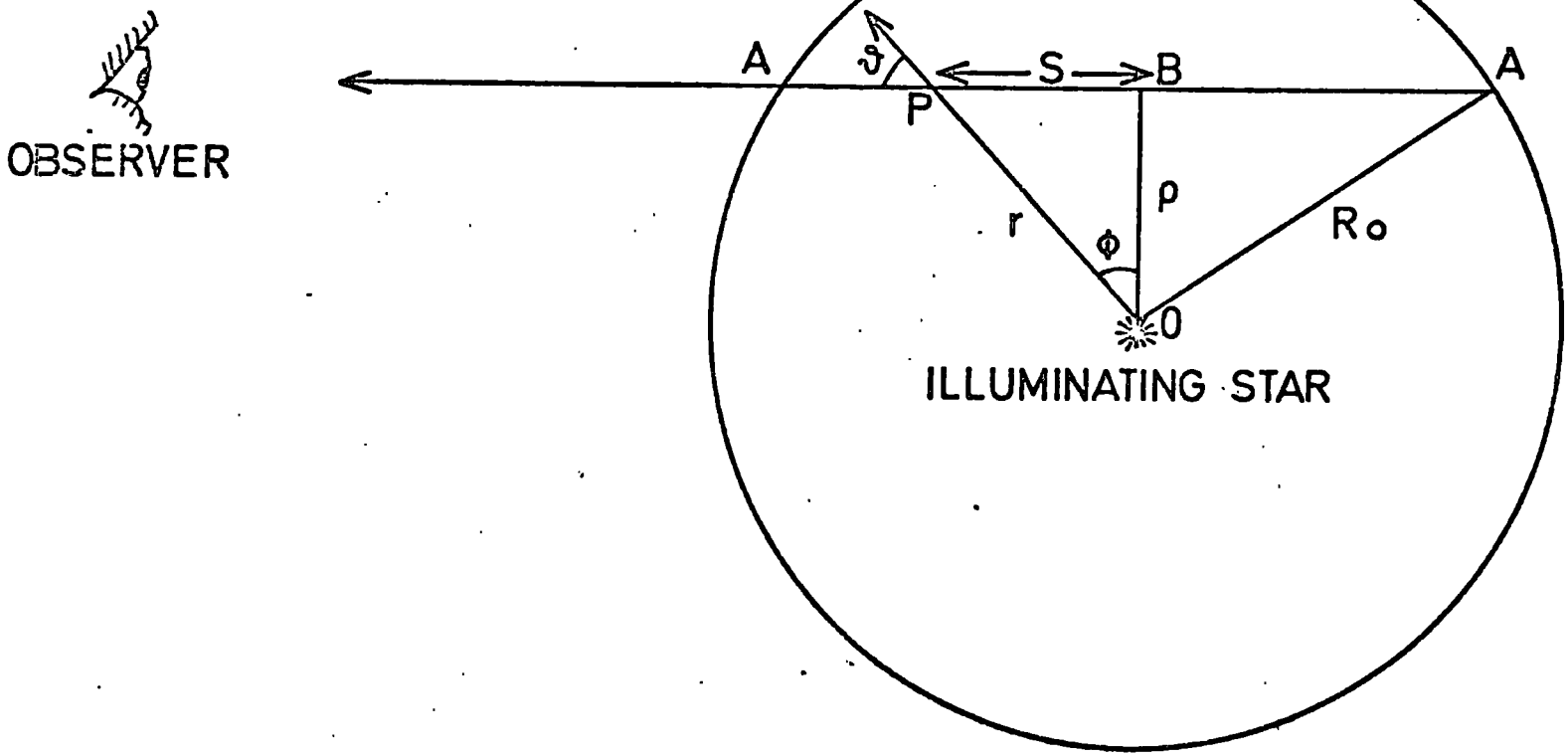

FIG. 25

The percentage polarisation of the scattered light for a discrete scattering angle θ will be

$$p = \frac{F_1(\theta) - F_2(\theta)}{F_1(\theta) + F_2(\theta)} \tag{7.2}$$

Before we can apply these quantities to the model we must reduce the model geometry to an analytical form. More precisely we must reduce it so that it depends solely on the scattering angle θ.

Let us consider first of all the polarised intensity I_p. If we wish to find the polarised intensity from the nebula at distance ρ from the central star

$$I_p = I_o \int_{-\ell}^{+\ell} (F_1(\theta) - F_2(\theta)) \frac{ds}{r^2} \tag{7.3}$$

where the total line of sight is 2l. This integral means that we merely add up each individual scattered component along the line of sight.

From the geometry the following reduction is readily observed.

$$\sin\theta = \rho/r$$

so that

$$\frac{\sin^2\theta}{\rho^2} = \frac{1}{r^2}$$

Also

$$\tan\theta = \rho/s$$

or

$$s = \rho \cot\theta$$

in which case

$$ds = -\rho \operatorname{cosec}^2\theta \, d\theta$$

Equation (7.3) becomes

$$I_p = -\frac{I_o}{\rho} \int_{-\ell}^{+\ell} (F_1(\theta) - F_2(\theta)) \, d\theta \tag{7.5}$$

The limits now become the angles θ_o and $\pi - \theta_o$ where

$$\theta_o = \sin^{-1}(\rho/R_o)$$

and equation (7.5) becomes

$$I_p = \frac{I_o}{\rho} \int_{\theta_o}^{\pi-\theta_o} (F_1(\theta) - F_2(\theta)) \, d\theta \tag{7.6}$$

where Ro is the radius of the nebula. It must be remembered that the symmetry of the geometry cannot be introduced into the integral since the functions $F_i'(\theta)$ are not symmetrical about $\theta=\frac{\pi}{2}$.

At this stage we may introduce a symmetrical dust density of the form

$$n_D = n_0/r^n$$

Equation (7.6) becomes

$$I_p = \frac{I_0 n_0}{\rho^{n+1}} \int_{\theta_0}^{\pi-\theta_0} (F_1(\theta) - F_2(\theta)) \sin^n\theta \, d\theta \qquad (7.7)$$

Likewise for the intensity of scattered light

$$I_s = \frac{I_0 n_0}{\rho^{n+1}} \int_{\theta_0}^{\pi-\theta_0} (F_1(\theta) - F_2(\theta)) \sin^n\theta \, d\theta \qquad (7.8)$$

7.2 Computational procedure

The models were computed using the IBM 370 at Newcastle linked with Durham. First checks had to be made. Various values of Qsca and Qabs were computed (see figures26-28) and compared with those calculated by Wickramasinghe (1972) and extremely good agreements were reached. The next task was to calculate the values of $S_i'(\theta,x)$ and then $F_i'(\theta)$. Since there are no analytical forms of $S_i'(\theta,x)$ an integration routine was used and values of $F_i'(\theta)$ were computed with one degree intervals. It is worth noticing that a good procedure was used because as x increases, the oscillations of $S_i'(\theta, x)$ become more rapid. This means that if a large step — length is introduced without a check many of the oscillations would be smoothed out during the calculation. So 360 values of $F_i'(\theta)$ are obtained for a particular distribution. To calculate equations (7.7) and (7.8) another integration procedure was used employing the Romberg method. (Note that in all these integrations, a check was used such that the error was one part in 10^4) Since the tabulated values of $F_i'(\theta)$ are in one degree intervals, an extrapolation routine was used that calculated the intermediate values of $F_i'(\theta)$. A check had to be employed, the most obvious one was to reduce the program to the Rayleigh case.

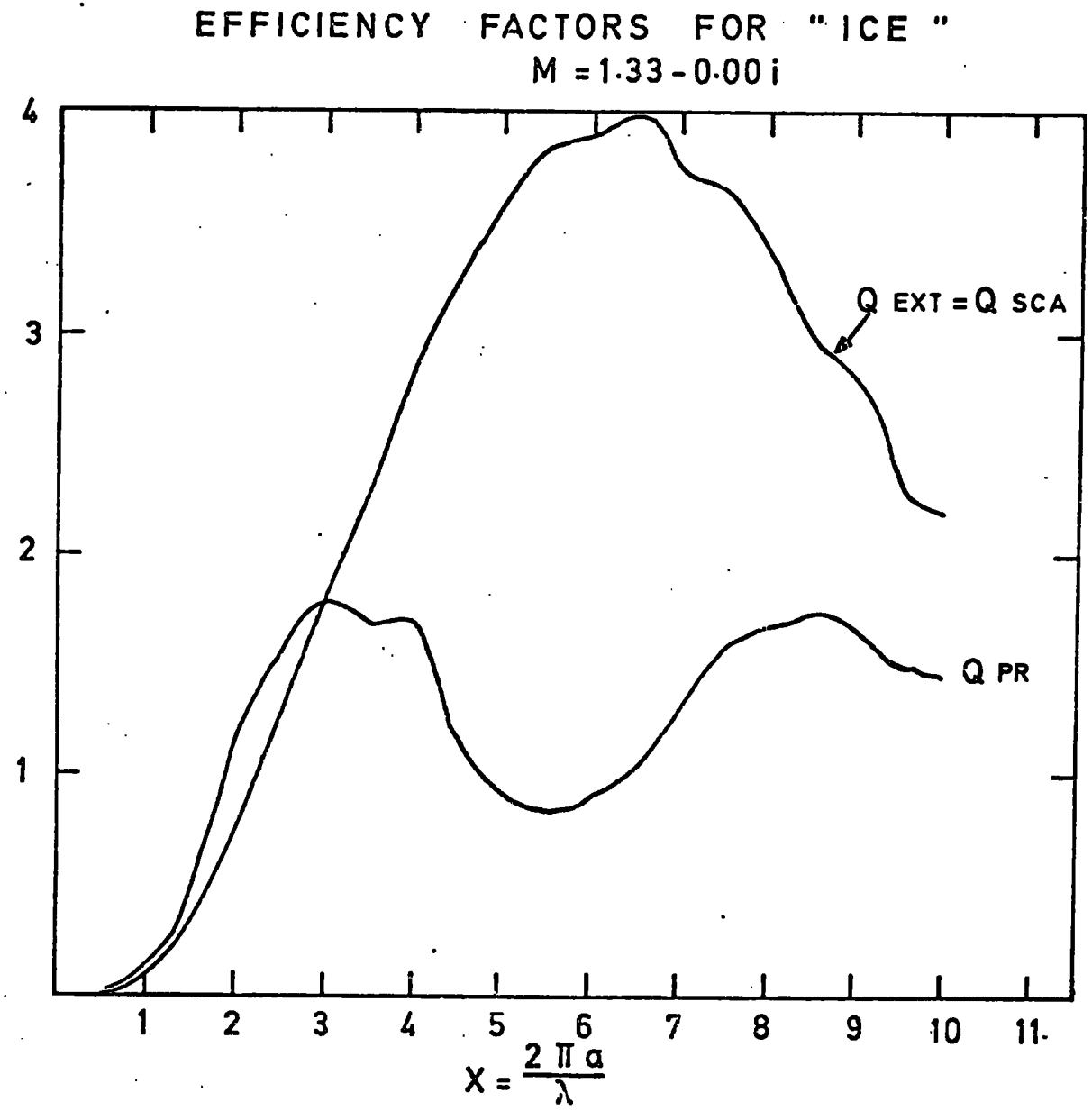
EFFICIENCY FACTORS FOR "ICE"
M = 1.33 - 0.00 i
Q EXT = Q SCA
Q PR
4
3
2
1
1
2
3
4
5
6
7
8
9
10
11
X = 2 π a / λ

FIG. 26

EFFICIENCY FACTORS FOR 'SILICATES' M = 1·70 - 0·30 i

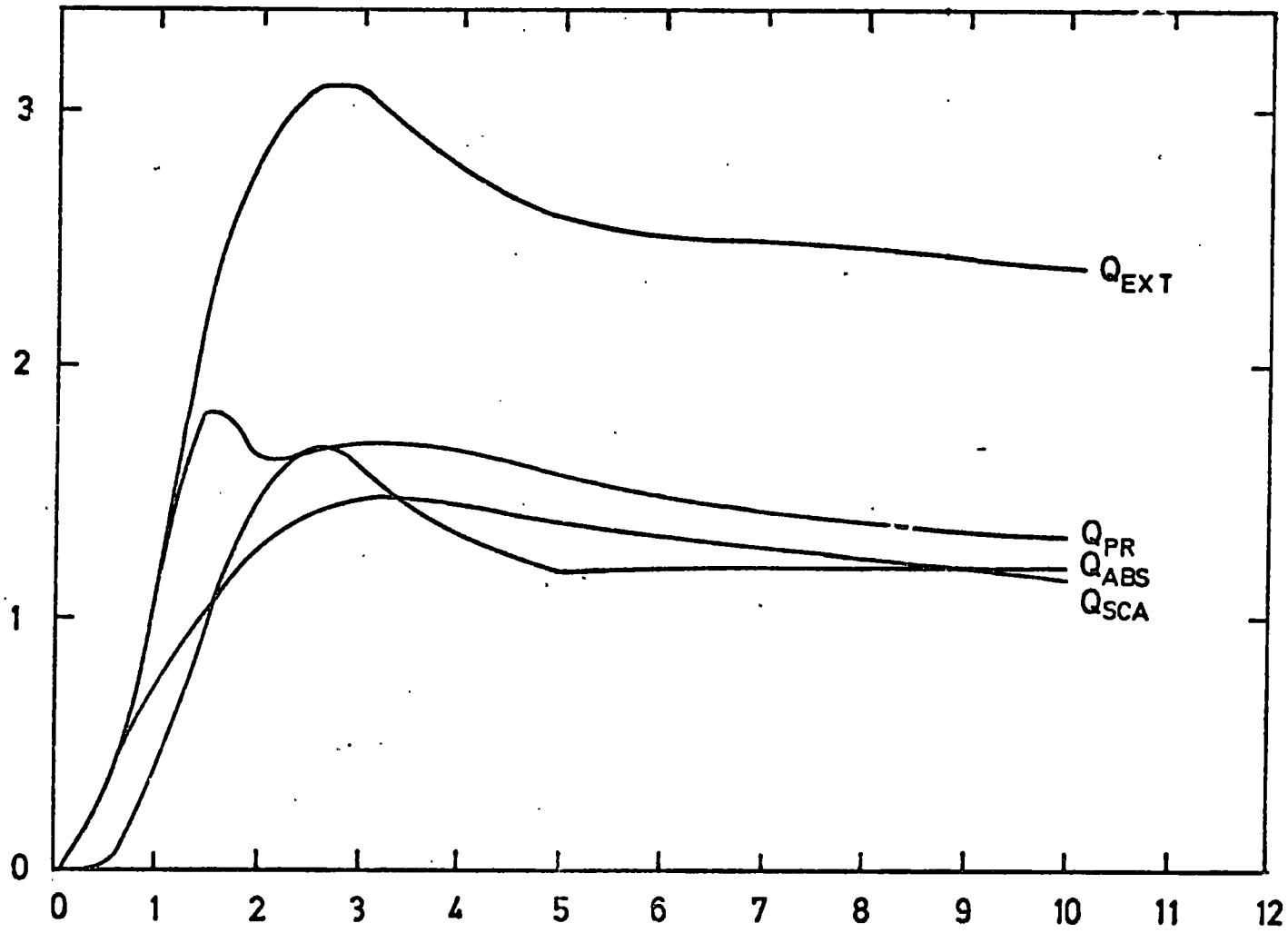

FIG. 27

EFFICIENCY FACTORS FOR "DIRTY" ICE

M = 1·33 - 0·05 i

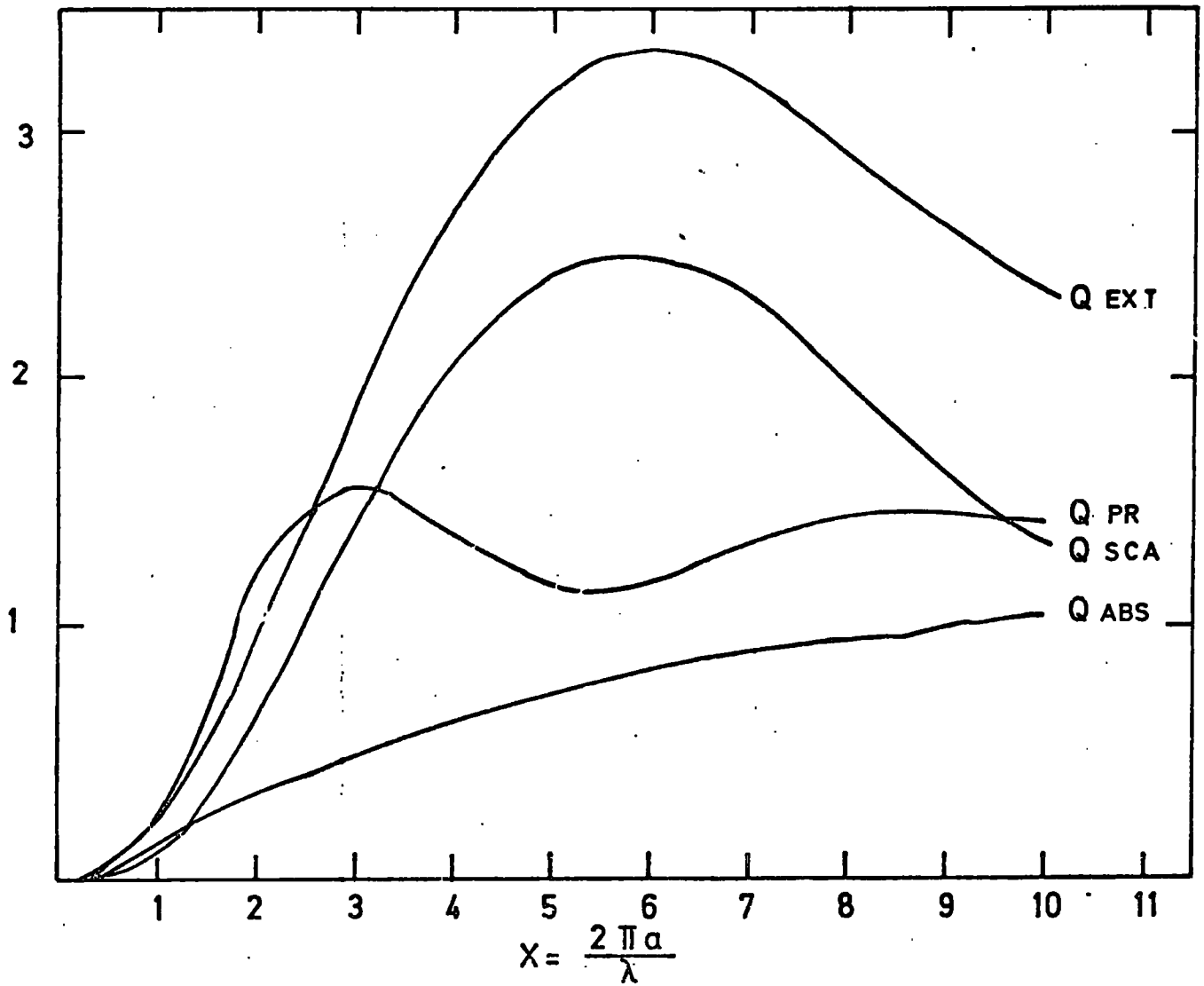

FIG. 28

7.3 The Rayleigh case

We use the Rayleigh case for the test since we can predict an analytical form for the state of polarisation and intensity. We refer back to figure (25). We first predict the polarised intensity. For each point along the line of sight the state of polarisation must be weighted against the intensity falling on the point.

Let the total intensity observed from the nebula at a distance ρ from the central star be $I_T(\rho)$, and the observed state of polarisation be $\Pi(\rho)$, then we can write

$$\Pi(\rho) I_T(\rho) = \int_{-\ell}^{+\ell} p(\theta) I(\theta)\, ds \tag{7.9}$$

where

$$p(\theta) = \frac{1-\cos^2\theta}{1+\cos^2\theta}$$

Since we are assuming an optically thin nebula.

$$I(\theta) = I_0 (1+\cos^2\theta)/r^2$$

which means that equation (7.9) becomes

$$\Pi(\rho) I_T(\rho) = \frac{I_0}{\rho} \int_{-\ell}^{+\ell} (1-\cos^2\theta) \frac{ds}{r^2} \tag{7.10}$$

We refer the geometry to the angle φ where $\varphi = \frac{\pi}{2} - \theta$

Applying the same analysis as in section 7.1

$$\Pi(\rho) I_T(\rho) = \frac{I_0}{\rho} \int_{\varphi_0}^{\pi-\varphi_0} \cos^2\varphi \, d\varphi \tag{7.11}$$

Likewise for $I_T(\rho)$ we have

$$I_T(\rho) = \frac{I_0}{\rho} \int_{\varphi_0}^{\pi-\varphi_0} (1+\sin^2\varphi)\, d\varphi \tag{7.12}$$

The state of polarisation for a point ρ from the star becomes

$$P(\rho) = \frac{\int_0^{\varphi_0} \cos^2\varphi \, d\varphi}{\int_0^{\varphi_0} 1+\sin^2\varphi \, d\varphi} \tag{7.13}$$

Note that we have used the symmetry of the geometry to change the limits of the integrals. Equation (7.13) becomes

$$P(\rho) = \frac{\varphi_0 + \frac{1}{2}\sin 2\varphi_0}{3\varphi_0 - \frac{1}{2}\sin 2\varphi_0} \qquad (7.14)$$

Since $\varphi_0 = \cos^{-1}\rho/R_0$

we use the variable $x = \rho/R_0$ which means that (7.14) is now

$$P(\rho) = \frac{\cos^{-1} x + x(1-x^2)^{1/2}}{3\cos^{-1} x - x(1+x^2)^{1/2}}$$

Values of P (ρ) were readily calculated. These values were compared with computer predictions using the Mie model for various values of the refractive index. It was found that the computer predictions were in error within two points in 10^4. This duly established the credibility of the computer model.

7.4. Results from computer models

We are now in a position to predict polarisation and intensity from model nebulae with the and of the model. All that is required is to imput the refractive index and size distribution of the grains. Since one can predict a multitude of results, we look at the affects on the results when the parameters are varied. The results presented here are the percentage polarisation plotted against the ratio of the distance of the point of observation from the star to the radius of the nebula. We have used two grain size distributions viz

$$n(a) = n_0 \exp(-a/a_0)^3 \qquad (7.15)$$

and

$$n(a) = n_0 a^{3/2} \exp(-\tfrac{1}{2} a/a_m)^3 \qquad (7.16)$$

Let us first look at the affect on the results when the mean grain size, $\bar{x}$, is varied. Figure (29) shows the polarisation for a spherical nebula containing dirty ice ($m = 1.33-0.05i$) along with the size distribution whown in equation (7.16). The predicted line, A, is far $\bar{x} = 2.0$ while B is far $\bar{x} = 3.0$. Clearly, dramatic effects occur when $\bar{x}$ is changed. What happens if we now change the grain size distribution? Figure (30) shows the case for dirty ice again only

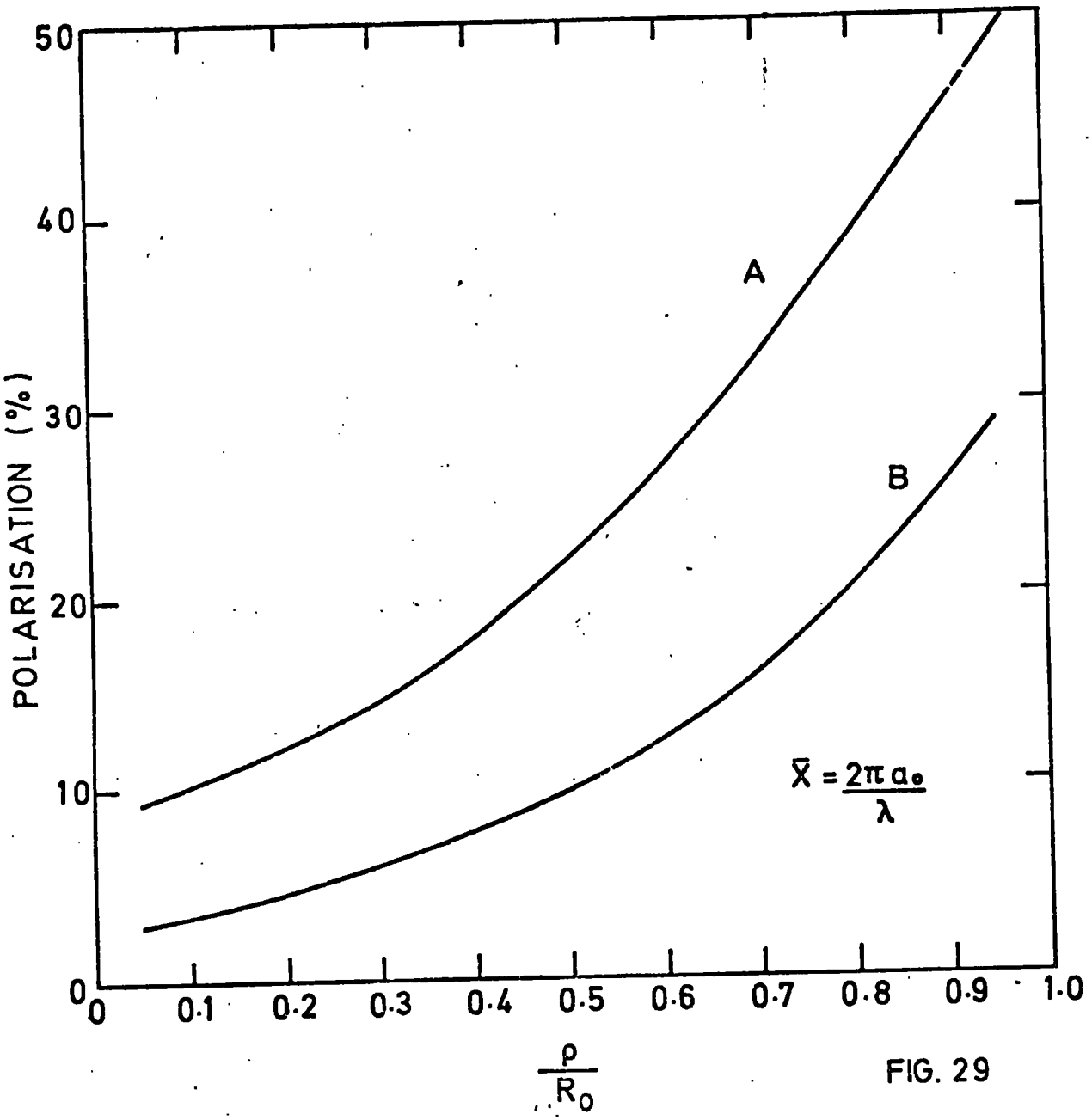
50
40
30
20
10
0
POLARISATION (%)
A
B
$\bar{X} = \frac{2\pi a_0}{\lambda}$
0
0.1
0.2
0.3
0.4
0.5
0.6
0.7
0.8
0.9
1.0
$\frac{\rho}{R_0}$

FIG. 29

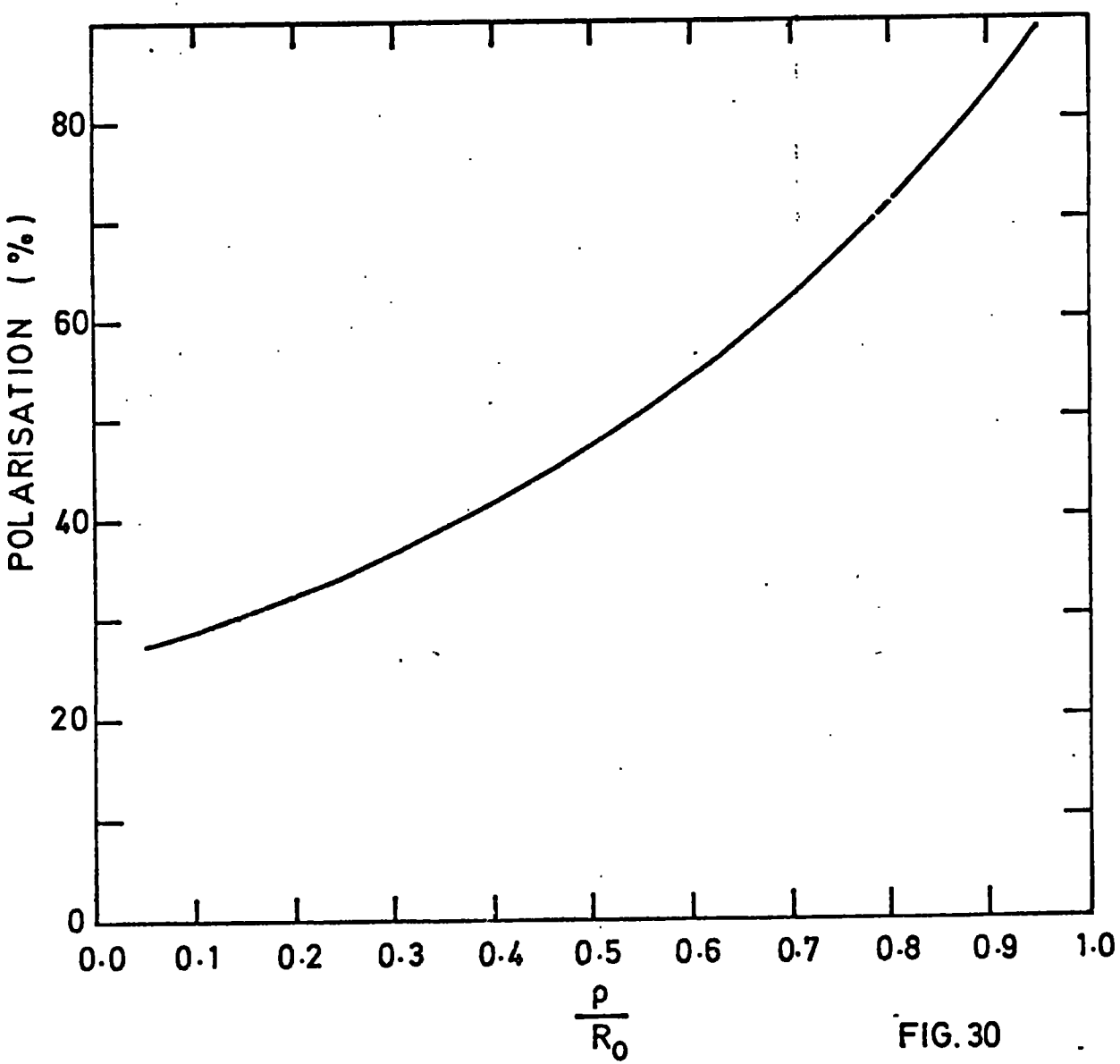

FIG. 30

this time the distribution shown in equation (7.15) is used along with $\bar{x} = 2.0$. Here the polarisation is increased dramatically when compared with line A, of figure (29). This indicates that the distribution is just as important as $\bar{x}$. The increase in polarisation encountered, when using the 'Greenstein' distribution (equation 7.15) is easily understood from the equation. The Greenstein distribution will contain many Rayleigh particles whereas the 'Wickramasinghe' distribution (equation 7.16) has the '$a^{3/2}$' factor coupled with the exponential thus reducing the number of Rayleigh particles present.

We now turn our attention to the geometry. We now invoke a 'slab' like geometry, the results using this are shown in figure (31). Here, as indicated, we have used the two size distribution with dirty ice and $\bar{x} = 2.0$. The Greenstein distribution can be compared with the curve in figure (30) which uses a spherical geometry. It is seen on comparison that the shape of the curves vary greatly. Using the same geometry with the Wickramasinghe distribution and holding $\bar{x} = 2.0$, we now use silicate grains. (seen in figure 32). Comparing the curves for ice and silicate, a great decrease in percentage polarisation is observed.

The only parameter left to investigate is the variation in the dust density. Figure (33) shows a spherical model using the Wickramasinghe size distribution with silicate grains only with $\bar{x} = 1.0$. This is very near the Rayleigh limit. A dust density of the form n_0/r^n was used. The curves A, B and C indicate the percentage polarisation for n = 0, 1 and 2 respectively. It must be added however, that as one increases $\bar{x}$, the difference in polarisations between the curves tends to decrease.

7.5. Discussion of results

From the previous section we are able to state to what extent the variation of the parameters affect the results. Usually, if one was dealing with data, the approach taken would be to assume the geometry of the object, although error in judgement can affect the results greatly. Secondly, the type of grains present can be found from infra-red absorption measurements, although again error here

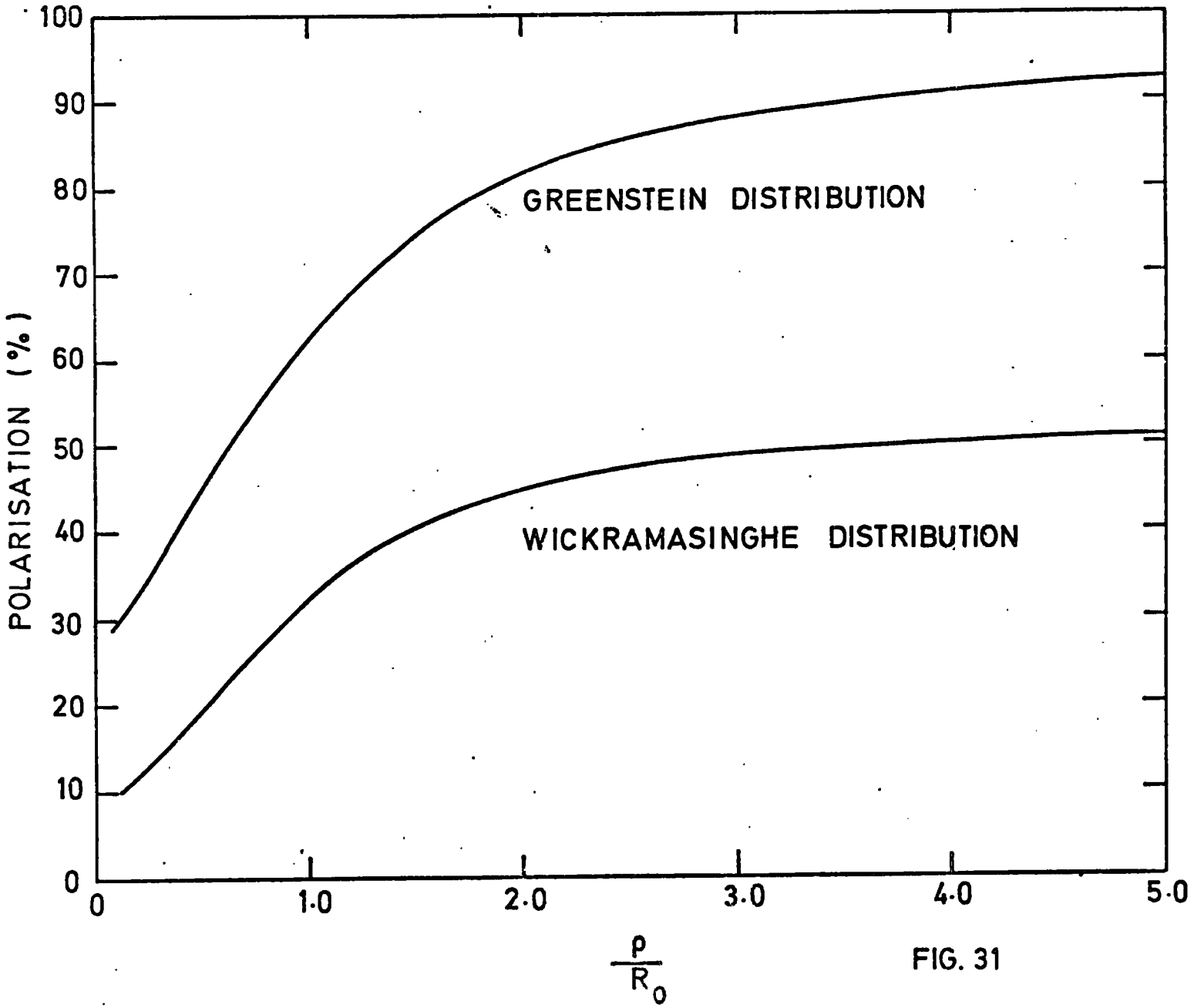
100
90
80
70
60
50
40
30
20
10
0
POLARISATION (%)
GREENSTEIN DISTRIBUTION
WICKRAMASINGHE DISTRIBUTION
0
1·0
2·0
3·0
4·0
5·0
ρ/R0

FIG. 31

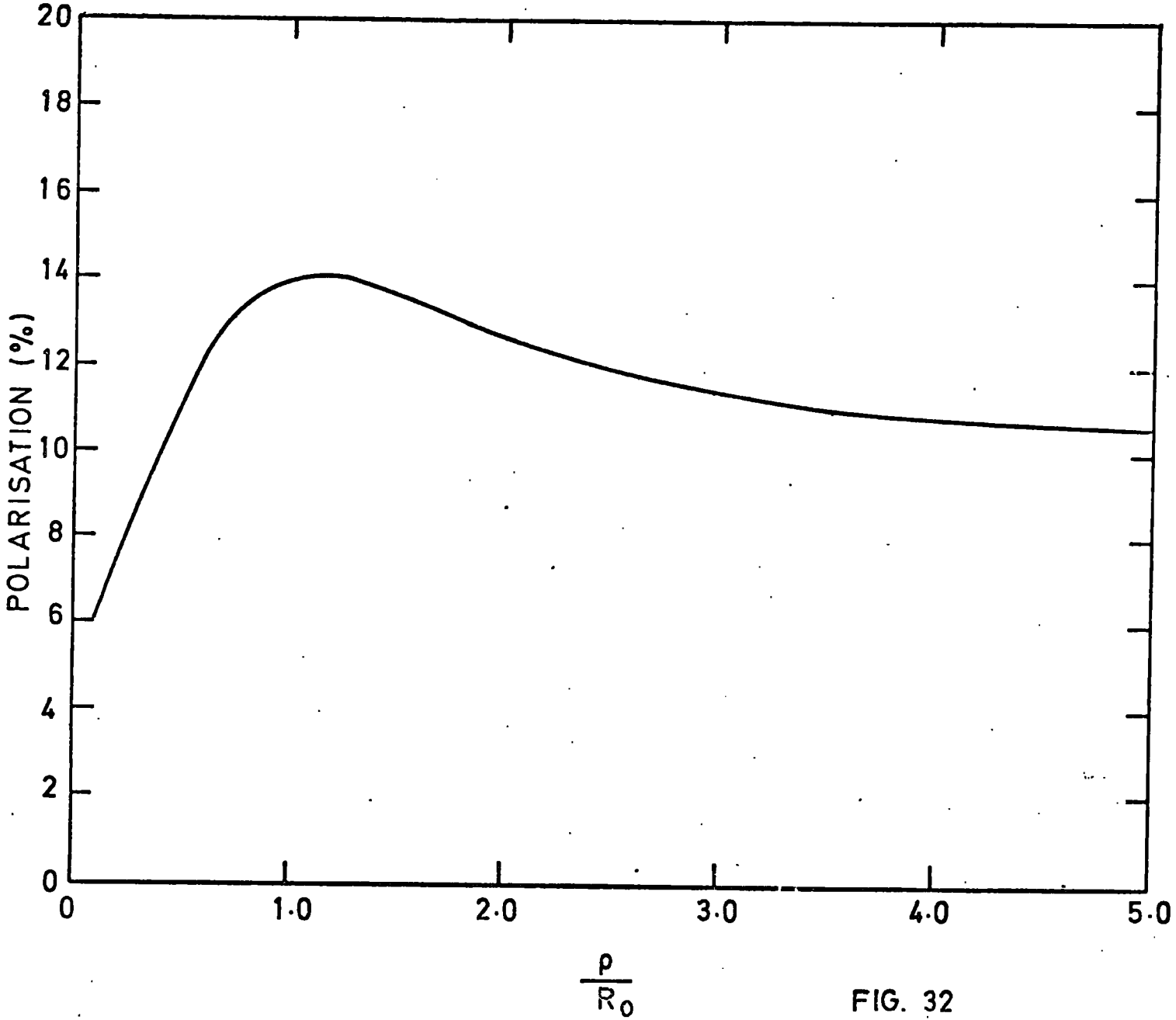

FIG. 32

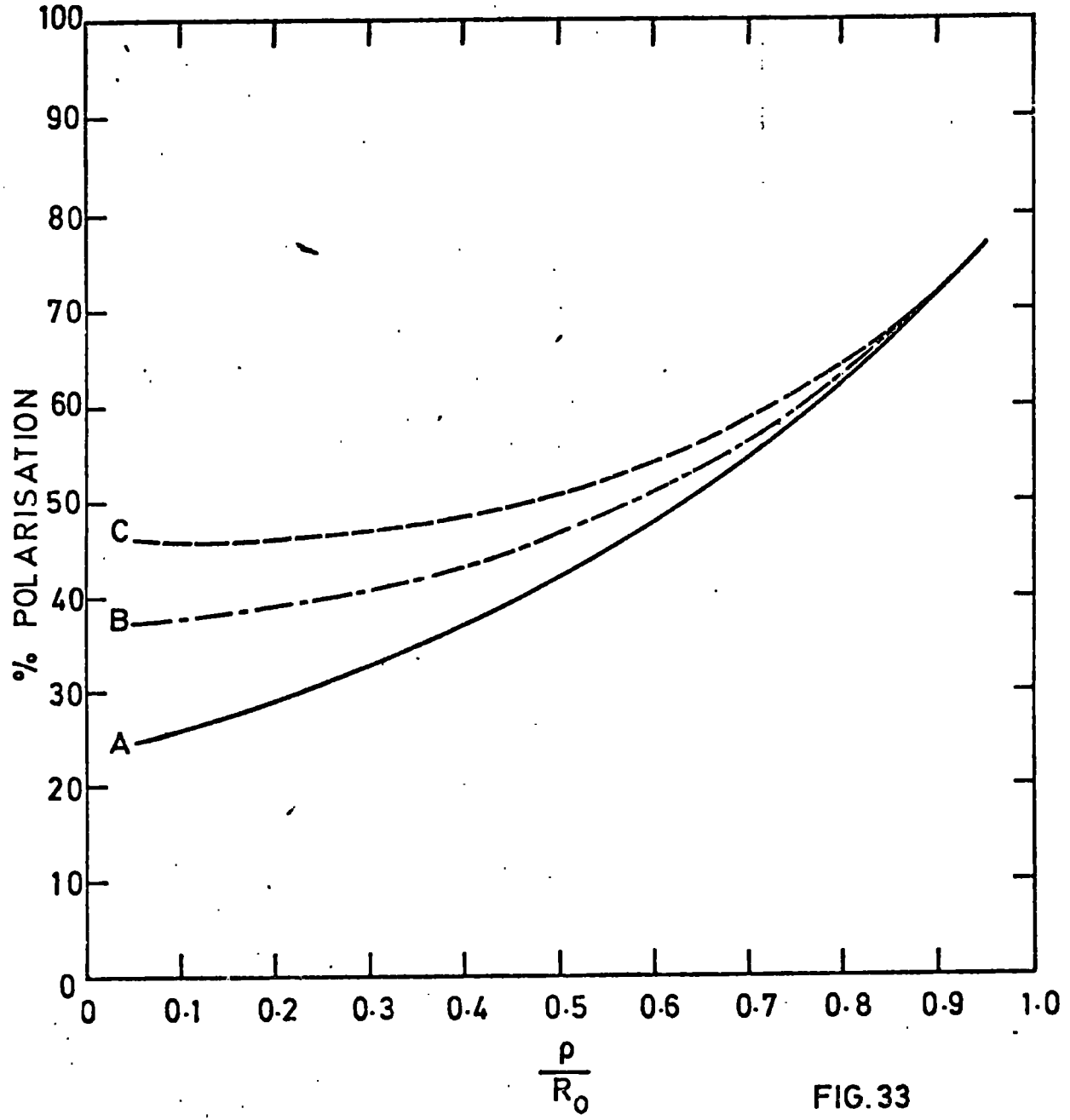
100
90
80
70
60
50
40
30
20
10
0
% POLARISATION
C
B
A
0
0·1
0·2
0·3
0·4
0·5
0·6
0·7
0·8
0·9
1·0
ρ/R0

FIG. 33

will greatly affect the results. The size distribution has probably the greatest affect on the results overall. The problem is twofold however, we not only need knowledge of the distribution but also of the mean grain size, $\overline{x}$, which also has a great affect on the results. It is clear from this that more study is required into this problem.

The dust density introduced is not such an important quantity. The effect on the polarisation is obvious after some thought. If a radial decrease in the dust density is introduced then when summing polarisation components along a line of sight more light will be scattered where the scattering angle is of the order of about ninety degrees, then when scattered at the edges of the nebula. Around these angles occur the greatest percentage polarisation.

There is one other problem that we have failed to mention that of the optical depth. Vanysek (1973) has found, by using a Monte-Carlo method, that as the optical depth of nebula is increased the polarisation decreases. This is because the number of scatterings has increased within the nebula (the models here assumes single scattering). As the light passes through the nebula the scattering angles will change for each point of scattering. This has the effect of 'diluting' the polarisation. Clearly a proper analytical approach to this will be extremely difficult.

GENERAL CONCLUSIONS

It is obvious from this thesis that polarisation measurements is one of the most important techniques for investigating grains in nebulae and galaxies. It also has other uses, particularly in deciding whether stars are embedded in certain nebulae, as was in the case of the Orion nebula (Pallister et. al. 1977) it can also be used in detecting magnetic fields, as in M104 (Scarrott et. al. 1977).

As polarisation has been considered here, its main purpose is to find out certain properties of grains in nebulae and galaxies. We have seen that there are two domains to consider, these being the Rayleigh domain and the Mie domain. If a nebula consists of Rayleigh particles the formulation becomes relatively simple however, the properties of the grains are lost since the polarisation is independent of the refractive index, and a grain size distribution is not required so that little can be said about the grains except that a limit on the size can be placed. The situation of M82 is very unusual. In this case, properties of the galaxy as well as some measure of the grain density can be found, but the chances of finding many observable galaxies like M82 must be very small indeed. M82 is an example that shows the versatility of polarisation in leading us to the answers.

The opposite occurs for Mie grains. In this case there are many parameters to be considered, the refractive index, the geometry of the nebula and the grain size distribution. The size distribution is not particularly of interest physically, but the theory requires a grain size distribution to be used. As in mathematical equations, the more variables present, the more equations are required to solve for the variables. An analogy can be drawn here since we have so many parameters we require many forms of measurements. These take the form of infra-red, colour measurements (e.g. B - V), spatial polarisation and variation of polarisation with wavelength. The problem now is to model the nebula, combined with the data.

The greatest problem here is the optical depth of the nebula for once the optical depth goes beyond the order of unity, multiple scattering arises. No analytical approach to this problem has yet been established, it is usually tackled by a Monte-Carlo procedure. Consider the possibility of using wavelength variation of polarisation. Knowledge of this property would be a great boon in the investigation of the grains' properties. However, if polarised intensity is used, knowledge of the variation with wavelength of the illuminating sources' intensity is a prerequisite. More fundamentally the geometry of the nebula has to be established initially before any modelling can be attempted. Assuming that the means of obtaining these measurements are at hand, what type of nebula should be approached? The answer appears to be an optically thin spherical reflecting nebula. However, it is usually found that most optically thin nebulae are not spherical. The other disadvantage is that an optically thin nebula will be of low intensity. Planetary nebulae might be of some interest since their geometry is more or less secured, however, the problem of scattering of emission light will be encountered in the shell. In any event the reduction of the model will require immense computing time. Clearly, from the arguments presented here, more work is required in the treatment of the theory.

Appendix A

Mathematical reduction of the M82 model

The analysis that follows is based upon Solingers' (1975) reduction. We refer back to figure (8). We define the angle θ as the scattering angle and the angle ψ as the angle between the scattering plane and the line of sight. Solinger shows that in this geometry the Stokes' parameters will be

$$\begin{pmatrix} I_e \\ I_r \\ U \end{pmatrix} = \frac{3}{4}\begin{pmatrix} \cos^2\theta\cos^2\psi + \sin^2\psi \\ \cos^2\theta\sin^2\psi + \cos^2\psi \\ (1-\cos^2\theta)\sin 2\psi \end{pmatrix} I_o \qquad (A.1)$$

or

$$\begin{aligned} I_e &= \tfrac{3}{4} I_o (\cos^2\theta\cos^2\psi + \sin^2\psi) \\ I_r &= \tfrac{3}{4} I_o (\cos^2\theta\sin^2\psi + \cos^2\psi) \\ U &= \tfrac{3}{4} I_o (1-\cos^2\theta)\sin 2\psi \end{aligned} \qquad (A.2)$$

From definition

$$I = I_e + I_r$$

and

$$\varphi = I_e - I_r$$

so that

$$I = I_e + I_r = \tfrac{3}{4} I_o (1+\cos^2\theta) \qquad (A.3)$$

$$\varphi = I_e - I_r = \tfrac{3}{4} I_o \cos 2\psi (\cos^2\theta - 1) \qquad (A.4)$$

$$U = \tfrac{3}{4} I_o \sin 2\psi \sin^2\theta \qquad (A.5)$$

From the diagram we define

$$\begin{aligned} \underset{\sim}{r_D} &= r_D\cos\varphi\,\underset{\sim}{i} + r_D\sin\varphi\,\underset{\sim}{j} \\ \underset{\sim}{R_1} &= Y\underset{\sim}{j} + Z\underset{\sim}{k} \\ \underset{\sim}{R_2} &= r_D\cos\varphi\,\underset{\sim}{i} + (Y - r_D\sin\varphi)\underset{\sim}{j} + Z\underset{\sim}{k} \\ \underset{\sim}{R} &= (X - r_D\cos\varphi)\underset{\sim}{i} + (Y - r_D\sin\varphi)\underset{\sim}{j} + Z\underset{\sim}{k} \end{aligned} \qquad (A.6)$$

and

$$\underset{\sim}{R}' = X\,\underset{\sim}{i} + Y\,\underset{\sim}{j} + Z\,\underset{\sim}{k}$$

where ($\underset{\sim}{i}$, $\underset{\sim}{j}$, $\underset{\sim}{k}$) are the Cartesian unit vectors.

From this we find

$$\cos\theta = \frac{\underset{\sim}{r}\cdot\underset{\sim}{R}}{|\underset{\sim}{R}|} = \frac{(X - r_D\cos\varphi)}{R} \tag{A.7}$$

and

$$\cos^2\psi = \frac{(Y - r_D\sin\varphi)^2}{(R_2^2 - r_D^2\cos^2\varphi)} \tag{A.8}$$

Equation (A.3) becomes

$$I = \tfrac{3}{4} I_0 \left(1 + \frac{(X - r_D\cos\varphi)^2}{R^2}\right) \tag{A.9}$$

Equation (A.4) can be reduced using

$$2\cos^2\psi - 1 = \frac{2(r_D\sin\varphi - Y)^2 - (R_2^2 - r_D^2\cos^2\varphi)}{(R_2^2 - r_D^2\cos^2\varphi)}$$

along with

$$R_2^2 - r_D^2\cos^2\varphi = (Y - r_D\sin\varphi)^2 + Z^2$$

so that

$$2\cos^2\psi - 1 = \frac{(Y - r_D\sin\varphi)^2 - Z^2}{(Y - r_D\sin\varphi)^2 + Z^2}$$

also

$$\cos^2\theta - 1 = \frac{(X - r_D\cos\varphi)^2 - R^2}{R^2}$$

$$= -\frac{(Y - r_D\sin\varphi)^2 - Z^2}{R^2}$$

this means that

$$\varphi = \tfrac{3}{4}\frac{I_0\,(Z^2 - (Y - r_D\sin\varphi)^2)}{R^2} \tag{A.10}$$

Finally we look at equation (A.5). It can easily be shown that

$$\sin 2\psi = 2\sin\psi\cos\psi = \frac{2Z(Y - r_D\sin\varphi)}{(Z^2 + (Y - r_D\sin\varphi)^2)}$$

so that

$$(1 - \cos^2\theta)\sin 2\psi = \frac{2Z\,(Y - r_D\sin\varphi)}{R^2}$$

or

$$U = \tfrac{3}{2} I_0 \frac{2Z(Y - r_D \sin\varphi)}{R^2} \qquad (A.11)$$

Let us now turn our attention to the galactic disk. Let the surface brightness of the disk be

$$B(r_D) = B_0 e^{-k r_D}$$

so that by integrating over the disk we have

$$L_D = \int B \, da \qquad (A.12)$$

where

$$da = r_D \, dr_D \, d\varphi$$

Consider an element of intensity, dIo, from the disk. Then

$$dI_0 = \frac{B(r_D)\, da}{4\pi R^2} = \frac{B_0 e^{-k r_D} da}{4\pi R^2}$$

and using equation (A.12)

$$dI_0 = \frac{2 L_D k^2 \exp(-k r_D)\, da}{16\pi^2 R^2 (1 - 6e^{-5})}$$

where, following Solinger, the upper limit of r = 5/k. Now equations (A.9; A.10; A.11) are Stokes' parameters for one point along the line of sight with the incident light eminating from one element in the disk. We now have to integrate over the disk and the line of sight in order to predict the observed Stokes parameters. The predicted parameters become

$$I_D = A' \int_{-\ell}^{+\ell} \int_0^{2\pi} \int_0^{r_D'} \frac{1}{R^2} \left(1 + \left(\frac{X - r_D \cos\varphi}{R^2}\right)^2\right) e^{-k r_D} r_D \, dr_D \, d\varphi \, dx$$

$$Q_D = A' \int_{-\ell}^{+\ell} \int_0^{2\pi} \int_0^{r_D'} \left(\frac{Z^2 - (Y - r_D \sin\varphi)^2}{R^4}\right) e^{-k r_D} r_D \, dr_D \, d\varphi \, dx$$

$$U_D = A' \int_{-\ell}^{+\ell} \int_0^{2\pi} \int_0^{r_D'} \frac{2Z(Y - r_D \sin\varphi)}{R^4} e^{-k r_D} r_D \, dr_D \, d\varphi \, dx$$

where A' is a constant. Note that these are the Stokes parameters observed from light eminating from the disk. For the nuclear parameters we simply place $r_D = 0$

and find

$$I_N = B' \int_{-\ell}^{+\ell} \left(1 + \frac{X}{R'^2}\right) \frac{dx}{R'^2}$$

$$Q_N = B' \int_{-\ell}^{+\ell} \frac{z^2 - y^2}{R'^4}\, dx$$

$$U_N = B' \int_{-\ell}^{+\ell} \frac{2yz}{R'^4}\, dx$$

where B' is a constant which depends on the nuclear luminosity. Note that these equations use a constant dust density distribution.

REFERENCES

Abadi, H. I., Bohren, C. F.1977 Astron & Astrophys 60 125

Axon, D. J., Taylor K. 1978 Nature 274 37

Bahng, J. 1966 Colloqium on Late Type stars (Trieste Observatorio Astronomico de Trieste) p. 225

Bates, D. R., Spitzer, L., 1951. Ap, J. 113 441

Bless, R. C., Savage, B. D. 1970 Ultraviolet Stellar Spectra and Groundbase Observations (Houziaux & Butler Eds., D. Riedel Co.)

Bingham, R. G., McMullan, D., Pallister, W. S., White, C., Axon, D. J., Scarrott, S. M., 1976. Nature 259 463

Chandrasekhar, S., 1960 Radiative Transfer, Dover.

Cotrell, G. A., 1977 Mon. Not. R. astr. Soc. 178 577

Deirmendjian, D. 1969. Electromagnetic scattering of spherical polydispersions. American Elsevier. Publ. Co. New York.

Elvius, A. 1963 Lowell Observatory Bull. 5 271
1972 Astron. & Astrophys 19 193

Elvius, A., Hall, J. S. 1967 Interstellar Grains (London: Chapman and Hall).

Gilra, D. P. 1971. Nature 169 322

Greenberg, J. M. 1966 Ap. J. 132 672
1968 Stars and stellar systems (Chicago: Chicago Univ. press) 7

Greenstein, J. L., Davis, L. 1951 Ap. J. 114 206

Hackwell, J. A., Gehrz, R. O., Woolf, N. J. 1970 Nature 227 822

Hall, J. S. 1949 Science 109 166

Hargrave, P. J. 1974 Mon. Not. R. astr. Soc. 168 49

Harper, D. A., Low, F. J. 1973 Ap. J. 182 L89

Hartman, W. K. 1970 Mem. Soc. R. Sci. Liege 19 215

Hayakawa, S., Yamashita, K., Yoshioka, S. 1969 Astrophys & Space. Sci 5 493

Henyey, L. G., Greenstein, J. L. 1941 Ap. J. 93 70

Hiltner, W. A., Hall, J. S. 1949 Science 109 165

Hoyle, F., Wickramasinghe, N. C. 1962 Mon. Not. R. astr. Soc. 124 417
1968 Nature 217 415
1970a Nature 226 62
1970b Nature 227 473

Johnson, H. L. 1968 Stars and stellar systems (Chicago: Chicago Univ. press) 7

Knacke, R. F., Gaustad, J. E., Gillet, F. C., Stein, W. A. 1969 Ap. J. Lett 155 L189

Linblad, B. 1935. Nature 135 133

Low, F. J., Krishna-Swamy, K. S. 1970 Nature 227 1333

Lynds, C. R. 1961 Ap. J. 134 659

Lynds, C. R., Sandage, A. R. 1963 Ap. J. 137 1005

Mathis, J. S. 1973 Ap. J. 183 41

Ney, E. P., Allan, D. A. 1969 Ap. J. Lett 155 L193

O'Dell, C. R. 1965 Ap. J. 142 604

O'Dell, C. R., Hubbard, W. B. 1965 Ap. J. 142 591

O'Dell, C. R., Hubbard, W. B., Peimbert, M. 1965 Ap. J. 143 743

Osterbrock, D. E. 1974 Astrophysics of gaseous nebulae (W. H. Freeman Co. San Fransisco).

Pallister, W. S. 1976 Ph.D. Thesis Durham.

Pallister, W. S., Perkins, H. G., Scarrott, S. M., Bingham, R. G., Pilkington, J. D. H. 1977 Mon. Not. R. astr. Soc. 178 93p

Platt, J. R. 1956 Ap. J. 123 486

Platt, J. R., Donn, B. D. 1956 Astron. J. 61 11

Reddish, V. C. 1967 Mon. Not. R. astr. Soc. 135 251

Roberts, M. S. 1972 External Galaxies and Quasi-stellar objects ed. D. S. Davies (New York: Springer - Vierlag) p 12

Sandage, A. R., Miller, E. C. 1964 Science 130 1421

Sandage, A. R., Visvanathan, N. J. 1972 Ap. J. 176 57

Sanders, R. H., Balamore, D. S. 1971 Ap. J. 166 7

Scarrott, S. M., White, C., Pallister, W. S., Solinger, A. B. 1977 Nature 265 32

Schalen, C. 1939 Upsala. Obs. Ann. 1. No. 2

Schiffer, F. H., Mathis, J. S. 1974 Ap. J. 194 597

Schild, R. E. 1977 Astron. J. 82 337

Schmidt, G. D., Angel, J. R. P., Cromwell, R. H. 1976 Ap. J. 206 888

Schmidt, Th. 1958 Z Astrophys. 46 145

Solinger, A. B. 1969a Ap. J. 155 403
1969b Ap. J. Lett. 150 L21
1969c Ibid 158 L25

Solinger, A. B., Markert, T. 1975 Ap. J. 197 309

Solinger, A. B., Morrison, P., Markert, T. 1977 Ap. J. 211 707

Stebbins, J. 1934. Publ. Washburn, Obs. 15 part 5

Stebbins, J., Huffer, C. M., Whitford, A. E. 1939 Ap. J. 96 209

Stecher, T. P., 1969 Ap. J. 157 L125

Stein, W. A., Gillet, F. C. 1969 Ap. J. Lett 155 L197

Van de Hulst, H. C. 1949 Rech. Astron. Obs. Utrecht. 11 part 2
1957 Light scattering by small particles (John Wiley & Sons New York).

Van den Bergh 1971 Astron. & Astrophys. 12 474

Vanysek, V. 1973 Interstellar Dust and Related Topics. I.A.U. Sympos. No. 52 (Ed. Greenberg & Van de Hulst, D. Reidel Publ. Co. Holland).

Weliachew, L., Gottesman, S. T. 1977 Ap. J. 211 47

Wickramasinghe, N. C. 1963 Mon. Not. R. astr. Soc. 126 99
1967 Interstellar Grains (Chapman & Hall: London).
1972 Interstellar Matter (Publ. Geneva. Obs: Switzerland)
1973 Light scattering functions for small particles. (Adam Hilger: London).

Wickramasinghe, N. C., Guillaume, C. 1965. Nature 207 366

Wickramasinghe, N. C., Nandy, K. 1970 Nature 222 51
1971 Mon. Not. R. astr. Soc. 153 205

Witt, A. N. 1968 Ap. J. 152 59

White, C. 1977 M.Sc. Thesis Durham.

Woolf, N. J., Ney, E. P. 1969 Ap. J. Lett 155 L181

ACKNOWLEDGEMENTS

I wish to thank Dr. S. M. Scarrott for his tireless academic and moral support during my term as a research student at Durham. I would also like to thank Dr. W. S. Pallister for the time and effort spent in providing me with the data. I must also thank Dr. R. G. Bingham and Dr. A. B. Solinger for the many hours spent in fruitful discussion.

Professor A. W. Wolfendale, F.R.S., and Professor B. H. Bransden are thanked for allowing the use of the ficilities of the department. This thesis would not have been possible but for the financial support of the S.R.C.

Lastly, I would like to thank Janet Reid and Olive Wright from Kenton Comprehensive School, who under much pressure, produced emmaculate typing on time.